WALL MODELS FOR LARGE-EDDY SIMULATION BASED ON OPTIMAL CONTROL THEORY

by

Jeremy A. Templeton, Parviz Moin and Meng Wang

Prepared with the support of the
Air Force Office of Scientific Research
under Grant No. F49620-03-1-0132

Report No. TF-98

Flow Physics and Computation Division
Department of Mechanical Engineering
Stanford University
Stanford, California 94305

January 2006

Abstract

Large-eddy simulation (LES) requires very high resolution in high Reynolds number, attached turbulent boundary layers due to the need to capture the small, dynamically important near-wall eddies. Resolving these eddies causes the computational expense of the LES to scale almost as strongly with the Reynolds number as direct numerical simulation for these flows. Wall modeling is a technique which enables LES to be performed on grids that do not resolve the wall layer. Instead, it provides approximate boundary conditions to the LES at solid boundaries, thus allowing a much weaker scaling of the LES grid size with the Reynolds number.

Unfortunately, wall models based on purely physical reasoning often lead to an inaccurate LES, particularly on coarse grids and at high Reynolds numbers, because they do not account for the numerical and SGS modeling errors that become large in these types of simulations. To address these errors, optimal control-based wall models have been developed by previous investigators. While these have the demonstrated ability to account for the aforementioned errors, they have two primary drawbacks: 1) high computational expense, due to the optimization procedure, and 2) a lack of predictability, because the control targets are prescribed *a priori*.

The goal of this work is to address these two issues in order to make control-based wall modeling feasible for engineering applications. To reduce the expense, the adjoint equations, which are used to determine the gradients needed for the optimization, have been reformulated to minimize the effort required in the optimization procedure. Further, the optimization algorithm has been modified to only use near-wall information so no work is wasted in regions of the flow which

are insensitive to the control. Such an approach reduces the computational cost of the method by an order of magnitude without a reduction in the accuracy of the simulation.

To make the method predictive, a near-wall Reynolds-averaged Navier-Stokes (RANS) model has been coupled to the LES/controller system to provide a target for the control. This coupling is accomplished by using the LES to provide the velocity boundary conditions for RANS away from the wall, while the RANS feeds back into the LES through the definition of the cost function that is minimized by the control. An additional degree of coupling enables the RANS to provide the mean wall stress for the LES. The control then provides the fluctuating wall stress which minimizes the cost function. Using this method in plane channel flow, an accurate prediction of the mean velocity profile has been obtained over a range of Reynolds numbers and on different grids. The results are comparable to those from previous control-based, non-predictive models, and are much more accurate than the predictions of traditional wall models.

Acknowledgements

This work was funded by the Air Force Office of Scientific Research through contract number F49620-03-1-0132. Computer time was provided by NAS at NASA Ames Research Center and the DOD's High Performance Computing Modernization Program though ARL/MSRC.

The authors are indebted to Professors Franck Nicoud and Bijan Mohammadi for their helpful ideas and suggestions. The authors also gratefully acknowledge Professors Sanjiva Lele, Juan Alonso, and George Papanicolaou for their comments on a draft of this manuscript.

Nomenclature

Re	Reynolds number
Re_τ	Reynolds number based on friction velocity
$\mathbb{R}$	set of all real numbers
x, y, z	spatial coordiates
t	time
Ω	spatial domain
T	terminal time
A	area of a plane
x_i	ith spatial coordinate
x^+	x in inner units
$\vec{x}$	vector of x, y, z
Δx	grid spacing in x
$\mathbf{X}$	entire range of x
u, v, w	velocity components
p	pressure
$\langle u \rangle$	average of u
$\bar{u}$	filter of u
$\hat{u}$	test filter of u
u'	linearized u
u^*	adjoint of u
$\tilde{u}$	perturbation to u
q	vector representation of the state u, v, w, p
q_0	initial conditions

q_r	RANS state
τ_{ij}	stress tensor
τ^w	wall stress
S_{ij}	strain rate tensor
ν	molecular kinematic viscosity
ρ	density
ν_t	eddy viscosity
ν_t^r	RANS eddy viscosity
κ	von Karman constant
h	channel half-height
$\mathcal{N}$	Navier-Stokes operator
$\mathcal{R}$	RANS operator
f	body force
Δ	filter width
J	cost function
ϕ	control
$\langle u, v \rangle$	inner product of u and v
$\mathcal{L}^2$	vector space of square integrable functions
j	functional on Ω
δ_u	functional of u
$\frac{Dj}{D\phi}$	Fréchet derivative of j with respect to ϕ
$\frac{\mathcal{D}j}{\mathcal{D}\phi}$	partial Fréchet derivative of j with respect to ϕ
ψ, β	Crank-Nicolson parameters
α	penalty weighting factor
ω_x	x component of vorticity
P^k	production of turbulent kinetic energy
C_u^ϕ	correlation coefficient of u and ϕ

Contents

List of Tables

List of Figures

Chapter 1

Introduction

1.1 Wall Modeling Background

The ability to accurately simulate fluid flows has important applications in engineering design and analysis. One of the most significant impediments to such simulations is the change from laminar flow, in which flow features are present only over a small number of spatial and temporal scales, to turbulent flow, where a very wide range of dynamically important scales in both space and time are present. Resolving all these scales is the most serious impediment to high fidelity simulations of fluid dynamics. It has been estimated that the required number of grid points for a fully resolved simulation scales as $Re^{9/4}$, where Re is the Reynolds number which measures the relative importance of inertial and viscous forces. A simulation that resolves all flow scales, and hence requires no models, is called a direct numerical simulation (DNS). For a recent review of DNS, see Moin and Mahesh (1998).

In an effort to mitigate the high computational expense associated with DNS, the technique of large-eddy simulation (LES) has been developed. The computational cost is reduced by applying a low-pass filter to the turbulent flow, thereby eliminating many of the small scales from the LES field. From a physical and engineering perspective, the high frequency information that is lost tends to be of less importance to practical problems. However, the short wavelength physics can have

a significant impact on the evolution of the flow, and so its effects on the LES field are incorporated through the use of models. These models are denoted sub-grid scale (SGS) models to indicate that they supply information from scales too small to be accurately captured by the numerical grid. Much effort has been put into developing effective models and techniques to perform LES, and good introductions to these and other issues found in LES are provided by Carati (2001), Sagaut (2002) and Meneveau and Katz (2000).

Over the years, models have been developed that allow LES to be successfully applied in many types of flow situations. One area, however, that has proved particularly challenging for SGS models is the near-wall region of attached flows. This is primarily due to the fact that near the wall, flow structures scale in viscous units. Hence, if the grid spacing is set to capture the large-, or integral-length, scales of the flow, then near the wall, many of the important physical scales of the flow become small relative to the grid. In addition, flow structures in this area tend to be anisotropic, and since SGS models are designed to model isotropic eddies that represent only a small fraction of the total energy of the flow, they cannot accurately represent the turbulent stresses in the vicinity of a wall (Jimenez and Moser, 2000). The number of grid points required to resolve the near wall shear stress producing eddies scales as Re_τ^2 (Baggett *et al.*, 1997). This makes the near-wall resolution requirements of LES almost as high as DNS.

In order to perform simulations of attached flows at high Reynolds numbers, wall models have been introduced to supply boundary conditions to the LES in an effort to eliminate the need to resolve the features near the wall. This is the reason the use of wall modeling in LES is almost as old as LES itself (Deardorff, 1970; Schumann, 1975): the computational expense when the near-wall region is not resolved becomes much more tractable. Wall models continue to be of interest to this day because of the desire to simulate flows at the high Reynolds numbers found in many engineering applications. Examples of many efforts in this field can be found in the reviews of Piomelli and Balaras (2002) and Cabot and Moin (2000).

A typical wall model is one that replaces the standard no-slip velocity boundary conditions at a solid surface with approximate conditions to enable the LES to accurately capture the large-scale features of the flow away from the surface without the inner layer being resolved. In addition to the strong wall-normal velocity gradients, this region also contains many streaky structures that scale in the inner units. The structures are known to be important for the generation and transport of turbulent kinetic energy and shear stress. A fully resolved LES must resolve the bulk of these features. Approximate boundary conditions instead account for the effects of the near-wall turbulence on the outer flow.

One set of approximate boundary conditions that have several advantages are wall stresses. They are directly related to the large scale body forces and accelerations present in the flow since they are some of the few external forces that can act on the fluid. This relationship implies that they must be correct for the flow to be accurate. In addition, it is possible to relate the stresses directly to the state of the flow in the mean sense through a known mean velocity profile. As will be shown in subsequent sections in this chapter, many methods have been developed that utilize such a relationship.

1.1.1 Alternatives to Wall Models

Off-the-Wall Models

Before giving a detailed overview of wall models, it will be useful to consider alternatives to them to motivate their necessity. The first alternative to be considered is the use of off the wall Dirichlet boundary conditions. This type of method cuts the LES off above the wall layer so there is no need to simulate the near-wall region. Instead, velocities are prescribed where the LES is cut-off, and the simulation is performed normally otherwise. Using these boundary conditions, it is possible to utilize a grid designed to capture the outer scales of the flow. Unfortunately, prescription of these velocities can prove challenging, as demonstrated by Baggett *et al.* (1997).

In Baggett *et al.*, a resolved LES was performed and the velocity history at the

cut-off region was recorded. This velocity history was then used directly as an off the wall boundary condition for an LES that did not resolve the wall, successfully recovering the resolved LES solution. While this demonstrated the theoretical feasibility of this approach, difficulties were encountered when more challenging tests were attempted. Next, the velocity history was distorted while maintaining a constant energy level to test the sensitivity of the simulation to the the boundary conditions. When the phase of the boundary data was scrambled but retained the same spectra and cospectra, the simulation was still able to produce reasonably accurate results. However, higher levels of scrambling that disrupted these spectra, and only retained the second-order statistics, created an artificial buffer layer above the cut-off layer before the flow transitioned to a logarithmic profile. This result demonstrated the need for a significant amount of physical information, including turbulent fluctuations, to be included in any off-wall boundary conditions.

The approach of Baggett was extended by Nicoud *et al.* (1998) and Jimenez and Vasco (1998) with similar results. The former group used a scaled velocity from the interior of the flow as the boundary condition. This was done by assuming that the velocities at two wall-parallel planes had self similar time scales so that the two could be related. It was determined the scaling ratio needed to be determined dynamically from the LES to obtain the best results. With this done, the statistics remained symmetric across the channel despite the fact that this boundary condition was only applied on one side of the channel while a no-slip boundary condition was used at the other. Unfortunately, when this boundary condition was used at both walls, it was found that the accuracy of the LES was diminshed. No definitive conclusions could be drawn, however the authors suggested that having one physical boundary condition helped to maintain a physical realization of the flow.

The work of Jimenez and Vasco (1998) involved prescribing velocity boundary conditions at the center of the channel as a feasibility study before attempting to prescribe velocities in the energetically and dynamically important wall layer. When scrambled velocity data from a full channel were provided as boundary conditions, results similar to those of Baggett (1997) were obtained. In an effort to design a

predictive model, the velocities from a plane near the boundary at the previous time step were used as a boundary condition, after being scaled to match the known rms fluctuations at the center. The velocities were further modified to ensure $\overline{uv} = \overline{vw} = 0$. However, this produced an unphysical peak in the pressure fluctuations near the upper boundary. This phenomenon was somewhat mitigated by setting the transpiration velocity to satisfy continuity requirements based on the gradients of the other two velocity components, but in the end the results were not accurate enough to warrant further investigation.

Another approach to off-the-wall boundary conditions was recently proposed by Iovieno *et al.* (2004). In this work, it was noted that if the filter size does not decrease to zero as the distance to the wall becomes small, then the unfiltered no-slip conditions no longer apply. The filter width is then taken as a function of the wall-normal distance with a minimum size such that the near wall structures can still be resolved. By expanding the velocity near the wall in a Taylor series, and doing likewise for the filter width, the corresponding boundary conditions off the wall can be obtained. However, due to the need for an accurate expansion of the variables, the off the wall boundary condition must be imposed between $1 \leq y^+ \leq 7$. While the method produces reasonable results at low to moderate Reynolds numbers, the proximity of the boundary conditions to the wall require that most of the near-wall turbulence be resolved. Hence, this method is best viewed as a means of correcting boundary conditions in wall-resolved LES for a non-zero filter width at the wall rather than a technique that will extend LES to very high Reynolds numbers.

Hybrid RANS/LES Approaches

A second alternative to wall modeling involves merging LES and RANS directly into a hybrid simulation. Since LES requires high resolution near the wall, RANS equations are instead used in this region to reduce the number of grid points. This is because RANS eddy viscosity models are designed to supply all of the turbulent stress, as opposed to LES SGS models which provide only a small fraction thereof. Thus, a RANS layer is used as part of the simulation near the wall to account for

more unresolved stress. This means the no-slip boundary conditions can be directly applied.

The difficulty with the hybrid approach comes from providing the matching conditions at the boundary between the two simulations. The LES requires a fluctuating field that transports turbulent stresses across the interface, while the RANS can only provide a mean field without the turbulent fluctuations. Such a model was suggested by Quemere *et al.* (2000), who attempted to resolve this issue by using either a predictor simulation or by adding random perturbations to the mean field. In these cases, the method and results become quite similar to the off-the-wall boundary conditions used by Baggett (1997) and Nicoud *et al.* (1998).

Alternatively, SGS models have been developed that behave like RANS models near the wall, allowing this region to be resolved only to the degree required for an accurate RANS computation, but that transition to LES models away from the wall. This technique alleviates the difficulties of prescribing matching conditions present in the previous methods. The most well known approach of this type is that of Spalart *et al.* (1997) called detached-eddy simulation (DES). This method uses a modified formulation of the one-equation Spalart-Allmaras (SA) eddy viscosity model. Unlike the RANS version, this model uses a length scale that is the distance from the wall in the near-wall region and switches to the LES filter width away from the wall. DES was originally conceived for massively separated flows with LES resolving the separated region while RANS computes the boundary layer. Further investigations of this approach examined the use of this technique in plane channel flow of varying Reynolds numbers to determine how it would behave in flows without separation (Nikitin *et al.*, 2000). Some encouraging results were obtained, as the viscous sub-layer and near-wall logarithmic profile were well predicted over a range of Reynolds numbers. However, the skin friction coefficient was under-predicted by about 15% due to the development of a spurious buffer layer in the logarithmic layer which shifted the mean velocity upwards. Piomelli *et al.* (2003) were able to mitigate this problem by using stochastic forcing (see section 1.2.1 for a more complete discussion). A similar under-prediction of the skin friction coefficient was

observed for attached flow over a flat plate (Caruelle and Ducros, 2003). In addition, when used to study pressure induced separation on a flat plate, DES over-predicted the length the separated region by over a factor of 2.

While the DES approach has been extended by Strelets (2001) to other RANS turbulence models, it is also possible to blend viscosity models to smoothly transition from RANS near the wall to LES away from it. A simple example from Baggett (1998) is

$$\tau_{ij} - \frac{1}{3}\tau_{ij}\delta_{ij} = -\left((1-\beta(y))\nu_{\mathrm{LES}} + \beta(y)\nu_{\mathrm{RANS}}\right) S_{ij}. \tag{1.1}$$

In this equation, the blending function $\beta(y)$ is 1 when the viscosity is purely RANS and 0 when it is purely LES. Typically, β is taken to be 1 at the wall, followed by a smooth transition to 0 at a location away from the wall. Above this location, the simulation uses only the LES viscosity. While this approach can be tuned to yield good results in certain situations, β cannot be determined theoretically and is expected to be different depending on the numerical method, grid resolution, and SGS models used in a given computation. We are also unaware of any technique for dynamically adjusting β. Other authors (Germano, 1999; Speziale, 1998; Arunajatesan and Sinha, 2001) have also worked on constructing universal models that asymptotically approach RANS or LES models depending on the grid spacing and flow conditions, all with limited success.

Some authors in the meteorological community use a different technique that is similar to a blended eddy viscosity model. An extra stress is added to the Navier-Stokes equations with a prescribed form that is chosen to decrease to zero at some point away from the wall (Brown *et al.*, 2001). This gives an equation for the stress to be:

$$\tau_{i2} = -\int C_c a(y)\,|u|\,u_i dy, \tag{1.2}$$

with $a(y)$ being the aforementioned shape function, and the subscript 2 denoting the wall-normal direction. The equation is used to solve for the index $i = 1$ (the streamwise wall stress) and $i = 3$ (the spanwise wall stress). The magnitude of this model can be adjusted with C_c. Cederwell (2001) chose this constant to match

experimental observations of stress in a tree canopy, and it can also be tuned to enforce a logarithmic law in the mean velocity profiles, as was done by Chow *et al.* (2005). The difficulty with this type of model is that the shape must be adjusted by trial and error, and in the meteorological community, these functions have been adjusted to match the stresses from the *de facto* rough wall present in environmental flows consisting of trees, rocks, houses, etc.

1.2 Standard Wall Models

After examining some of the alternatives, wall models will now be considered. Wall models are categorized into three main groups: algebraic models that use a simple relationship between the wall stress and LES state, two-layer models that utilize some set of near-wall dynamics to prescribe the wall stresses, and control-based wall models that formulate controllers to regulate the LES via wall stress inputs. In the notation here, a standard wall model will denote either of the two former approaches, since these have been in use the longest.

An additional feature these models share is that they aim to provide boundary conditions only by accounting for unresolved physics. This is typically accomplished by prescribing wall stresses on the wall-parallel velocity components while the wall-normal velocity is set to zero. This restriction arises from the fact that it is difficult to determine an appropriate penetration velocity from purely physical reasoning since both this component and its wall-normal derivative are zero at the wall. An additional difficulty is that if the penetration velocity is non-zero, it must be set such that there is no net mass flux through the wall. This means that it will not be possible to determine this velocity from local LES data, requiring additional complexity from the wall model. Therefore, in the following discussion it should be understood that the models that are described are wall-stress models with zero penetration velocity. This will not be the case when control-based wall models are discussed, as a controller can provide an appropriate penetration velocity.

1.2.1 Algebraic Wall Models

Wall-stress models were the first type of near wall treatment considered for LES. This type of model replaces the classical no-slip boundary conditions in the streamwise and spanwise directions with wall stresses so that the near-wall turbulence need not be resolved. The first attempt at such a model was by Deardorff (1970) who used the following model in a LES of plane channel flow at infinite Reynolds number:

$$\frac{\partial^2 u}{\partial y^2} = -\frac{1}{\kappa y_1^2} + \frac{\partial^2 u}{\partial z^2} \tag{1.3}$$

$$\frac{\partial^2 w}{\partial y^2} = \frac{\partial^2 w}{\partial x^2}, \tag{1.4}$$

with u and w being the filtered streamwise and spanwise velocity components, respectively, while y_1 is the location of the first grid point off the wall and κ is the von Karman constant. These boundary conditions are unique in that they impose a condition on the second derivative at the wall. Note that in the mean, these conditions imply a logarithmic profile at the boundary. When combined with a no-penetration condition at the wall, the conditions on u and w provide all the wall data required by the simulation. Using this model, Deardorff was able to compute the flow in a plane channel, although the mean statistics were not in good agreement with the experimental data. This deficiency cannot be solely attributed to the wall model, however, as the grid resolution was too coarse to properly resolve even the outer length scales.

Schumann (1975) was the first to implement what is now considered a standard wall-stress model in a LES of plane channel flow. The wall stresses were determined by assuming that they were in phase with the velocities at the first interior grid point, and that the local deviation from the mean was proportional to the deviation from the mean of the LES velocity at the nearest wall-normal grid point.

Specifically, the following model was used:

$$\tau_{12}^w = (\nu + \nu_t)\frac{\partial u}{\partial y} = \frac{\langle \tau^w \rangle}{\langle u \rangle (y_1)} u(y_1) \tag{1.5}$$

$$\tau_{32}^w = (\nu + \nu_t)\frac{\partial w}{\partial y} = \nu \frac{w}{y_1}, \tag{1.6}$$

with $\langle \cdot \rangle$ denoting plane averaging, ν is the molecular viscosity, and ν_t the eddy viscosity. Also, $\langle \tau^w \rangle$ represents the averaged streamwise wall stress. This can either be taken to balance the applied mean pressure gradient (which is only applicable in channel flow) or iteratively solved to impose that the plane-averaged streamwise velocity at y_1, the first grid point in the channel interior, satisfies the logarithmic law of the wall by assuming the boundary layer is in equilibrium. This model produced much better results in channel flow than Deardorff's coarse grained calculations. Several improvements have been suggested to this type of model, such as the method by Piomelli *et al.* (1989) (see Section 1.2.3) which moved the matching point downstream to account for the inclination of near-wall vortical structures. Grötzbach (1987) used a model of this type to impose heat fluxes at the wall in computations involving heat transfer.

As mentioned in the previous section, wall modeling has also been of great importance in simulating environmental flows where the wall stresses are typically set based on enforcing the logarithmic profile locally and instantaneously (Mason and Callen, 1986). Mean velocity profiles other than the logarithmic law have also been used to compute the wall stress in (1.5). The work of Werner and Wengle (1991), for example, used a near-wall linear profile with a power law further from the wall. The predictions of these computations tend to be similar to those obtained by Schumann (1975) and Piomelli *et al.* (1989).

Mason and Thomson (1992) used a stochastic backscatter model in conjunction with the wall model of Mason and Callen (1986). This model attempted to account for the effects of the backscatter of energy from the small scales to the large scales by adding a random force to the Navier-Stokes equations in the near-wall region. By adjusting the amplitude of this force, they were able to significantly improve upon

the mean velocity profile of Mason and Callen (1986). Both Mason and Thomson (1992) and Piomelli *et al.* (2003) reported that the stochastic force "breaks up" the large structures and produces a less correlated velocity field. The exact manner in which this improves the prediction of the mean velocity in the outer layer is unclear, although it is likely that the random forcing adds energy which is transported to the outer flow. However, it is clear from the instantaneous flow contours that the resulting flow structures do not correspond to the well known features in attached boundary layers. In addition, there is currently no way of selecting the amplitude of the random force *a priori*. This result cannot therefore be used as a general purpose wall model, but does provide evidence that standard wall models must be corrected in order for a good prediction of the mean velocity profile to be obtained.

1.2.2 Two-Layer Wall Models

The other type of standard wall model uses simplified versions of the thin boundary layer equations (TBLE) to determine the wall stress. These equations are given by:

$$\frac{\partial u_i}{\partial t} + \frac{\partial u_i u_j}{\partial x_j} = -\frac{1}{\rho}\frac{\partial p}{\partial x_i} + \frac{\partial}{\partial y}(\nu + \nu_t)\frac{\partial u_i}{\partial y}, \tag{1.7}$$

where all diffusion terms not in the wall-normal direction are assumed to be small. The boundary conditions for (1.7) are taken to be no-slip at the wall and the LES velocity, u_i, at the outer boundary $y = y_m$. The wall-normal velocity is computed to satisfy the continuity equation

$$v(x, y, z) = -\int_0^y \left(\frac{\partial u}{\partial x} + \frac{\partial w}{\partial z}\right) dy', \tag{1.8}$$

for $y \in (0, y_m]$.

By neglecting the convective terms in (1.7), Hoffman and Benocci (1995) constructed a local model by integrating the TBLE in the wall-normal direction:

$$\tau_{12}^w = (\nu + \nu_t)\frac{\partial u}{\partial y}\bigg|_{y_m} - y_m\frac{\partial p_{\text{LES}}}{\partial x} - \frac{d}{dt}\int_0^{y_m} u_{\text{LES}}\, dy. \tag{1.9}$$

The LES pressure was used in these equations (assuming that pressure is constant in the wall-normal direction). The time derivative was evaluated directly from the LES computation so that the model could be evaluated instantaneously and locally without having to store the TBLE state. Finally, a mixing length eddy viscosity model was used to compensate for the neglected terms. This approach was implemented in plane and rotating channel flow with reasonable results.

In an effort to incorporate more physics into the wall-stress models, Balaras *et al.* (1994) introduced a two-layer approach that solves an additional set of dynamical equations near the wall. The near-wall equations are solved on a fine wall-normal grid, as shown in Fig. 1.1. The wall stress computed by the inner layer is then used as a boundary condition for the LES. Balaras *et al.* (1996) attempted a model of this type in a plane channel, square duct, and rotating channel using the full TBLE to compute a near-wall velocity field u_i on a fine mesh embedded in the first cell of the LES grid. Savings over the full LES equations are realized since the TBLE grid need only be refined in the wall-normal direction and uses the LES grid spacing in the wall parallel directions. Further, since the pressure is applied from the LES and v is solved to satisfy continuity, no pressure solution is required for the near-wall region. Note also that an eddy viscosity model is often used to compensate for the neglected terms and the large wall-parallel grid spacing, and most practitioners use some form of a mixing length model with near wall damping.

Since this was the same approach taken by Hoffman and Benocci (1995), but without neglecting non-linear terms, it was unclear what physics the near-wall model should retain and what could be neglected. Cabot (1996) considered a variety of different near-wall models in an LES of a backward facing step flow. The results were mixed for each model. In particular, some quantities, such as the pressure coefficient after the step, were poorly predicted by all the models. More recently, Wang and Moin (2002) used a two-layer model to compute an airfoil trailing edge flow. Several variants of (1.7) with a mixing-length eddy viscosity were considered: 1) setting wall-normal diffusion equal to zero, 2) wall-normal diffusion balancing the LES pressure gradient, and 3) the full TBLE equation. In case 3), they dynamically

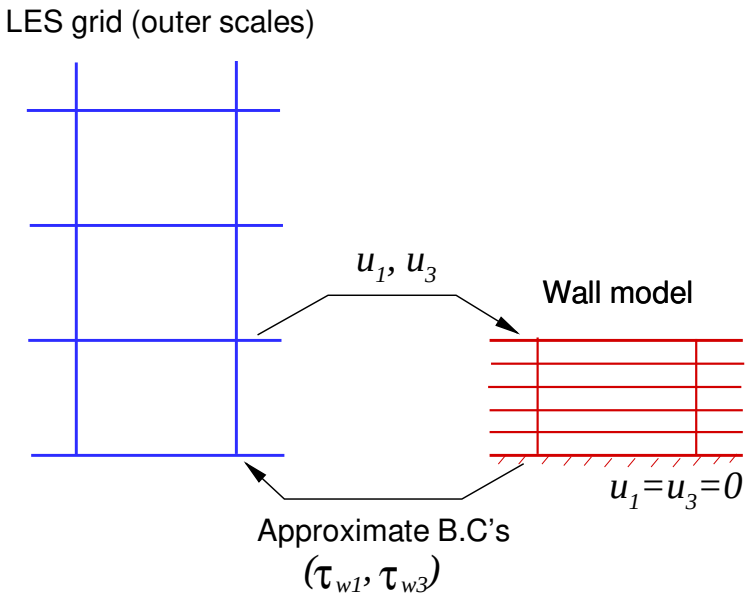

Figure 1.1: Two-layer model schematic.

adjusted the coefficient of the mixing-length eddy viscosity model to match the LES and RANS shear stresses at the interface. The most accurate results were achieved by the last approach. Mean velocity profiles and skin friction are presented in Fig. 1.2, which show good agreement with a resolved LES. However, when Catalano *et al.* (2003) used case 2 to compute flow over a cylinder at high (super-critical) Reynolds numbers, the Reynolds number dependence of the drag coefficient was not captured. Problems were also encountered when using very coarse grids in the trailing edge simulation. These results illustrate the primary difficulty with standard wall models. Although some success has been obtained using them in simple geometries at low to moderate Reynolds numbers, none has demonstrated the robustness needed to be used on very coarse grids at high Reynolds numbers.

The one-dimensional turbulence (ODT) model of Kerstein *et al.* (2001) was recently used as a SGS and wall model for pressure-driven plane channel flow by Schmidt *et al.* (2003). In order to apply this model to fully three-dimensional flow, the standard model, which only includes wall-normal diffusion, was augmented to include the LES pressure gradient and a convection term similar to (1.7), only here

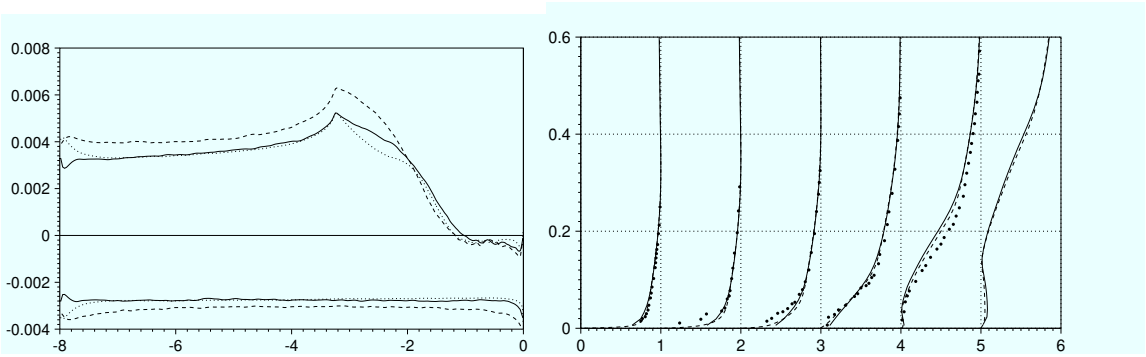

Figure 1.2: Trailing-edge skin friction coefficient (left) and mean velocity profiles (right); ——— : dynamic κ, - - - - : constant $\kappa = 0.4$ (left) and resolved LES (right), ····· : resolved LES (left), •: experiment of Blake (1975).

the convecting velocity is taken from an average over the LES time step in the cells in which the ODT model is used. The ODT is advanced using a smaller time step to include "eddy events": random perturbations to the velocity designed to mimic turbulent eddies. To couple the ODT to the LES, these events were allowed to extend out into the LES over its first few grid points. Reasonable results were reported over a variety of Reynolds numbers, although the slope of the logarithmic profile becomes increasingly over-predicted with increasing Reynolds number. Also, some discrepancies are noted in the wake region of the flow, particularly in the wall-normal rms velocity fluctuations. An additional issue is the high computational expense of the method.

1.2.3 Deficiencies of Standard Wall Models in High Reynolds Number Flow

The previous section illustrated that many variants of wall stress models have been proposed over the past thirty-five years. In plane channel flow, all of these models provide streamwise and spanwise wall stresses at each grid point on the wall while retaining a zero penetration velocity. In most cases, either an averaged or instantaneous logarithmic profile is used to predict the mean wall stress. Before moving on to control-based wall modeling techniques, it is useful to evaluate these models

in the test case that will be considered in this work.

The first model considered will be the shifted model of Piomelli *et al.* (1989). If we denote the streamwise wall stress by τ_{12}^w and the spanwise wall stress by τ_{32}^w, the shifted model specifies the local stresses by

$$\tau_{12}^w(x,z) = \frac{u(x+\delta, y_1, z)}{\langle u \rangle} \langle \tau^w \rangle \tag{1.10}$$

$$\tau_{32}^w(x,z) = \frac{w(x+\delta, y_1, z)}{\langle u \rangle} \langle \tau^w \rangle \tag{1.11}$$

with $\langle \tau^w \rangle$ being the mean streamwise wall stress computed by assuming a log-law velocity profile near the wall. Recall that in this and all other models, the transpiration velocity is taken to be zero.

The other model examined is a variant of the TBLE equation model (1.7). The following equations, as presented by Wang and Moin (2002), are used:

$$\frac{\partial}{\partial y}(\nu + \nu_t)\frac{\partial u_i}{\partial y} = 0, \qquad i = 1, 3 \tag{1.12}$$

with the mixing-length eddy viscosity model

$$\frac{\nu_t}{\nu} = \kappa y^+ \left(1 - e^{-y^+/A}\right)^2 \tag{1.13}$$

with $\kappa = .41$ and $A = 17.9$. In this form, the TBLE model is simply an ODE that can be analytically integrated to yield

$$u_i(y) = C_1 \int_0^y \frac{1}{\nu + \nu_t(y')}\, dy' + C_2. \tag{1.14}$$

The integration constants are set such that $C_2 = 0$, enforcing the no-slip condition, and C_1 is found by the matching condition $u_i(y_1) = u_{i,\mathrm{LES}}(y_1)$. The wall stress is directly identifiable as C_1.

Figure 1.3 demonstrates that both models perform nearly identically in channel flow at $Re_\tau = 4000$ using a uniform mesh of $32 \times 33 \times 32$ grid points and the agreement with the standard logarithmic law is not satisfactory. Additional evidence of

this insensitivity is offered by considering an extremely simple wall model:

$$\tau_{i2}^{w} = \rho u_{\tau}(u_i(y_1) - U_i) + h\frac{\partial \langle p \rangle}{\partial x_i} \tag{1.15}$$

for $i = 1, 3$, where the friction velocity is defined by $< \tau_{12}^{w} >= \rho u_{\tau}^{2}$ and h is the channel half height. In this model, U_i is a matching velocity set *a priori*, in this case to match the logarithmic profile at y_1, and the second term on the right-hand side is present to balance the mean pressure gradient. This model can be seen to be a simple feedback control setting the wall stress to target a mean value for the velocity. In fact, it is even simpler than a typical feedback controller since the gain is naively taken to be unity. However, the mean profile it produces when U_1 matches the law of the wall and $U_3 = 0$, as shown in Fig, 1.3, is almost identical to the other two models that use advanced techniques and knowledge of turbulent flows to predict the wall stress. It is reasonable to suppose that, despite their differences, all the models have an underlying structure that give the same wall stress predictions. It seems clear that a model based on these principles will encounter difficulties in flows at high Reynolds numbers on coarse grids.

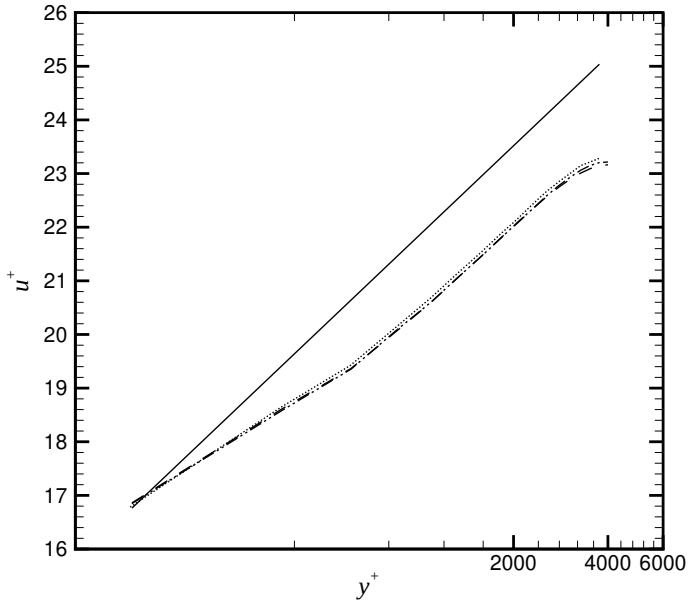

Figure 1.3: Mean flow profile using standard wall models; ····· : shifted model of Piomelli *et al.* (1989), - - - - : algebraic model of Wang and Moin (2002), —·— : simple wall model (1.15), —— : logarithmic profile ($u^+ = 2.41 \log y^+ + 5.2$).

1.3 Control-Based Wall Models

Algebraic and TBLE wall models have produced successes in certain cases, but none has been demonstrated to be robust enough to be used in a general setting. This is likely due to standard models relying on obtaining the missing physics from coarse simulations without addressing the effects of SGS modeling errors and numerical errors present near the wall. Cabot (1997) provided direct evidence of the significance of these errors by using the wall-stresses obtained from a resolved LES of a backward facing step as a wall model. These were then used in an LES with the same initial conditions and resolution away from the wall, but with the first ten near-wall points removed. The results demonstrated that even the "correct" wall stresses could not produce a wall model that was more accurate than standard phenomenologically derived techniques. What was needed was a method that could actively regulate an LES. The first attempts at such a technique were by Nicoud *et al.* (2001), who in fact tried two different approaches.

The first approach involved the application of optimal control theory to implement a regulator to provide the wall stresses, since it is unknown how to compensate for numerical and SGS errors. The approach used was similar to that of optimal flow control (Bewley and Moin, 1997). A cost function was defined that measured the plane-averaged deviation of the LES velocity from that of the logarithmic profile. Adjoint equations (see Chapter 2) were used to compute the gradient of this cost function with respect to the control, in this case taken to be the streamwise and spanwise wall stresses (the transpiration velocity was set to zero). Several approximations were made in the formulation of the adjoint equations, as well as the LES-based equations used to compute the physical state required for the adjoint's solution. Further, the controls were optimized over one time step only. These reductions imply that, while optimal control theory was used, the controller was in fact sub-optimal. Despite this, the results from a LES of channel flow at $Re_\tau = 4000$ using $32 \times 33 \times 32$ cells display a good prediction of the mean velocity profile throughout the domain (Fig. 1.4).

The second regulator implemented by Nicoud *et al.* was a feedback controller

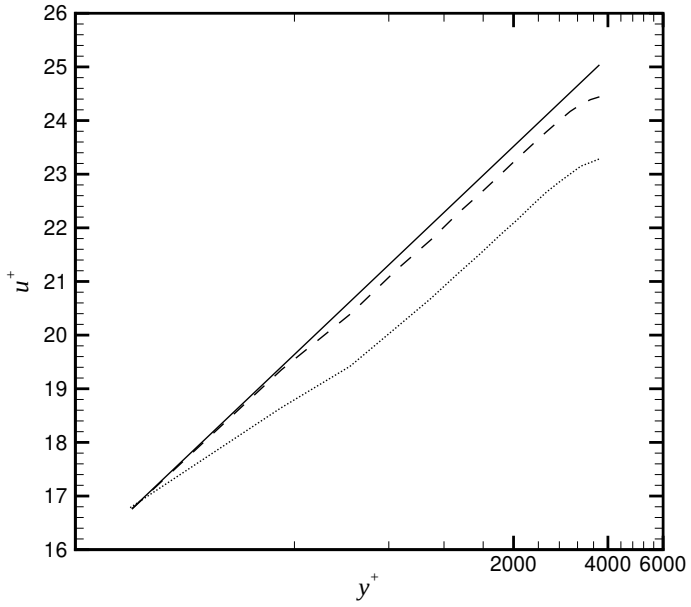

Figure 1.4: Mean flow profile using a control-based wall model; ····· : shifted model of Piomelli *et al.* (1989), - - - - : control-based model of Nicoud *et al.* (2001), —— : logarithmic profile.

constructed from the results of the sub-optimal control. A linear stochastic estimation (LSE) (Bagwell *et al.*, 1993) was performed on the wall stresses produced by the sub-optimal control framework to determine the optimal linear correlation between the velocity field and the wall stresses. The resulting controller was then of the form of a kernel convolved with the velocity field. Results of this regulator at $Re_\tau = 640$ and 20 000 showed a good prediction of the mean velocity profile.

Both the LSE and the suboptimal regulators were extended by Baggett *et al.* (2000). First, transpiration velocity was added to the control set of the sub-optimal regulator. However, this addition did not significantly improve the model's predictions relative to the improvement obtained when replacing a standard wall model with a control-based wall model. A cost function including terms measuring the deviation of the rms velocity fluctuations were also considered. The rms target profiles were taken from the LES of Kravchenko *et al.* (1996) using zonally embedded meshes. While minimization of this cost function did slightly improve the match between the predicted rms velocity fluctuations and those of Kravchenko *et al.*, a decrease in the accuracy of the prediction of the mean velocity also occured. This is possibly due to the control objectives being in conflict with each other. Baggett *et al.* also further investigated the use of the LSE feedback regulator by using the one previously obtained by Nicoud *et al.* in new channel flow simulations with different numerical methods. When implemented in a code using fourth order finite differencing to evaluate the spatial derivatives (Nicoud *et al.* used a second order formulation), the mean profile was not as well predicted. This indicates the controller was adjusting the wall stresses based on the discretization stencil used in the simulation. An even greater change was observed when the SGS model of Cabot and Moin (2000) was used to increase the eddy viscosity in the first cell. In this case, the slope near the wall was significantly over-predicted, resulting in the intercept of the law of the wall being too great. This result shows that the controller strongly reacts to the SGS model. Specifically, it increases the rms velocities to compensate for the SGS model not carrying enough turbulent stress.

The results of Nicoud *et al.* (2001) and Baggett *et al.* (2000) indicate that each

simulation will require its own active controller, at least for a sufficient time to derive an LSE-based regulator which can compensate for the numerical and SGS modeling errors present in the simulation. In addition to the significant cost of the sub-optimal control, its extension to more complex flows is limited by the need to have a target mean velocity profile known *a priori*, i.e. the method is not predictive.

These issues led Templeton *et al.* (2002) to propose a different type of feedback regulator. This approach uses a near-wall model similar to Wang and Moin to generate target velocity profiles. Since these models are valid only near the wall, the cost function is similarly only defined in this region. To reduce the computational cost, a predictor-corrector approach was used in that the wall stress determined by the near-wall model was used as an initial guess for the control. Then, one optimization iteration was performed by descending along the gradient direction of the cost function. Since an adjoint equation is difficult to formulate for the trailing edge airfoil flow, significant approximations were made to the gradient such that it was computed using surface data only (Mohammadi *et al.*, 2000). Unfortunately, this approximation proved too severe, indicating that a significant amount of accuracy in the gradient is required for a successful regulator (see Appendix A).

1.4 Research Objectives

There are two outstanding issues in the development of active LES regulators: predictability and cost. The latter is a significant issue because the purpose of a wall model is to reduce computational expense to make simulating high Reynolds number flows more tractable. In the work involving sub-optimal control, the cost of the wall model is on the order of ten times the cost of the rest of the simulation. This occurs because both the adjoint and LES equations must be solved once per iteration, and $O(10)$ iterations are required to obtain a converged solution. Therefore, one objective of this work was to reduce the computational effort required per iteration to enable the model to be used efficiently.

The other issue that must be resolved is the predictability of the method. In the

work of Nicoud *et al.*, the target profile used was prescribed *a priori*. While this can be done in canonical boundary layers since the mean velocity is known, in an arbitrary flow the mean velocity profile will not be known before the computation is performed. The problem of predictability will be addressed through the use of RANS equations to determine the target profile.

Chapter 2 will derive the continuous formulation of all the equations needed in this work. Issues related to the numerical solution of these equations will be presented in Chapter 3, with special emphasis on techniques to discretize the adjoint equations and the choice of cost functions consistent with those discretizations. This will be followed by Chapter 4 in which an efficient method for solving the optimization problem in plane channel flow will be presented. In order to make this approach predictive, Chapter 5 will demonstrate how RANS velocity profiles can be incorporated into the cost function definition. Some final thoughts and conclusions will be offered in Chapter 6.

1.5 Accomplishments

- Evaluated the applicability of cost function gradients computed using the method of incomplete sensitivities to the problem of control-based wall modeling (Appendix A).
- Demonstrated the importance of the interplay between cost function definition and adjoint discretization in constructing an accurate sub-optimal regulator (Chapter 3).
- Significantly reduced the computational expense of the optimal control-based wall model by taking advantage of the adjoint formulation and cost function structure (Chapter 4).
- Determined a method to incorporate RANS velocity profiles into the cost function definition to make wall models based on optimal control techniques predictive (Chapter 5).

Chapter 2

Derivation of the Continuous Equations

2.1 Introduction and Notation

In this chapter we present the continuous equations that will be considered in this work. The first set of equations presented will be the incompressible Navier-Stokes equations. For convenience, we will define $q = [\vec{u}, p]$ to represent the full state. In what follows, the velocity $\vec{u}$ will be written interchangeably as (u_1, u_2, u_3) or (u, v, w), which represent the components of the velocity field in the (x_1, x_2, x_3) directions, respectively. It will often be convenient to refer to the coordinate axes as (x, y, z). When considering velocity components individually, the notation (x, y, z) and (u, v, w) will be utilized. In this work, summation over repeated indices (i.e. i, j, etc.) is implied, except when specifically indicated.

The first set of equations that will be presented are those for incompressible, Newtonian fluid flow with constant density. Next, the LES equations are derived, which retain the large scales of the flow while modeling the small ones. Physical boundary conditions can be prescribed for the Navier-Stokes equations, but transferring these conditions to the LES equations can present some computational difficulties.

The goal of this work is to use optimal control techniques to remedy these difficulties by formulating a wall model, or alternate set of LES boundary conditions. In order to use such techniques efficiently, the adjoint equations of the LES system must be derived. The solution of these equations can be thought of as representing the sensitivities of the flow to disturbances, or of being Lagrange multipliers that account for the constraint of the LES system on the optimization process. In the process of constructing these equations, the LES equations will be formally linearized. The solution of the linearized equations will be denoted by $q' = [\vec{u}', p']$, where u_i' corresponds to the linearized state associated with u_i. Similar notation will be used for the adjoint state, $q^* = [\vec{u}^*, p^*]$, where each physical variable will have a corresponding adjoint variable.

Since much of this work involves the use of adjoint equations and optimal control techniques, it will be beneficial to express many of the equations in operator notation. In all cases, a non-linear operator acting on a vector will be written as $\mathcal{A}(q)$, while a linear operator will be denoted as $\mathcal{B}q$.

2.2 Navier-Stokes Equations

The Navier-Stokes operator, which is used to write the equations that govern incompressible, Newtonian flows, can be written as:

$$\mathcal{N}(q) = \begin{cases} \frac{\partial \rho u_i}{\partial t} + \frac{\partial \rho u_i u_j}{\partial x_j} + \frac{\partial p}{\partial x_i} - \frac{\partial}{\partial x_j}\mu\left(\frac{\partial u_i}{\partial x_j} + \frac{\partial u_j}{\partial x_i}\right) \\ \frac{\partial u_j}{\partial x_j} \end{cases} . \tag{2.1}$$

This operator defines the differential operations that are applied to the state q. The Navier-Stokes equations can be written compactly as

$$\mathcal{N}(q) = \vec{f}, \tag{2.2}$$

where $\vec{f}$, a vector with four entries at each spatial and temporal location, is the source term. The fourth entry, corresponding to the divergence operator in (2.1),

must be everywhere zero to enforce the divergence-free constraint on the velocity field. The other terms in $\vec{f}$ represent momentum sources, which can come from the physics or be control inputs into the system.

The final component required to define the Navier-Stokes system are initial and boundary conditions. The velocity and pressure fields are considered to exist on the closed set $\bar{\Omega}$, while the Navier-Stokes equations are valid on the open set $\Omega \subset \mathbb{R}^3$. The boundary of the set is defined as

$$\partial\Omega = \bar{\Omega} \setminus \Omega.$$

Without loss of generality, the system can be taken to start at $t = 0$, and hence the temporal domain is $(0, T]$. Therefore, the initial and boundary conditions are defined as

$$q|_{t=0} = q_0(\vec{x}) \tag{2.3}$$

$$\vec{g}(t, \vec{x}, q : \vec{x} \in \partial\Omega) = 0. \tag{2.4}$$

Note that, similarly to the source term $\vec{f}$, $\vec{g}$ can also contain control inputs to the system.

We denote the dimensionless value of quantity a by $a^\dagger$, and so each dimensionless variable is defined by:

$$\frac{u}{U} = u^\dagger, \qquad \frac{p}{\rho U^2} = p^\dagger, \qquad \frac{x}{D} = x^\dagger, \qquad \frac{tU}{D} = t^\dagger,$$

where U is the chosen velocity scale and D the chosen length scale. Substituting these expressions into (2.1) yields the dimensionless Navier-Stokes operator:

$$\mathcal{N}^\dagger(q^\dagger) = \begin{cases} \frac{\partial u_i^\dagger}{\partial t^\dagger} + \frac{\partial u_i^\dagger u_j^\dagger}{\partial x_j^\dagger} + \frac{\partial p^\dagger}{\partial x_i^\dagger} - \frac{\partial}{\partial x_j^\dagger}\frac{1}{Re}\left(\frac{\partial u_i^\dagger}{\partial x_j^\dagger} + \frac{\partial u_j^\dagger}{\partial x_i^\dagger}\right) \\ \frac{\partial u_j^\dagger}{\partial x_j^\dagger} \end{cases} \tag{2.5}$$

where there is now only one dimensionless parameter, the Reynolds number,

$$Re = \frac{\rho U D}{\mu}.$$

To ease the notation, all quantities should be taken to be dimensionless (without special designation) unless otherwise noted. The scales used to make the variables dimensionless will be presented as they appear.

2.3 Large-eddy Simulation

To construct the LES equations, a low-pass filter is applied to the state q in order to remove the small scales. The filtered q is denoted by $\bar{q}$. The effects of the small scales on the large ones must be modeled. The LES operator is written as:

$$\bar{\mathcal{N}}(\bar{q}) = \begin{cases} \frac{\partial \bar{u}_i}{\partial t} + \frac{\partial \bar{u}_i \bar{u}_j}{\partial x_j} + \frac{\partial \bar{p}}{\partial x_i} - \frac{\partial}{\partial x_j}\frac{1}{Re}\left(\frac{\partial \bar{u}_i}{\partial x_j} + \frac{\partial \bar{u}_j}{\partial x_i}\right) + \frac{\partial \tau_{ij}}{\partial x_j} \\ \frac{\partial \bar{u}_j}{\partial x_j}, \end{cases} \tag{2.6}$$

where τ_{ij} is called the sub-grid scale (SGS) stress and is given by

$$\tau_{ij} = \overline{u_i u_j} - \bar{u}_i \bar{u}_j, \tag{2.7}$$

which must be modeled based on the LES state.

In this work we will use an eddy viscosity models for τ_{ij}:

$$\tau_{ij} = 2\nu_t \bar{S}_{ij} \tag{2.8}$$

with $\bar{S}_{ij}$ being the filtered strain rate tensor,

$$\bar{S}_{ij} = \frac{1}{2}\left(\frac{\partial \bar{u}_i}{\partial x_j} + \frac{\partial \bar{u}_j}{\partial x_i}\right),$$

and ν_t the SGS eddy viscosity.

A common SGS eddy viscosity model is the Smagorinsky eddy viscosity model

(Smagorinsky, 1963):

$$\nu_t = C_S \Delta^2 \left|\bar{S}\right|, \tag{2.9}$$

where C_S is a model coefficient, Δ is the filter width, and

$$\left|\bar{S}\right| = \sqrt{2\bar{S}_{ij}\bar{S}_{ij}}.$$

The Dynamic model (Germano *et al.*, 1991; Lilly, 1992) allows C_S to be computed from the resolved velocity field:

$$C_S = \frac{[M_{ij}L_{ij}]}{[M_{kl}M_{kl}]}, \tag{2.10}$$

where

$$M_{ij} = \Delta^2 \widehat{\left|\bar{S}\right| \bar{S}_{ij}} - \Delta_F^2 \left|\hat{\bar{S}}\right| \hat{\bar{S}}_{ij} \tag{2.11}$$

$$L_{ij} = \widehat{\bar{u}_i \bar{u}_j} - \hat{\bar{u}}_i \hat{\bar{u}}_j \tag{2.12}$$

and $[\cdot]$ is an averaging operator. In (2.11), $\hat{\cdot}$ denotes a test filter with filter width $\Delta_F > \Delta$. In flows with homogenous directions, the averaging operator can be applied over these directions. If this is not the case, the dynamic localization procedure of Ghosal *et al.* (1995) can be used to compute the model coefficient. This model has been successfully tested in a range of applications and requires no parameters that are set *a priori*.

2.4 Derivation of the Adjoint Operator

In this section, the adjoint operator will be derived from the LES equations. This is in contrast to Nicoud *et al.* (2001) in which the adjoint equations were formulated after the state equation was already discretized in time. The temporal discretization used in that analysis was not consistent with the discretization actually used to advance the state equation. In contrast, we wish to determine what temporal

discretization or discretizations will perform the best in this context, with performance being measured by the accuracy of the flow statistics, evaluation effort, and amenability to approximation (to further reduce the evaluation effort). However, in order to consider the temporal discretization of the adjoint equations, it is first necessary to derive them in continuous form. This has been done many times before for slightly different formulations of the state equations (see e.g. Bewley *et al.* (2001)), but here we do it from (2.6).

Note that one could start with the fully discretized Navier-Stokes equations as solved in the code and then derive the adjoint equations based solely on them without ambiguity. While this would achieve the best possible accuracy because the exact gradient of the discrete system could be computed, the evaluation effort would be great and potential for approximation would be quite poor (Nadarajah and Jameson, 2000). Further, the effort required to construct them must be repeated for each new code, making it difficult to develop a general wall-model subroutine. In this section, only the adjoint operator will be determined. This is because the adjoint equations themselves will be determined by the specific control problem under investigation. Thus, one should look at the adjoint operator as a system that measures the sensitivity of the flow to an arbitrary perturbation, and adjoint equations as governing the response of the system to a specific perturbation.

In order to find the adjoint equations, it is necessary to first write the equation for the Fréchet derivative of the state with respect to a small perturbation to the control input, $\tilde{\phi}$. The Fréchet derivative of an arbitrary function, J, is defined to be

$$\frac{DJ}{D\phi}\tilde{\phi} = \lim_{\epsilon \to 0} \frac{J(\phi + \epsilon\tilde{\phi}) - J(\phi)}{\epsilon},$$

where $\tilde{\phi}$ is an arbitrary test function. Here, the gradient of J with respect to ϕ, $DJ/D\phi$, is a linear operator acting on the perturbation $\tilde{\phi}$. See Luenberger (1969) for additional mathematical details.

The work here will focus on taking the Fréchet derivative of the LES state governed by operator (2.6) with respect to a control input. This input could come through the initial conditions, boundary conditions, or source term. To ease the

notation, we introduce the shorthand:

$$q' = \frac{Dq}{D\phi}\tilde{\phi}. \tag{2.13}$$

Taking the Fréchet derivative of $\mathcal{N}(q)$ yields the linearized Navier-Stokes operator:

$$\mathcal{N}'_q q' = \begin{cases} \frac{\partial u'_i}{\partial t} + \frac{\partial (u'_i u_j + u_i u'_j)}{\partial x_j} + \frac{\partial p'}{\partial x_i} - \frac{\partial}{\partial x_j}\left((\nu + \nu_t)\left(\frac{\partial u'_i}{\partial x_j} + \frac{\partial u'_j}{\partial x_i}\right)\right) \\ \frac{\partial u'_j}{\partial x_j} \end{cases}, \tag{2.14}$$

where $\mathcal{N}'_q$ is a linear state equation acting on the linearized state q' about a base state of q, and $\nu = 1/Re$. Here we have ignored the sensitivity of ν_t to changes in ϕ. This approximation was shown to be reasonable for short time intervals by Chang and Collis (1999).

Fréchet differentiation can also be applied to (2.3) and (2.4) to identify the initial and boundary conditions for the linearized system:

$$q'(t = 0, \vec{x} \in \Omega) = q'_0 \tag{2.15}$$

$$g'(t, \vec{x}, q' : \vec{x} \in \partial\Omega) = 0. \tag{2.16}$$

Note in (2.16) g' represents the boundary conditions for the linearized system. To write the linearized Navier-Stokes equations, it only remains to take the Frechet derivative of the LES equations to obtain

$$\mathcal{N}'_q q' = f'. \tag{2.17}$$

As was mentioned earlier, the specific adjoint equations cannot be found until the optimization problem is stated, in contrast to the linearized equations which are fully known once the LES equations are prescribed.

The next step in developing the adjoint equations is to determine the inner product that defines the space in which the functions, q', exist. Therefore, we take each element of q' to be a function in $\mathcal{L}_2(\Omega \times [0, T])$. The inner product on this

space of $a, b \in \mathcal{L}_2(\Omega \times [0,T])$ is then

$$\langle a, b \rangle = \int_0^T \int_\Omega a(\vec{x},t) b(\vec{x},t)\, d\vec{x}\, dt. \tag{2.18}$$

Another way of identifying these vectors is to state that b is in the space of bounded linear functionals of $\mathcal{L}_2(\Omega \times [0,T])$, denoted by $\mathcal{L}_2^*(\Omega \times [0,T])$, which is the dual of the original space. In this particular case, the dual and original spaces are the same, and so b is also an element of the original space. For more information concerning dual spaces and the role they play in optimization, the interested reader is referred to Luenberger (1969).

In this formulation, the state q' is a member of the original space, while the adjoint state, q^*, is as yet an undetermined element in the dual space. The adjoint operator is then the linear operator, $\mathcal{N}_q^*$, acting on q^*, that satisfies the following identity

$$\left\langle \mathcal{N}_q' q', q^* \right\rangle = \left\langle q', \mathcal{N}_q^* q^* \right\rangle + \mathrm{BT}, \tag{2.19}$$

with BT being terms that are only evaluated at the temporal and spatial boundaries of the domain. Such an operator is guaranteed to exist (Luenberger, 1969). In the case of differential operators, Gauss' theorem is used to move the partial derivatives from q' to q^*, which results in the addition of the boundary terms, BT, which will be discussed following the presentation of the adjoint operator.

Deriving the adjoint equations is an exercise in integration by parts followed by identifying which terms are in which adjoint equation by comparing them with the inner product. The integration by parts for the $u'\mathcal{N}_q'u$ will be given below for clarity (it has been applied twice to the diffusion terms):

$$\begin{aligned}\int_0^T \int_\Omega u^* \Bigg(& \frac{\partial u'}{\partial t} + \frac{\partial}{\partial x}(uu' + u'u) + \frac{\partial}{\partial y}(uv' + u'v) + \frac{\partial}{\partial z}(uw' + u'w) + \frac{\partial p'}{\partial x} \\ & - \frac{\partial}{\partial x}\nu_T\left(\frac{\partial u'}{\partial x} + \frac{\partial u'}{\partial x}\right) - \frac{\partial}{\partial y}\nu_T\left(\frac{\partial u'}{\partial y} + \frac{\partial v'}{\partial x}\right) - \frac{\partial}{\partial z}\nu_T\left(\frac{\partial u'}{\partial z} + \frac{\partial w'}{\partial x}\right)\Bigg) d\vec{x}\, dt = \\ \int_0^T \int_\Omega \Bigg(& - u'\frac{\partial u^*}{\partial t} - (u'u + u'u)\frac{\partial u^*}{\partial x} - (v'u + u'v)\frac{\partial u^*}{\partial y} - (w'u + u'w)\frac{\partial u^*}{\partial z} - p'\frac{\partial u^*}{\partial x} \\ & - u'\frac{\partial}{\partial x}\nu_T\left(\frac{\partial u^*}{\partial x} + \frac{\partial u^*}{\partial x}\right) - u'\frac{\partial}{\partial y}\nu_T\frac{\partial u^*}{\partial y} - v'\frac{\partial}{\partial x}\nu_T\frac{\partial u^*}{\partial y} - u'\frac{\partial}{\partial z}\nu_T\frac{\partial u^*}{\partial z} \\ & - w'\frac{\partial}{\partial x}\nu_T\frac{\partial u^*}{\partial z}\Bigg) d\vec{x}\, dt, \quad (2.20)\end{aligned}$$

where the shorthand $\nu_T = \nu + \nu_t$ has been used to write the equation more compactly. The notation on the RHS has been chosen to suggest the next step in deriving the adjoint equations, that being identifying all the terms multiplied by u' (including those coming from equations multiplied by v^*, w^* and p^* terms which were not shown) into the equation for u^*. This approach is implied by the inner product formulation. Grouping such terms yields the adjoint operator:

$$\mathcal{N}_q^* q^* = \begin{cases} -\frac{\partial u_i^*}{\partial t} - u_j\frac{\partial u_i^*}{\partial x_j} - u_j\frac{\partial u_j^*}{\partial x_i} - \frac{\partial p^*}{\partial x_j} - \frac{\partial}{\partial x_j}\left((\nu + \nu_t)\left(\frac{\partial u_i^*}{\partial x_j} + \frac{\partial u_j^*}{\partial x_i}\right)\right) \\ -\frac{\partial u_j^*}{\partial x_j} \end{cases} . \quad (2.21)$$

It is important to note that these are the adjoint equations that would be found following Bewley *et al.* (2001). Nicoud *et al.* (2001) arrive at a slightly different form by applying the divergence-free constraint to the convective terms of the linearized system. This results in the third term in (2.21) being

$$+u_j^*\frac{\partial u_j}{\partial x_i}.$$

The equivalence between the two formulations is found by taking into account the adjoint pressure equation. We can write:

$$-u_j \frac{\partial u_j^*}{\partial x_i} = -\frac{\partial u_j u_j^*}{\partial x_i} + u_j^* \frac{\partial u_j}{\partial x_i}.$$

The resulting source term in the adjoint pressure equation is

$$-\frac{\partial}{\partial x_i} u_j \frac{\partial u_j^*}{\partial x_i} = -\frac{\partial^2 u_j u_j^*}{\partial x_i^2} + \frac{\partial}{\partial x_i} u_j^* \frac{\partial u_j}{\partial x_i}.$$

Since in both formulations the equation for p^* is an invertible Laplace equation, we have

$$p_1^* = p_2^* - u_j u_j^*,$$

where p_1^* is the adjoint pressure following Bewley *et al.* and p_2^* is the same quantity from Nicoud *et al.*. When this is used in (2.21), it is seen to be identical to the formulation of Nicoud *et al.* (2001). However, their formulation requires knowledge of the adjoint source term, f^*, and so is slightly less general. Therefore, the formulation presented here will be used, although if the divergence of the adjoint state is constrained to be zero, the two approaches are equivalent.

Of course, the application of Gauss' theorem, which resulted in the derivatives being moved from q' to q^*, yields a series of terms which must be integrated over the spatial and temporal boundaries. To specify these terms, it will be helpful to introduce some new notation. First, the vector n_{x_i} is the component of the outward facing normal vector to $\partial\Omega$ in the x_i direction. Second, to help represent the integration by parts in time, denote

$$a|_0^T = \int_\Omega a(\vec{x}, T)\, d\vec{x} - \int_\Omega a(\vec{x}, 0)\, d\vec{x}.$$

The boundary terms arising from (2.20) can then be written as

$$\begin{aligned}\mathrm{BT}_u = u'u^*|_0^T + \int_{\partial\Omega} \Bigg(& u^* \left((uu' + uu')n_x + (uv' + u'v)n_y + (uw' + u'w)n_z + p'n_x\right) \\ & + (\nu + \nu_t) \Bigg(- u^* \left(\frac{\partial u'}{\partial x} + \frac{\partial u'}{\partial x}\right) n_x + (u'n_x + u'n_x)\frac{\partial u^*}{\partial x} - u^* \left(\frac{\partial u'}{\partial y} - \frac{\partial v'}{\partial x}\right) n_y \\ & + (u'n_y + v'n_x)\frac{\partial u^*}{\partial y} - u^* \left(\frac{\partial u'}{\partial z} + \frac{\partial w'}{\partial x}\right) n_z + (u'n_z + w'n_x)\frac{\partial u^*}{\partial z}\Bigg)\Bigg) d\vec{x}\, dt, \quad (2.22)\end{aligned}$$

where the integral is understood to be a surface integral over $\partial\Omega$. When added to the boundary terms arising from v, w, and p, the full boundary term is given by

$$\begin{aligned}\mathrm{BT} = u_i' u_i^*|_0^T + \int_{\partial\Omega} \Bigg(& u_i^*(u_i u_j' + u_i' u_j) n_{x_j} + p' u_i^* n_{x_i} \\ - (\nu + \nu_t) & \left(u_i^* \left(\frac{\partial u_i'}{\partial x_j} + \frac{\partial u_j'}{\partial x_i}\right) n_{x_j} - (u_i' n_{x_j} + u_j' n_{x_i})\frac{\partial u_i^*}{\partial x_j}\right) + p^* u_i' n_{x_i}\Bigg) d\vec{x}\, dt, \quad (2.23)\end{aligned}$$

where the last term comes from the continuity equation. Now, (2.19) is complete.

The adjoint equations for q^* are given by

$$\mathcal{N}_q^* q^* = f^* \quad (2.24)$$

with initial and boundary information

$$q^*_{t=T,\vec{x}\in\Omega} = q_0^* \quad (2.25)$$

$$g^*(t, \vec{x}, q^* : \vec{x} \in \partial\Omega) = 0. \quad (2.26)$$

The adjoint boundary conditions, g^*, depend on the control set and cost function and will be determined in later chapters. An important piece of information to note is that the "initial" condition for the adjoint equations is specified at the terminal time T. This is because the sign of the time derivative changes in going from the linearized equations to the adjoint equations. Hence, characteristics of the adjoint

equations propagate backwards in time, not forwards.

All of the equations needed for this work have now been presented in their continuous form. The next chapter will detail how the continuous equations are discretized for numerical solution.

Chapter 3

Discretization of the Continuous Equations

3.1 Introduction

In Chapter 2 the continuous equations that are of interest in this work were derived. In order to obtain solutions to the LES equations in the high Reynolds number flows of engineering interest, it is necessary to solve them numerically. Since adjoint-based optimization techniques are used, an important issue that must be addressed is how the adjoint equations are discretized. As mentioned in Chapter 2, the approach taken iis to first derive a continuous set of adjoint equations from the continuous LES equations, and then discretize them. The alternative is to formulate discrete adjoint equations directly from the discrete LES operator. In applications involving optimization of physical systems, it is unclear which formulation is superior. Adjoints derived from the discrete equations typically achieve greater cost function reduction, however, some of this reduction may be unphysical in that the optimization takes advantage of peculiarities in the discrete system that do not exist in the continuous system. This type of adjoint is also often more complex to derive and evaluate.

In the present application, it is clear that for maximum accuracy to be achieved,

the adjoint equations formulated from the discrete LES system should be used. This is because the entire purpose of the optimization is to manipulate the discrete system, not to optimize an engineering cost function in a physical system. Unfortunately, this observation conflicts with the need to have the evaluation of the adjoint equations be as inexpensive as possible. It is therefore necessary to derive the continuous adjoint equations and consider only a subset of the possible methods used for the time advancement. A further complication is that the choice of the cost function can impact the performance of various temporal discretization schemes. This effect will result in certain cost functions proving more appropriate than others for this application. The effectiveness of the cost functions coupled with the temporal discretization will be evaluated in Chapter 4 based on the accuracy of the prediction of the mean velocity profiles, the cost, and the potential for approximation (to further reduce the computational cost).

3.2 Discretization of the LES Equations

Many techniques exist for discretizing the Navier-Stokes equation. For an introduction to some of them, see Moin (2001). The specific method chosen for this work are low-order finite difference schemes to evaluate the spatial derivatives with Runge-Kutta time advancement. These methods have been selected because of their relative simplicity, not for their accuracy, since the end goal is to generate wall models for the coarse LES needed for industrial applications. Higher order numerical methods, particularly spectral methods, are well suited to the flow geometry that will be used in this work (see e.g. Moser *et al.* (1999)). However, it has been observed by Baggett *et al.* (2000) that the numerical techniques used in a simulation can affect what is required wall stresses, so these will be eschewed in favor of methods that will be used in engineering applications to evaluate the behavior of the wall model in those situations.

The specific spatial discretization used will be a centered, second-order finite difference technique on a staggered grid. A schematic illustrating the system is

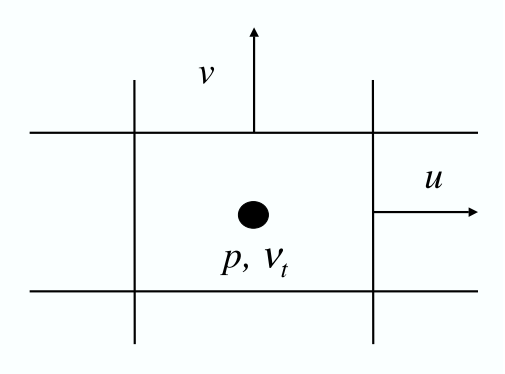

Figure 3.1: Staggered grid schematic.

shown in Figure 3.1 in a two-dimensional plane. The LES equations are advanced in time using a low-storage, third-order Runge-Kutta technique (Spalart *et al.*, 1991) to advance the convective terms and the Crank-Nicolson method for the diffusion terms. The final aspect of the time advancement that must be addressed is the computation of the pressure. In the present work, this is handled using the fractional step method that allows for pressure to be used as a Lagrange multiplier to ensure that the resulting velocity fields are divergence free (Kim and Moin, 1985). The eddy viscosity and wall-boundary conditions are updated only at the beginning of each Runge-Kutta advancement to reduce the expense of the method (Le *et al.*, 1997).

3.3 Discretization Approaches for Adjoint Equations

Given the adjoint equations formulated in a continuous setting, they must be discretized so that they may be solved numerically. As previously mentioned, there are several objectives in analysing the discretization process, and one of them is amenability to approximation. Making the approximations necessary to have a system that can be solved relatively easily will depend on the form of the equations. Two approximations will be made in all discretization attempts. The first is that the optimal control problem will be solved independently over each time step. In

this sense, we are computing a sub-optimal control since a fully optimal control would require solving the adjoint equations over a sufficiently large time horizon that the flow could converge to a statistically steady state and statistics could be measured. In addition to the computational burden this entails, the memory requirements can also be quite prohibitive due to the need to store the time history of q over this entire interval (Bewley *et al.*, 2001). The second approximation made will be to use a single step method for time advancement, as opposed to the three step Runge-Kutta scheme used to solve the LES equations.

The first step of the discretization will be to consider the spatial derivatives. In all cases, they will be approximated in a way consistent with the second-order treatment of these derivatives in the Navier-Stokes equations. The justification for such a discretization is that the derivative operators acting on equation (2.14) are matrix operators for spatially discrete variables and the adjoint of this matrix is simply its transpose. On any grid, this means that the two operators are of the same form (since they are square), but on a uniform grid, the matrix is symmetric and so applying the same discretization is consistent with this formulation.

The more challenging discretization to construct is the temporal one. It would be possible to construct the exact adjoint of the discrete, three-step system, but using a three-step approach is computationally burdensome. Using a one-step approach immediately reduces the computational cost of each iteration by 2/3. Further, such an approach will make it easier to use this technique in other codes with different time-stepping schemes since it is not desirable to have to re-derive the adjoint equations for each new code. A further complication in choosing the time-advancement approach is how it interacts with the choice of the cost function. Therefore, we first examine the impact this choice has on the discrete adjoint equations.

3.3.1 Cost Function Options and the Resulting Adjoint Systems

In this section, different cost function formulations will be presented and their effects on the discrete adjoint equations analyzed. The two main formulations of the cost function we will consider here are distinguished according to whether they measure quantities from the LES at all times or just the terminal time. When considering the optimization over one time step, it may seem that this is trivial, but it does bring about changes in the discrete adjoint equations that must be examined to determine which will produce the best results. The cost function defined over all time, denoted by J_1, is:

$$J_1 = \langle j(q(t,\vec{x})), j(q(t,\vec{x}))\rangle \,, \tag{3.1}$$

where j is a function that maps the state to the set of of real numbers. This inner product formulation is the same as was used to define the adjoint operator in Chapter 2. This makes J_1 a positive semi-definite function.

Using this formulation, boundary conditions, initial conditions, and source term of the adjoint system can be set such that the gradient may be identified through the solution of the adjoint equations. The gradients as functions of the adjoint state will be found via the $\left\langle \mathcal{N}_q' q', q^* \right\rangle$ term, the boundary values, or the terminal ($t = 0$) values of the adjoint state, depending on whether the control inputs are body forces, boundary conditions, or initial conditions, respectively. This means that the gradient of the cost function must appear in (2.19) through either the initial adjoint conditions or the source term since

$$\left\langle q', \mathcal{N}_q^* q^* \right\rangle = \langle q', f^* \rangle \,.$$

In order to determine exactly how the cost function gradients should be represented in the adjoint identity, it is necessary to first take the Fréchet derivative of (3.1) using the chain rule:

$$\frac{DJ_1}{D\phi}\tilde{\phi} = 2\left\langle j\frac{Dj}{Dq}, \frac{Dq}{D\phi}\tilde{\phi}\right\rangle, \tag{3.2}$$

recalling $\tilde{\phi}$ is an arbitrary function in $\mathcal{L}^2((\Omega \times (0,T])^4)$. We note though that since Dj/Dq is a linear operator acting over all the values of q',

$$q' \equiv \frac{Dq}{D\phi}\tilde{\phi}, \tag{3.3}$$

we can rewrite (3.2) as

$$\frac{DJ_1}{D\phi}\tilde{\phi} = \left\langle q', 2\frac{Dj}{Dq}\right\rangle. \tag{3.4}$$

This formulation suggests that the correct way to incorporate this information into the adjoint identity is to prescribe the adjoint source term to be

$$f_1^* = \begin{bmatrix} \frac{Dj}{Du} \\ \frac{Dj}{Dv} \\ \frac{Dj}{Dw} \\ \frac{Dj}{Dp} \end{bmatrix}, \tag{3.5}$$

while the initial conditions are

$$u_{i,1}^*(t = T, \vec{x}) = 0. \tag{3.6}$$

This choice results in

$$\left\langle q', \mathcal{N}_q^* q^* \right\rangle = \frac{DJ_1}{D\phi}\tilde{\phi}.$$

An alternative to computing a cost function that maintains a running track of the deviation of the LES from its target is to have one that only measures this deviation at the terminal time T. Mathematically, this cost function is constructed

as

$$J_2 = \int\int\int \left[j(q(T,\vec{x}))\right]^2 \, d\vec{x}, \tag{3.7}$$

where j is the same as in 3.1. From a physical perspective, J_1 is more appropriate since the LES quantities that are controlled are well defined only after plane and temporal averaging. However, since we will only be considering the sub-optimal approach applied over one time step, the number of samples available in each framework will be identical. It will therefore remain to be seen which approach can produce the most accurate results at the least expense.

This formulation will have the gradients as functions of the adjoint state identified in the same way as J_1. Also, while the boundary conditions of the two systems will be the same, the gradient of 3.7 must be evaluated to determine

$$\frac{DJ_2}{D\phi}\tilde{\phi} = \int\int\int 2j(q(T,\vec{x}))\frac{Dj}{Dq}q(T,\vec{x})' \, d\vec{x}. \tag{3.8}$$

Since the term depending on q' contains no integration in time, the initial conditions will be used to generate the correct cost function gradient. Thus, they are taken to be:

$$q^*|_{t=T} = \begin{bmatrix} 2j(q(T))\frac{Dj}{Du} \\ 2j(q(T))\frac{Dj}{Dv} \\ 2j(q(T))\frac{Dj}{Dw} \\ 2j(q(T))\frac{Dj}{Dp} \end{bmatrix}. \tag{3.9}$$

Then the correct adjoint source term is

$$f^*_{i,2} = 0. \tag{3.10}$$

This choice of initial and boundary conditions, as well as the source term, results in the initial conditions in (2.19) becoming

$$u_i' u_i^*|^T = \int\int\int u_i'(T,\vec{x})u_i^*(T,\vec{x}) \, d\vec{x} = \int\int\int q'(T)2j(q(T))\frac{Dj}{Dq} \, d\vec{x}. \tag{3.11}$$

This result is, not unexpectedly, similar to the previous result for J_1. However, the

formulation of these problems will make them more or less amenable to different temporal discretization schemes, as will be discussed next.

Effect of Cost Function on Temporal Discretization

The time integration and differentiation found in the expressions for the adjoint equations and the cost function gradients now need to be addressed when discretizing the equations. The time advancement, since we restrict our attention to single-step methods, can be any combination of implicit or explicit methods applied to each term. Quadrature for integration can be handled similarly. Determining a good way to do this is important since nearly all of these approaches will be first-order accurate in time and so we do not know *a priori* which will perform the best in this application. Further, the best method may depend on how the Navier-Stokes equations themselves are advanced. We will now present the equations using several temporal discretization schemes. These will be compared in the next section.

The first time-advancement approach we shall consider is a fully explicit scheme. Here, all the spatial derivatives and source terms are evaluated at the beginning of the time step. We denote variables at the beginning of a time step by n and those at the end of the time step by $n+1$. Further, let Δt be the time-step size for a given advancement, and, where appropriate, the multiplier 2β will be used in front of it when we wish to consider the changes over only one Runge-Kutta sub-step. This is consistent with the time advancement approach used for the Navier-Stokes equations. Therefore, an explicit scheme will be

$$u^*_{i,n+1} = u^*_{i,n} + \Delta t \Bigg(u_{j,n} \frac{\partial u^*_{i,n}}{\partial x_j} + u_{j,n} \frac{\partial u^*_{j,n}}{\partial x_i} + \frac{\partial p^*_n}{\partial x_j} + \frac{\partial}{\partial x_j} \left(\nu + \nu_t\right) \left(\frac{\partial u^*_{i,n}}{\partial x_j} + \frac{\partial u^*_{j,n}}{\partial x_i} \right) + f_{i,n} \Bigg). \tag{3.12}$$

The physical variables are aligned with the adjoint ones by noting that the time of T for the physical variables corresponds to time 0 of the adjoint state and $n = 0$ denotes the initial conditions of the adjoint equations. In all cases considered, the

adjoint pressure will be evaluated using a fractional step formulation whereby an intermediate value for $u^*_{i,n+1}$ is computed using every term from equation (3.12) except for the adjoint pressure gradient. The adjoint pressure is then computed in the same way as the physical pressure by solving a Poisson equation with the appropriate source term such that subtraction of the pressure gradient from the intermediate adjoint state removes its divergence. In practice, fully explicit schemes such as this are rarely used since they are unstable. However in this application, since we will only use the advancement over one time step, this issue is not relevant and so any method can be applied.

Next an implicit time advancement scheme is considered. In this case, all the terms are evaluated at time level $n+1$:

$$u^*_{i,n+1} = u^*_{i,n} + \Delta t \Bigg(u_{j,n+1}\frac{\partial u^*_{i,n+1}}{\partial x_j} + u_{j,n+1}\frac{\partial u^*_{j,n+1}}{\partial x_i} + \frac{\partial p^*_{n+1}}{\partial x_j} + \frac{\partial}{\partial x_j}(\nu+\nu_t)\left(\frac{\partial u^*_{i,n+1}}{\partial x_j} + \frac{\partial u^*_{j,n+1}}{\partial x_i}\right) + f_{i,n+1}\Bigg). \tag{3.13}$$

To reduce computational expense, ν_t is not evaluated at time level $n+1$ which is consistent with the assumption that the control cannot significantly affect its value. By incorporating the parameter $\psi \in [0,1]$, we can generalize the above methods by writing

$$\begin{aligned} u^*_{i,n+1} = u^*_{i,n} &+ \Delta t\psi \Bigg(u_{j,n}\frac{\partial u^*_{i,n}}{\partial x_j} + u_{j,n}\frac{\partial u^*_{j,n}}{\partial x_i} + \frac{\partial p^*_{n}}{\partial x_j} + \frac{\partial}{\partial x_j}(\nu+\nu_t)\left(\frac{\partial u^*_{i,n}}{\partial x_j} + \frac{\partial u^*_{j,n}}{\partial x_i}\right) + f_{i,n}\Bigg) \\ &+ \Delta t(1-\psi)\Bigg(u_{j,n+1}\frac{\partial u^*_{i,n+1}}{\partial x_j} + u_{j,n+1}\frac{\partial u^*_{j,n+1}}{\partial x_i} + \frac{\partial p^*_{n+1}}{\partial x_j} + \frac{\partial}{\partial x_j}(\nu+\nu_t)\left(\frac{\partial u^*_{i,n+1}}{\partial x_j} + \frac{\partial u^*_{j,n+1}}{\partial x_i}\right) + f_{i,n+1}\Bigg). \end{aligned} \tag{3.14}$$

By selecting a value for ψ, the resulting expression can be weighted to any degree

towards an explicit or implicit formulation. This can also be done individually term by term. Note that the advancement for the Navier-Stokes equations used is either fully explicit or fully explicit in all terms but wall-normal diffusion, which is handled using a semi-implicit scheme with $\psi = 1/2$.

What is important in this application is not the specific time-advancement scheme used, but how it interacts with the temporally discretized cost function and the approximations that have already been made. Since the cost functions are reduced to only being evaluated at one instant in time, there is no choice as to which integration quadrature should be used to evaluate them. Since the state at the initial time is fixed, the quadrature for quantities involving the state must be such that the only contribution to temporal integrals come from the next time step. Similarly, since only one control input will be found, integrals involving the control inputs are evaluated such that the only term in them comes from the current control under consideration. When fully explicit advancement for the Navier-Stokes equations are used, the control is taken to be at the same time as the initial state and so the quadrature for the state variables and control variables are reversed. For the semi-implicit formulation, this quantity must be taken as the appropriate time average, and the quadrature adjusted accordingly.

Given these definitions of quadrature, it is seen that, when considered over only one time step with appropriate constants, $J_1 = J_2$. However, the discrete equations used to solve for their gradients are different. The reason for this is the order Δt difference that comes from the time advancement of the initial state. As $\Delta t \to 0$, this difference goes to zero so that in the limit the two gradients are identical. Thus, the deviation can be seen as caused by approximating the functions discretely in time, however such deviations can be large since in the LES we are interested in, large time steps will be used. It is also important to note that while we regulate the indicated cost functions, the quantities that are actually of interest are the long-time averaged flow statistics. Thus, we must determine which formulation produces the best results for these quantities.

The difference in the equations can be immediately seen when considering the explicit discretization of each. For J_1, the explicit evaluation is:

$$u^*_{i,n+1} = (f_i(u_i(t=T))) = \begin{bmatrix} \frac{Dj}{Du} \\ \frac{Dj}{Dv} \\ \frac{Dj}{Dw} \\ \frac{Dj}{Dp} \end{bmatrix}. \tag{3.15}$$

Note that since the initial conditions are all zero, the only remaining term is the source term. It is evaluated at time T not because of the explicit formulation, but to be consistent with the cost function. Also, $\Delta t = T$ in this case, which is why it is cancelled out in the denominator of the source term. The pressure will also be absent here if the source term is divergence free, otherwise it must be included.

Now, we can compare (3.15) with the same equation formulated from J_2:

$$\begin{aligned} u^*_{i,n+1} =& u^*_{i,n} + \Delta t \left(u_{j,n}\frac{\partial u^*_{i,n}}{\partial x_j} + u_{j,n}\frac{\partial u^*_{j,n}}{\partial x_i} + \frac{\partial p^*_n}{\partial x_j} + \frac{\partial}{\partial x_j}(\nu+\nu_t)\left(\frac{\partial u^*_{i,n}}{\partial x_j} + \frac{\partial u^*_{j,n}}{\partial x_i}\right)\right) \\ =& \begin{bmatrix} \frac{Dj}{Du} \\ \frac{Dj}{Dv} \\ \frac{Dj}{Dw} \\ \frac{Dj}{Dp} \end{bmatrix} + \Delta t \Bigg(u_{j,n}\frac{\partial u^*_{i,n}}{\partial x_j} + u_{j,n}\frac{\partial u^*_{j,n}}{\partial x_i} \\ & + \frac{\partial p^*_n}{\partial x_j} + \frac{\partial}{\partial x_j}(\nu+\nu_t)\left(\frac{\partial u^*_{i,n}}{\partial x_j} + \frac{\partial u^*_{j,n}}{\partial x_i}\right)\Bigg). \end{aligned} \tag{3.16}$$

In this case, all the terms are retained because the cost function information enters through the initial conditions. Hence, it is likely that (3.16) will provide a better gradient estimate than (3.15) since it incorporates the turbulent features (through terms containing u) and more information about the structure of the equations (through the differential operators).

A somewhat different pattern emerges when we examine the implicit formulation. Here, for the J_1 adjoint equations we have

$$\begin{aligned} u^*_{i,n+1} =& u^*_{i,n} + \Delta t \Bigg(u_{j,n+1} \frac{\partial u^*_{i,n+1}}{\partial x_j} + u_{j,n+1} \frac{\partial u^*_{j,n+1}}{\partial x_i} \\ & + \frac{\partial p^*_{n+1}}{\partial x_j} + \frac{\partial}{\partial x_j} (\nu + \nu_t) \left(\frac{\partial u^*_{i,n+1}}{\partial x_j} + \frac{\partial u^*_{j,n+1}}{\partial x_i} \right) + f_i(u_i(t=T)) \Bigg) \\ =& \begin{bmatrix} \frac{Dj}{Du} \\ \frac{Dj}{Dv} \\ \frac{Dj}{Dw} \\ \frac{Dj}{Dp} \end{bmatrix} + \Delta t \Bigg(u_{j,n+1} \frac{\partial u^*_{i,n+1}}{\partial x_j} + u_{j,n+1} \frac{\partial u^*_{j,n+1}}{\partial x_i} \\ & + \frac{\partial p^*_{n+1}}{\partial x_j} + \frac{\partial}{\partial x_j} (\nu + \nu_t) \left(\frac{\partial u^*_{i,n+1}}{\partial x_j} + \frac{\partial u^*_{j,n+1}}{\partial x_i} \right) \Bigg), \end{aligned} \tag{3.17}$$

while for J_2 we have

$$\begin{aligned} u^*_{i,n+1} =& u^*_{i,n} + \Delta t \Bigg(u_{j,n+1} \frac{\partial u^*_{i,n+1}}{\partial x_j} + u_{j,n+1} \frac{\partial u^*_{j,n+1}}{\partial x_i} \\ & + \frac{\partial p^*_{n+1}}{\partial x_j} + \frac{\partial}{\partial x_j} (\nu + \nu_t) \left(\frac{\partial u^*_{i,n+1}}{\partial x_j} + \frac{\partial u^*_{j,n+1}}{\partial x_i} \right) \Bigg) \\ =& \begin{bmatrix} \frac{Dj}{Du} \\ \frac{Dj}{Dv} \\ \frac{Dj}{Dw} \\ \frac{Dj}{Dp} \end{bmatrix} + \Delta t \Bigg(u_{j,n+1} \frac{\partial u^*_{i,n+1}}{\partial x_j} + u_{j,n+1} \frac{\partial u^*_{j,n+1}}{\partial x_i} \\ & + \frac{\partial p^*_{n+1}}{\partial x_j} + \frac{\partial}{\partial x_j} (\nu + \nu_t) \left(\frac{\partial u^*_{i,n+1}}{\partial x_j} + \frac{\partial u^*_{j,n+1}}{\partial x_i} \right) \Bigg). \end{aligned} \tag{3.18}$$

These equations are identical. For semi-implicit methods, the differences will be found in the explicit terms, in which J_1 will have none while J_2 will include them. Therefore for single step methods, J_2 is more robust with respect to the numerical discretization. To illustrate these results, numerical experiments have been conducted using the different discretization formulations and cost functions in plane channel flow (see Chapter 4 for more details). The predicted mean velocity profiles

are presented in Figure 3.2. Clearly, both formulations perform well when considered with implicit temporal discretization, while when explicit discretization is used, the mean velocity profile is poorly predicted.

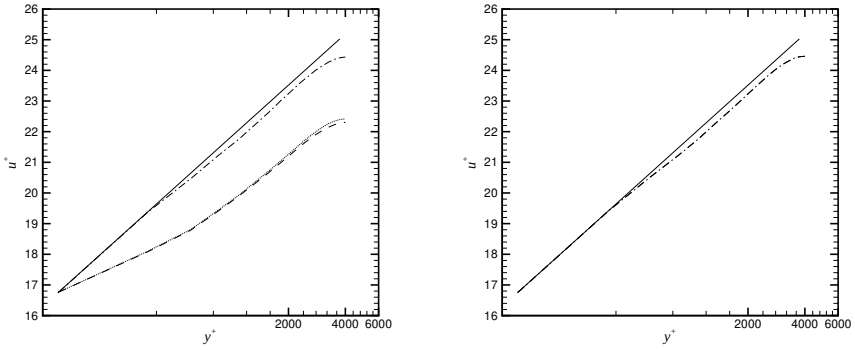

Figure 3.2: Effects of adjoint discretization and cost function choice for $\psi = 0$ (left) and $\psi = 1$ (right), ——— : $u^+ = 2.41\log(y^+) + 5.2$,, - - - - : J_1, —·— : J_2, ····· : single Runge-Kutta sub-step adjoint evaluation.

The next question is that, if the implicit formulations produce the exact same equations for cost function we know to be identical, would that not be the best formula to use? The answer, at least in some cases, is no. This is because the formulation of the Navier-Stokes equations must be taken into account. The solution of the Navier-Stokes system is computed using a three-step Runge-Kutta advancement with each sub-step either being a fully explicit advance or a semi-implicit advance with wall normal diffusion handled using $\psi = 1/2$ and all other terms being fully explicit. In these two cases, it will be straightforward to derive the appropriate adjoint equations exactly from the temporally discretized state equations.

We will first consider the semi-implicit case since that fits into the above framework more easily. Here, the equation for the Frechet derivative of u_i is

$$\mathcal{N}'_q q' = \begin{cases} u'_i - 2\beta\Delta t \left(\frac{\partial p'}{\partial x_i} + \frac{\partial}{\partial y}\left(\nu + \nu_t\right) \frac{\partial u'_i}{\partial y} \right) = 0 \\ \frac{\partial u'_j}{\partial x_j} = 0. \end{cases} \tag{3.19}$$

This will lead to the adjoint equations becoming

$$\mathcal{N}_q^* q^* = \begin{cases} u_i^* + 2\beta\Delta t \left(\frac{\partial p^*}{\partial x_i} - \frac{\partial}{\partial y} \left(\nu + \nu_t \right) \frac{\partial u_i^*}{\partial y} \right) \\ -\frac{\partial u_j^*}{\partial x_j}. \end{cases} \tag{3.20}$$

In this case, very little information from the turbulent flow is included in this formulation since only the initial conditions and ν_t depend on the LES velocity field. Since Nicoud *et al.* (2001) demonstrated the importance of prescribing the wall stress fluctuations, it is important that the turbulent state enter the adjoint equations so that the resulting wall stresses contain this unsteadiness. Direct evidence of this is also provided in Fig. 3.2 since the mean velocity profile computed using this formulation is almost indentical to the explicit adjoint construction using J_1.

The final formulation, when a fully explicit time advancement scheme is used, will be demonstrated to provide even less information from the turbulent state. Unfortunately, the lack of derivatives applied to u_i^{n+1} means that the previous formulation will not work and we must consider the fully discrete equations. Before doing this, we must define the operator Δ_i which will be a discrete difference operator in the ith direction:

$$\Delta_i a \equiv \frac{a(x_{i+1}, x_j, x_k) - a(x_i, x_j, x_k)}{x_{i+1} - x_i}, \tag{3.21}$$

with each x being an arbitrary discrete coordinate in one direction, and hence the need for three of them to specify a spatial location. The state equations in this formulation become

$$\mathcal{N}(q) = \begin{cases} u_{i,n+1,\mathrm{in}} - \Delta_i p = \mathrm{RHS}_n \\ u_{n+1,\mathrm{w}} - \Delta_u p = \mathrm{RHS}_n + \mathrm{sign(w)} \frac{\phi_u}{\Delta y} \\ v_{n+1,\mathrm{w}} = 0 \\ w_{n+1,\mathrm{w}} - \Delta_w p = \mathrm{RHS}_n + \mathrm{sign(w)} \frac{\phi_w}{\Delta y} \\ \Delta_j u_{j,n+1} = 0, \end{cases} \tag{3.22}$$

where "w" stands for quantities in cells adjacent to the walls and "in" stands for quantities in the interior of the domain (not adjacent to the walls). The terms ϕ_u and ϕ_w are the streamwise and spanwise control inputs, respectively, which enter (3.21) in the specific form they do because the represent the streamwise and spanwise wall stresses. This occurs since only the change in the wall stress can effect the state either directly on the terms at the wall (w) or through altering the divergence and changing p everywhere.

Taking the Frechet derivative of (3.22) gives us the linear system

$$\mathcal{N}_q' q' = \begin{cases} u'_{i,n+1,\text{in}} - \Delta_i p' = 0 \\ u'_{n+1,\text{w}} - \Delta_u p' = \text{sign(w)} \frac{\tilde{\phi}_u}{\Delta y} \\ v'_{n+1,\text{w}} = 0 \\ w'_{n+1,\text{w}} - \Delta_w p' = \text{sign(w)} \frac{\tilde{\phi}_w}{\Delta y} \\ \Delta_j u'_{j,n+1} = 0. \end{cases} \tag{3.23}$$

In this case, the inner product used is a weighted summation that is analogous to integration in the continuous sense. Since we are on a uniform grid, the transpose operation to construct the adjoint equations can be expressed with the same notation

$$\mathcal{N}_q^* q^* = \begin{cases} u^*_{i,n+1,\text{in}} + \Delta_i p^* \\ u^*_{n+1,\text{w}} + \Delta_i p^* \\ v^*_{n+1,\text{w}} = 0 \\ w^*_{n+1,\text{w}} - \Delta_w p^* \\ -\Delta_j u^*_{j,n+1}. \end{cases} \tag{3.24}$$

Using the same source term as in the the J_1 formulation, we arrive at an expression for the gradient via the adjoint identity

$$\frac{D\mathcal{J}}{D\phi}\tilde{\phi} = \sum \sum_w u_i^* \text{sign(w)} \frac{\tilde{\phi}_i}{\Delta y} \Delta x \, \Delta z, \tag{3.25}$$

$$\frac{D\mathcal{J}}{D\phi_i} = \text{sign}(w)\frac{u_i^*}{\Delta y}. \tag{3.26}$$

Note that in the two expressions that are exact for the Runge-Kutta sub-step, very little information about the physics or state of the flow enters into the formulation. It is therefore reasonable to expect that over an entire Runge-Kutta step (or the whole computation), these will not perform as well as the formulations starting from the continuous equations since the state and physics would enter into the adjoint of the full Runge-Kutta step.

While the two cases considered above are extreme, it should also be pointed out that if any single step time advancement is used with the parameter ψ for the Navier-Stokes equations, then the corresponding exact adjoint equations over one time step will have the same formulation but with parameter $1 - \psi$ on the $t + \Delta t$ terms and 0 on the terms at time t. This is because the terms at time t are fixed and are therefore completely insensitive to the control. In this case, it can be seen that if the Navier-Stokes equations are solved with a fully implicit method, the corresponding adjoint equations will be fully explicit, while when the Navier-Stokes equations are solved with a fully explicit method, none of the adjoint equations discussed above (except 3.24) are appropriate. In fact, the fully implicit adjoint solution does not correspond to any time advancement scheme over one time step for the Navier-Stokes equations that does not alter the terms at time t.

3.4 Conclusions

The analysis performed in this chapter can be used to make several choices with respect to the cost function and adjoint equations that will be used in the remainder of this work. First, adjoint equations based on one Runge-Kutta sub-step of the exact discrete system have been shown to contain very little information about the turbulent flow. The effect is that they will be ineffective for computing the fluctuating component of the wall stress required to obtain an accurate mean velocity profile. Therefore, the three step Runge-Kutta method will be approximated by a singe-step method over the same interval instead of computing the exact optimal

control for one Runge-Kutta sub-step and applying it over all three sub-steps.

Second, when using the terminal valued cost function J_2, defined by (3.7), the discretization of the adjoint equations using any single-step method retains a significant amount of information regarding the turbulent velocity field. This result is in contrast to the cost function J_1 defined using an inner product (see (3.1)). The latter loses information about the LES state as it becomes increasingly explicit through the parameter ψ in (3.14). Therefore, J_2 will be used throughout the remainder of this work. The advantage of this formulation is that a range of time integration methods can be used with it.

The optimization procedure used in this work is given by the following algorithm:

1. Compute the eddy viscosity using the dynamic Smagorinsky model.
2. Forward solve the LES state (2.6) using an Euler step.
3. Compute j from (3.7).
4. Backward solve the adjoint equations (4.13) to compute the cost function gradient.
5. Update the control using steepest descent (4.27).
6. Repeat from 2. until the control converges.
7. Advance the LES state (2.6) using third-order Runge Kutta.

The next chapter will demonstrate how the computational cost of solving the adjoint equations can be reduced through a judicious choice of the time advancement scheme.

Chapter 4

Methods to Reduce Computational Expense

4.1 Introduction

The end goal of this work is to provide a general wall model that can be easily used with an arbitrary LES. In order to achieve this, the three components of the adjoint solver must be relatively automatic in order to interface with any given code and to be of relative ease of use to practioners. These three components are 1) the analytic derivation, 2) the numerical implementation, and 3) the computational resources required. The work presented in discussed Chapter 3 has the advantage that, since the adjoint equations are derived in their continuous form and then discretized in time and space, their analytic derivation is general and need not be repeated for every code. The formulation also allows for researchers to examine different discretization techniques.

However, the adjoint solutions require an extensive programming effort. Specifically, all the data structures and routines to handle the full set of adjoint equations must be written. The complexity of this code is almost that of the standard Navier-Stokes solver itself. Also, the adjoint formulation depends directly on the Navier-Stokes solver's numerical methods, primarily the spatial discretization. It

is impractical then to require that a new adjoint solver be written for every code in which a wall model is desired, particularly those using more complex numerical techniques such as curvilinear coordinates or unstructured meshes. Preferably, a model would be developed that can be called from a subroutine and used directly with as little modification as possible.

In addition to the difficulty involved with writing the computer programs to solve the adjoint equations, their actual solution requires access to significant computational resources. This is at odds with the objective of making LES easily affordable. The reason for this expense is that the adjoint equations require roughly the same computational effort to solve as the Navier-Stokes equations. While typically one-step methods are used to advance these equations, when combined with the iterations required for the optimization as well as the solutions of the Navier-Stokes equations at each iteration to provide the adjoint coefficients, the cost can become prohibitively expensive.

In order to work toward the goal of affordable LES, the issues of algorithmic complexity and computational expense must be addressed. This chapter examines methods of mitigating both of these problems by restricting the solution of the adjoint equations to the near wall region. The justification for this restriction is that it is the near-wall flow that is where the SGS models have the most difficulty and where numerical errors are greatest due to the large magnitude of the physical second derivative of velocity. Furthermore, since the adjoint equations are solved over only one time step, the sensitivity of the control to the outer flow is small. These observations will allow the entire optimization process to be conducted only over the near-wall region, reducing the complexity and expense of the wall model.

In this chapter, the specific problem under consideration will be presented, and a quick summary of the application of the general results found in Chapters 2 and 3 will be applied to it. The problem is that of flow in a pressure-gradient driven plane channel, and it is chosen because of the large body of knowledge available for this flow. This makes it much easier to determine what exactly the wall model is doing and to obtain a deeper understanding of the dynamics of the system. In addition,

as has been shown in Chapter 1, this is a challenging test case for standard wall models and the work can be readily compared to the previous work in control-based wall modeling by Nicoud *et al.* (2001) and Baggett *et al.* (2000).

4.2 Application of the Adjoint Problem to Channel Flow

In this section, the specific LES, linearized LES, and adjoint operators for plane channel flow will be extended from the results in Chapter 2. Of important note here will be the precise definition of the applied control, the boundary conditions, initial conditions, and actual equations. We start with the continuous LES operator,

$$\mathcal{N}(q) = \begin{cases} \frac{\partial u_i}{\partial t} + \frac{\partial u_i u_j}{\partial x_j} + \frac{\partial p}{\partial x_i} - \frac{\partial}{\partial x_j}\left(\nu + \nu_t\right)\left(\frac{\partial u_i}{\partial x_j} + \frac{\partial u_j}{\partial x_i}\right) \\ \frac{\partial u_j}{\partial x_j} \end{cases} \tag{4.1}$$

with boundary conditions

$$\nu \frac{\partial u}{\partial y_n} = \phi_u \tag{4.2}$$

$$v = 0 \tag{4.3}$$

$$\nu \frac{\partial w}{\partial y_n} = \phi_w. \tag{4.4}$$

In this application, the boundary conditions in the streamwise and spanwise directions are the control inputs, ϕ. In pressure-gradient driven plane channel flow, the LES equations are written succinctly as

$$\mathcal{N}(q) = \begin{bmatrix} 1 \\ 0 \\ 0 \\ 0 \end{bmatrix}, \tag{4.5}$$

with the source term representing the imposed mean pressure gradient. Note that the flow variables have been scaled by the friction velocity, u_τ, for the velocity, the channel half-height, h, for length, and ρu_τ^2 for pressure. This results in the mean pressure gradient always being -1 since the velocity is non-dimensionalized with u_τ.

4.2.1 Continuous Adjoint Operator

To construct the adjoint equations, it is first necessary to find the linearized LES operator. As in Chapter 2, this is accomplished by taking the Fréchet derivative of $\mathcal{N}(q)$:

$$\mathcal{N}'_q q' = \begin{cases} \frac{\partial u_i'}{\partial t} + \frac{\partial (u_i' u_j + u_i u_j')}{\partial x_j} + \frac{\partial p'}{\partial x_i} - \frac{\partial}{\partial x_j}\left(\nu + \nu_t\right)\left(\frac{\partial u_i'}{\partial x_j} + \frac{\partial u_j'}{\partial x_i}\right), \\ \frac{\partial u_j'}{\partial x_j} \end{cases} \tag{4.6}$$

Recall we have ignored the sensitivity of ν_t to changes in ϕ. In the same way, the initial and boundary conditions for the equations are found to be:

$$\nu \frac{\partial u'}{\partial y_n} = \tilde{\phi}_u \tag{4.7}$$

$$v' = 0 \tag{4.8}$$

$$\nu \frac{\partial w'}{\partial y_n} = \tilde{\phi}_w. \tag{4.9}$$

The linearized Navier-Stokes equations are

$$\mathcal{N}'_q q' = 0. \tag{4.10}$$

It is clear that (4.7) cannot be solved since the boundary conditions contain the unknown function $\tilde{\phi}$, motivating the need for the adjoint equations.

Using the analysis developed in Chapter 2, the adjoint equations are found to be

$$\mathcal{N}_q^* q^* = \begin{cases} -\frac{\partial u_i^*}{\partial t} - u_j \frac{\partial u_i^*}{\partial x_j} - u_j \frac{\partial u_j^*}{\partial x_i} - \frac{\partial p^*}{\partial x_j} - \frac{\partial}{\partial x_j}(\nu + \nu_t)\left(\frac{\partial u_i^*}{\partial x_j} + \frac{\partial u_j^*}{\partial x_i}\right). \\ -\frac{\partial u_j^*}{\partial x_j} \end{cases} \tag{4.11}$$

By applying the periodic boundary conditions in the homogenous directions, the only boundary terms remaining from (2.23) occur at the walls ($y = \pm 1$) and the temporal boundaries:

$$\mathrm{BT} = u_j' u_j^* \big|_0^T - (\nu + \nu_t) u_j^* \left(\frac{\partial u_j'}{\partial y} + \frac{\partial v'}{\partial x_j}\right)\Bigg|_{-1}^{1} + (\nu + \nu_t) u_j' \left(\frac{\partial v^*}{\partial x_j} + \frac{\partial u_j^*}{\partial y}\right)\Bigg|_{-1}^{1} + p' v^* |_{-1}^{1}, \tag{4.12}$$

where the following notation is used:

$$\begin{aligned} a|_0^T &= \int_\Omega a(\vec{x}, T)\, d\vec{x} - \int_\Omega a(\vec{x}, 0)\, d\vec{x} \\ a|_{-1}^{1} &= \int_0^T \int_{\mathbf{X}} \int_{\mathbf{Z}} a(x, 1, z, t)\, dx\, dz\, dt - \int_0^T \int_{\mathbf{X}} \int_{\mathbf{Z}} a(x, -1, z, t)\, dx\, dz\, dt. \end{aligned}$$

Note that the boundary conditions $v|_w = v'|_w = 0$ have already been used to reduce the expression. With these terms known, the adjoint identity (2.19) is complete.

The adjoint equations themselves define the solution of q^* that satisfies

$$\mathcal{N}_q^* q^* = f^*, \tag{4.13}$$

with initial and boundary information given by

$$q^*_{t=T, \vec{x} \in \Omega} = q_0^* \tag{4.14}$$

$$g^*(t, \vec{x}, q^* : \vec{x} \in \partial\Omega) = 0. \tag{4.15}$$

How to prescribe the source term, initial conditions, and boundary conditions with the given cost function will be the subject of the next section.

4.2.2 Cost Function Definition and Resulting Boundary and Initial Conditions

Based on the results in Chapter 3, the cost function used will be the one defined at the terminal time. In this case, it is given by

$$J_2 = \int_{-1}^{1} (\delta'_u(y)^2 + \delta'_w(y)^2) dy, \tag{4.16}$$

where

$$\delta'_{u_i}(y) = \frac{1}{A} \int_{\mathbf{X}} \int_{\mathbf{Z}} (u_i(t=T) - u_{i,\mathrm{REF}}) dx\, dz. \tag{4.17}$$

Before specifying the initial conditions implied by this cost function, it is first necessary to examine the gradient of J_2:

$$\frac{DJ_2}{D\phi}\tilde{\phi} = \int\int\int_{\Omega} \left(\frac{2\delta'_u}{A} u' + \frac{2\delta'_w}{A} w' \right) d\vec{x}. \tag{4.18}$$

Since the term depending on q' contains no integration in time, the initial conditions will be used to generate the correct formulation. Thus, they are taken to be:

$$q_0^* = \begin{bmatrix} \frac{2\delta'_u}{A} \\ 0 \\ \frac{2\delta'_w}{A} \\ 0 \end{bmatrix}, \tag{4.19}$$

while the boundary conditions are

$$\frac{\partial u^*}{\partial y_n} = 0 \tag{4.20}$$

$$v^* = 0 \tag{4.21}$$

$$\frac{\partial w^*}{\partial y_n} = 0 \tag{4.22}$$

Then, the correct adjoint equation to solve is

$$\mathcal{N}_q^* q^* = 0. \tag{4.23}$$

This choice of initial and boundary conditions, as well as the source term, results in the following form for (2.19)

$$\frac{DJ_2}{D\phi}\tilde{\phi} = -\int_0^T \int\int_{y=\pm 1} \text{sign}(y)(u^*\tilde{\phi}_1 + w^*\tilde{\phi}_3)\, dx\, dy\, dt, \tag{4.24}$$

where application of (4.7) and (4.19)-(4.20) have reduced the boundary terms from (4.14) to those appearing in (4.24). The expressions for the gradient of J_2 are then

$$\frac{DJ_2}{D\phi_u} = -\text{sign}(y)u^* \tag{4.25}$$

$$\frac{DJ_2}{D\phi_w} = -\text{sign}(y)w^*. \tag{4.26}$$

4.3 Computational Domain

In order to test the models proposed in this work, a pressure-gradient driven plane channel flow at $Re_\tau = 4000$ will be considered in order to compare with the LES results of Kravchenko *et al.* (1996). The boundary conditions used are periodic in the streamwise (x) and spanwise (z) directions, with wall stress conditions applied to the streamwise and spanwise velocities (respectively u, w) at the walls located at $y = \pm 1$. The total channel dimensions are $2\pi \times 2 \times 4\pi/3$, after being made dimensionless by the channel half-height, h. The penetration velocity v at these walls will be set to zero. In order to reduce the effort required to solve the adjoint equations, the mean pressure gradient is kept constant while the mass flow rate is allowed to fluctuate.

A centered second-order finite difference scheme is used on a staggered grid using $32 \times 33 \times 32$ points uniformly distributed in each direction. Velocity components are stored at cell faces to which they are normal while pressure and viscosity are

stored at the cell centers. Note that this configuration implies that the data needed directly at the boundaries are

$$uv - \nu\frac{\partial u}{\partial y},\ v,\ \text{and}\ wv - \nu\frac{\partial w}{\partial y},$$

which will be provided by the control.

To advance the equations in time, a third-order low-storage Runge-Kutta scheme is used. At each Runge-Kutta sub-step, the momentum equations are advanced explicitly except for the wall-normal diffusion terms, which are handled using the Crank-Nicolson technique. In wall-resolved simulations, this is done to avoid the wall-normal CFL constraint. Due to the coarse grids used in this work, this constraint is not as significant but this method is retained since it does not substantially increase the computational effort. The time step is fixed at $\Delta t u_\tau/h = 0.0015$, which produces a maximum CFL value of approximately 0.3. Given the time advancement method used, this is well below the bounds required for stability, but it was found to be necessary to have the solution independent of Δt.

4.3.1 Optimization Technique

In the optimization routine, it is necessary to iterate on the adjoint and LES equations in order to compute the cost function gradients. As previously discussed for the adjoint equations, a one-step method in time will be used to advance both sets of equations within the optimization routine in order to reduce the computational expense of the method. The LES equations are advanced for one complete time-step using an explicit Euler scheme, thus obtaining the state variables required in (4.11).

If an implicit solution is used to solve the adjoint equations, it must have a good initial guess to avoid many iterations. In this work, it is taken to be the right-hand side vector of (3.18), which is an $O(1)$ approximation to the solution. Note that Nicoud *et al.* (2001) took the initial guess to be the adjoint solution from the previous iteration, which resulted in slower convergence of the optimization

procedure.

With the gradients determined from the adjoint state, the control is updated using a steepest descent method. Let the index k denote the sub-iterations performed in the optimization routine, and so the update equation for the controls ϕ is

$$\phi^{k+1} = \phi^k - \mu \frac{DJ}{D\phi^k}, \tag{4.27}$$

where μ is a descent parameter set *a priori* to be 5×10^5 to match the value used by Nicoud *et al.* (2001). Theoretically, this method is not guaranteed to converge, however in this application this has not been observed to be an issue. Again, to match Nicoud *et al.*, convergence is measured in the L_2-norm of the change in control between sub-steps:

$$\frac{\|\phi^{k+1} - \phi^k\|^2}{\phi_s^2} \leq \epsilon, \tag{4.28}$$

with $\epsilon = 2 \times 10^{-5}$. In this case, ϕ_s is of order unity because the mean wall stress is one when u_τ is used as the velocity scale. This approach is recommended for cases in which the scales of the cost function are unknown (Dennis, 1983).

In order to regularize the cost function, a penalty term on the fluctuations of the controls is included. This is done by defining the cost function in the following manner:

$$J = J_T + J_{P,1} + J_{P,3}, \qquad J_{P,i} = \frac{\alpha}{AT} \int_0^T \int \int \left(\phi_i - \bar{\phi}_i\right)^2 \, dx \, dz. \tag{4.29}$$

This is necessary to prevent the control from using very large fluctuations to reduce the cost function, which can destabilize the simulation. In the present work, $\alpha = 10^{-6}$, corresponding to the value used by Nicoud *et al.* (2001). In general, α should be set to the smallest value that allows the simulation to be performed stably.

4.4 Techniques to Reduce Computational Expense

4.4.1 Definition of a Near-Wall Cost Function and its Dependence on Pressure Variables

An important goal of this work is to reduce the amount of computational effort that the wall modeling routine must exert away from the wall. Doing so has two primary advantages. The first is that the operation count and data storage requirements of the model are significantly reduced if only the data near the wall must be stored and manipulated. Secondly, by defining the cost function near the wall, it may be possible to use TBLE similar to Wang and Moin (2002) to provide a target for the controller. This subsection illustrates how such a construction can be accomplished.

The first step in restricting the equations solved in the wall model to the near-wall region is to define a cost function that only measures the flow there. Take the wall to be located at $y = 0$ and define $y = y_m$ to be the upper edge of the near-wall region. Then the cost function is written as

$$J_2 = \int_0^{y_m} (\delta_u^2 + \delta_w^2)\, dy. \tag{4.30}$$

Unfortunately, the smallest value of y_m that will produce a good solution is unknown, and this value could vary with the Reynolds number, numerical techniques, and grid resolution used. However, a reasonable value can be obtained by examining the flow obtained using standard wall models. In these predictions, an unphysical transition occurs in the mean profile from the near-wall flow, in which the slope of the logarithmic profile is under predicted, to the outer flow, which more accurately represents this slope. It is reasonable to assume that it is in this region where SGS and numerical errors are dominant, and so this is where the cost function should be measured. In the present LES ($Re_\tau = 4000$), this transition occurs after the third wall-normal velocity grid point at $y = 0.15/h$ or $y^+ = 605$, so m is chosen to match this value. Figure 4.1 shows the mean velocity profiles obtained when choosing m corresponding to the second and third streamwise velocity nodes, with figure 4.2

showing the RMS velocity fluctuations. The latter case shows significantly better agreement than the former with the results obtained when the cost function is defined over the whole domain, providing evidence that the supposition about the transition region is correct. This same region can be determined in other flows by performing a coarse LES using a standard wall model and noting where the transition from near-wall to outer flow takes place, although the results of this work suggest that the number of overlap grid points is independent of grid resolution and Reynolds number.

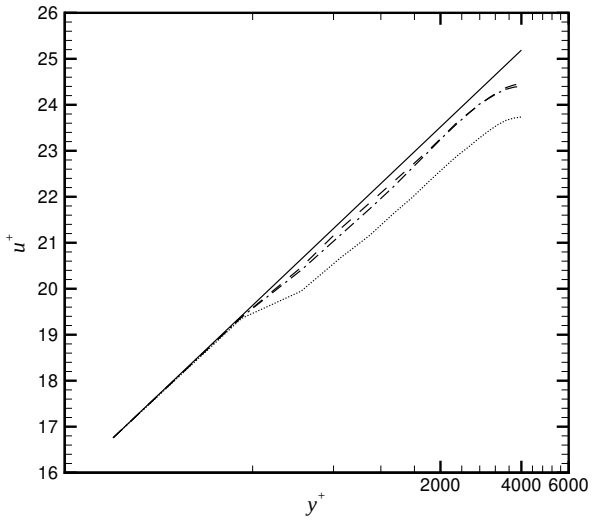

Figure 4.1: Mean velocity profiles at $Re_\tau = 4000$, ——— : $u^+ = 2.41 \log(y^+) + 5.2$, - - - - : full channel cost function, —·— : $y_m^+ = 605$ (3 points), ····· : $y_m^+ = 363$ (2 points).

Now that a cost function has been defined near the wall, it is important to determine its sensitivity to the flow variables. The first variable that is considered will be the pressure. Since a fractional step method is being used to advance the state equations, the state can be written as

$$u_i = u_i^\dagger - \Delta t \frac{\partial p}{\partial x_i}, \tag{4.31}$$

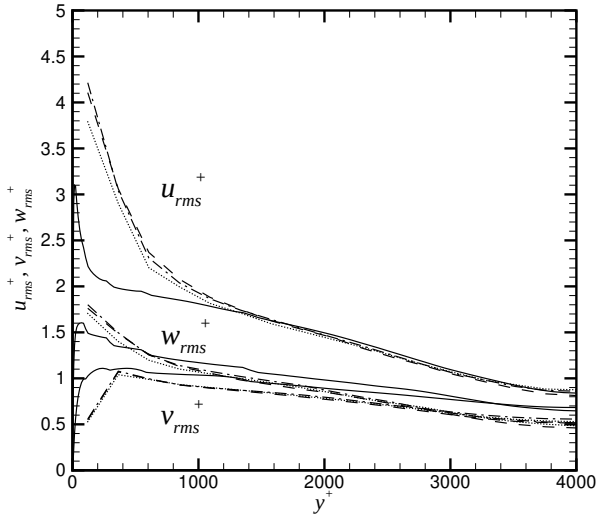

Figure 4.2: RMS velocity fluctuations at $Re_\tau = 4000$, ——— : Kravchenko *et al.* (1996), ---- : full channel cost function, —·— : $y_m^+ = 605$ (3 points), ····· : $y_m^+ = 363$ (2 points).

with $u^\dagger$ being the intermediate, non-divergence free state arising from advancing the momentum equations without the most recent pressure. Inserting this into (4.17) results in

$$\begin{aligned}\delta_{u_i}(y) &= \int_{\mathbf{X}}\int_{\mathbf{Z}} (u^\dagger_{i,\mathrm{LES}}(\vec{X},T) - \Delta t\frac{\partial p}{\partial x_i} - u_{i,\mathrm{REF}}(\vec{x},T))\,dx\,dz \\ &= \int_{\mathbf{X}}\int_{\mathbf{Z}} (u^\dagger_{i,\mathrm{LES}}(\vec{X},T) - u_{i,\mathrm{REF}}(\vec{x},T))\,dx\,dz - \Delta t\int_{\mathbf{X}}\int_{\mathbf{Z}}\frac{\partial p}{\partial x_i}\,dx\,dz.\end{aligned}$$

Since the second integral is over the homogenous directions and involves derivatives in them, it is identically zero. Hence, the final evaluation of the pressure does not have an effect on the cost function value.

In order to take advantage of pressure not entering the cost function value, the only LES state data that can be used is that from the old time. If data at the new time is required, it is coupled with the adjoint operator and can affect the value and distribution of the adjoint solution. This implies that the best choice for

the discretization of the adjoint equations is a fully implicit method. Using this technique, all the LES state information appearing as coefficients in the adjoint equations is at the old time. This means that a pressure solution for the LES equations is not required to perform the optimization. Then, only one iteration on the implicit equations will be performed, which is equivalent to the approach taken by Nicoud *et al.* (2001).

4.4.2 Reduction in Expense of Navier-Stokes and Adjoint Solutions

If a one step, explicit advance is used for the LES state in the adjoint equations, the effects of the control will never be applied to any point other than the one nearest the wall. However, if the wall-normal diffusion is handled implicitly, then the effects of the wall stresses will be applied everywhere in the flow. An important property that can be leveraged here is the linearity of this term. The time advancement can be written succinctly as (with no summation implied over the index i)

$$W_i u_i = f_i + b_i, \tag{4.32}$$

with W being a matrix representing the implicit wall-normal diffusion and time advancement, and f and b being the right-hand side vectors arising from the discrete LES equations and boundary conditions, respectively. Since f will not change during the course of the iterations, the term

$$u_i^f = W_i^{-1} f_i$$

need only be solved once per optimization procedure. Since f has non-zero entries everywhere, this equation must be solved over the entire domain. The total velocity field at the new time is then written as

$$u_i = u_i^f + W_i^{-1} b_i. \tag{4.33}$$

Note that since the cost function only measures the deviation in the streamwise and spanwise velocity profiles from their mean values, (4.33) need not be solved for the wall-normal velocity component in fully developed channel flow.

Approximations can also be made in the solution of the adjoint equations. Since a fully implicit method is used to advance these equations, the only term that will appear on the right-hand side, and hence in the initial guess for the adjoint state, will be the adjoint initial conditions. This state varies only in the wall-normal direction because it is the plane-wise averaged deviation of the LES and target velocities, so many of the terms that appear in (4.11) are zero. When only the gradients in the wall-normal direction are retained, along with removing v^* and p^* since they are zero, the adjoint operator becomes

$$\mathcal{N}_q^* q_{t=T}^* = \begin{cases} -\frac{\partial u^*}{\partial t} - v\frac{\partial u^*}{\partial y} - \frac{\partial}{\partial y}\left(\nu + \nu_t\right)\frac{\partial u^*}{\partial y} \\ -\frac{\partial v^*}{\partial t} - u\frac{\partial u^*}{\partial y} - w\frac{\partial w^*}{\partial y} - \frac{\partial}{\partial x}\left(\nu + \nu_t\right)\frac{\partial u^*}{\partial y} - \frac{\partial}{\partial z}\left(\nu + \nu_t\right)\frac{\partial w^*}{\partial y} \\ -\frac{\partial w^*}{\partial t} - v\frac{\partial w^*}{\partial y} - \frac{\partial}{\partial y}\left(\nu + \nu_t\right)\frac{\partial w^*}{\partial y} \\ 0 \end{cases} . \quad (4.34)$$

Furthermore, since the initial conditions do not vary with x or z, the gradients need only be computed once for each wall, which is the advantage when using this form of the adjoint "convective" terms. If the other formulation is used, gradients of the local turbulent velocities must be obtained, making the method more expensive (see Section 4.2.1) but more generally applicable.

4.4.3 Near-Wall Approximation to Implicit Equations

In the optimization process, the LES state only contributes to the cost function over the matching region near the wall. Similarly, the adjoint solution only affects the control inputs, and hence the LES, through its value at the wall. Therefore, the solution of the equations throughout the outer domain contributes relatively little to the overall performance of the LES. The difficulty in eliminating this outer region is that it does affect the near-wall region through the implicit equations that

are solved to advance the LES and adjoint states. These are the adjoint pressure equation and implicitly discretized wall-normal diffusion. The wall-normal diffusion can be handled directly.

The structure of b in (4.33) can be used to reduce the computational effort in its solution. This is done by noting that the only non-zero entries of b will be those at the wall containing the applied control inputs. The effect of these terms far away from the wall over one time step will be quite small. Therefore, W will be approximated by W_{nw} which is identical to W near the wall but contains only zeros away from it, with a Neumann boundary condition used to approximate the reduction in sensitivity of the outer flow to the wall stress. This condition will be placed on point $m+1$ so as to mitigate the effect of this approximation on the region that defines the cost function. The total velocity field at the new time is then written as

$$u_i = u_i^f + W_{i,nw}^{-1} b_i. \tag{4.35}$$

Using this technique, only the near-wall wall-normal diffusion needs to be computed for the LES system during the optimization iterations, significantly reducing the computational expense.

The final equation that needs to be addressed is for the pressure in the adjoint solution. Again, the only non-zero terms will be near the wall, specifically at the first $m+1$ points in the wall-normal direction, but the pressure can affect the field in the whole domain. In order to advance these equations, the pressure is modified in a similar manner to the wall-normal diffusion in the LES equations. A Neumann condition is used to close the adjoint pressure solution at $m+1$. This is reasonable since the only pressure values that will affect the controls will be those at the wall if only one iteration is performed. Therefore, as long as the value near the wall is a good approximation of the correct adjoint pressure, the adjoint equations need only be solved near the wall as well. In Figures 4.3 and 4.4, the adjoint equations are solved only at the first $m+1$ points and then the pressure is computed as has just been described. The results demonstrate that the method is still capable of accurately predicting the mean velocity profile.

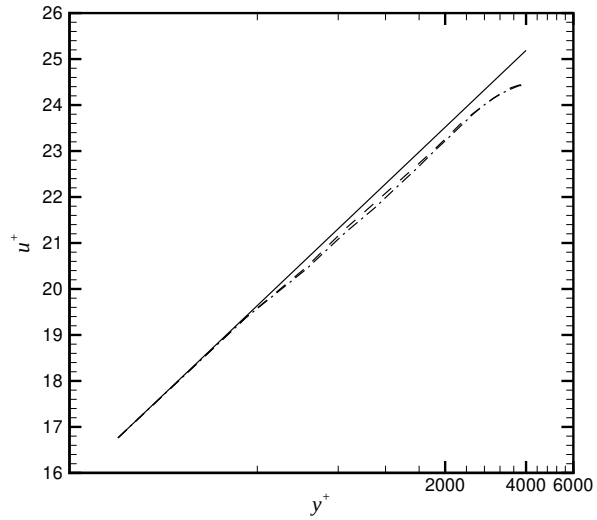

Figure 4.3: Mean velocity profiles, —— : $u^+ = 2.41 \log(y^+) + 5.2$, ---- : original formulation, —·— : reduced cost formulation.

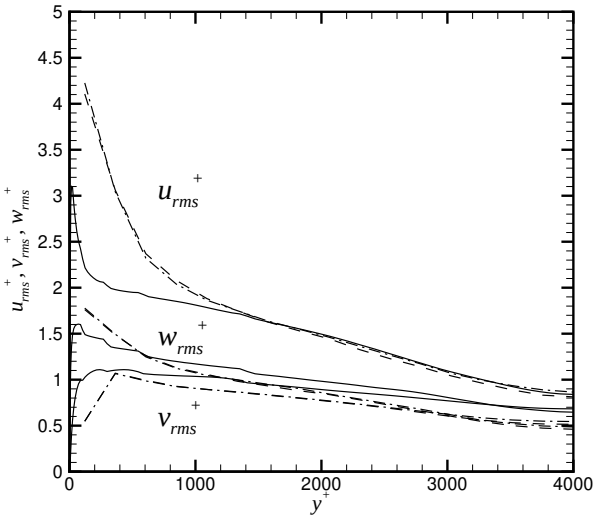

Figure 4.4: RMS velocity fluctuations, —— : Kravchenko *et al.* (1996), ---- : original formulation, —·— : reduced cost formulation.

4.5 Conclusions

A method has been presented that significantly reduces the computational effort required to implement a wall model based on sub-optimal control theory. Without this method, the wall model is approximately 13 times as expensive as the LES solution, while with the method, the wall model is between 1 and 2 times the cost of the LES. A further advantage of this approach is that only data near the wall is needed to define the cost function, and the optimization procedure must only solve the LES and adjoint equations in this region. Thus, applying this technique to flows in complex geometries is more feasible since near-wall approximations can be used in defining a predictive target profile and constructing the numerical techniques used in the optimization routine.

In order to obtain such advantages, the structures of the cost function and adjoint equation discretization are exploited. This paradigm could have utility in other applications where limited computer resources dictate that significant increases in the efficiency of the optimization procedure is more important than a very accurate gradient evaluation. In such cases, the most general formulation of the continuous adjoint equations should be found, which be discretized and approximated to maximize accuracy while minimizing expense. Therefore computational efficiency can be taken into consideration in the construction of the optimization procedure.

Chapter 5

Coupling LES and RANS via the Sub-Optimal Control Formulation

5.1 Introduction

In this chapter we will discuss how RANS equations can be utilized in the optimal control framework to provide the target profile needed by the controller. There are many ways in which RANS can be incorporated with varying models, physics, and, perhaps most importantly, coupling to the rest of the system. We will first consider a general RANS model arbitrarily coupled to the LES state and the control inputs. To make the presentation more succinct, only the terminal time cost function without penalties will be considered, but the analysis could be applied to any formulation. Penalty terms will be examined separately later in the chapter. Also, the term RANS will be used loosely to describe any system that can capture an "average"-type behavior of the near-wall physics, which will ensure the spatially and temporally averaged LES solution accurately captures the mean velocity profile.

As a matter of practicality, it is best to use the cheapest RANS system that meets the above requirements. However, an important constraint is that the cost to solve the RANS system can only scale weakly with the Reynolds number. This is

achieved by having he RANS system resolve the strong wall-normal mean velocity gradients while retaining the same coarseness in the wall-parallel directions as the LES. However, in the derivation of the adjoint equations the RANS system will first be treated a general continuous operator. The specific RANS system used will be considered in the discretization process. Examples of several appropriate near-wall RANS equations of varying levels of complexity are presented in Wang and Moin (2002).

5.2 LES Control Algorithm using RANS Targets

A control algorithm will be devised to compute the wall stresses that are required as inputs to the LES. However, in order to apply a control algorithm, it is necessary to have a quantity to regulate. Many such flow quantities are possible, including both volume integrals and wall-normal fluxes of flow properties such as momentum, stress, energy, and vorticity. However, since a predictive method is required, it will be necessary to define a cost function that can use data obtained from RANS-based computations. This is because RANS is the only technique that, at present, can obtain reasonably accurate information at a modest cost in most attached near-wall flows. The primary cost function considered will then be based on the plane averaged deviation of the LES profile from the RANS profile, although other cost functions will be considered. An additional reason for using such a cost function is that previous calculations by Nicoud *et al.* (2001) and those presented in Chapter 4 demonstrated that this definition, at least for the case of a fixed target velocity, was able to yield accurate mean velocity profiles.

The RANS model will be of the form used by Wang and Moin (2002), since they demonstrated the effectiveness of near-wall RANS modeling in supplying wall stresses for a moderately resolved LES in complex geometry. The cost function is then defined to be

$$J(\phi) = \int_0^{y_m} (\delta_u(y)^2 + \delta_w(y)^2)\, dy, \tag{5.1}$$

which is a function of the control input ϕ. In the case of channel flow, $\phi \in (\mathcal{L}^2(\partial\Omega \rightarrow$

$\mathbb{R}))^2$ since each element is a function mapping points on the walls to $\mathbb{R}$. There are two such functions corresponding to each of τ_{12}^w and τ_{32}^w on both walls. For clarity, the notation $\phi_u = \tau_{12}^w$ and $\phi_w = \tau_{32}^w$ will be used.

With $\mathbf{X}$ and $\mathbf{Z}$ used to designate the extent of the domain in the streamwise and spanwise directions, the specific quantities appearing in the first term of (5.1) are defined as

$$\delta_{u_i}(y) = \frac{1}{A}\int_{\mathbf{X}}\int_{\mathbf{Z}}(u_{i,\mathrm{LES}}(x,y,z,T) - u_{i,\mathrm{RANS}}(x,y,z,T))dx\,dz, \tag{5.2}$$

where the subscripts l and r denote state variables from the LES and RANS equations, respectively. Note that both are functions of ϕ, with $u_{i,\mathrm{LES}}$ satisfying the constraint that $\mathcal{N}(q) = 0$. While the RANS velocity can be taken as a fixed target from an independent calculation, it is more useful to have it coupled with the LES state and control inputs.

Now that the cost function is defined, its derivative must be calculated to apply the control algorithm. Taking the Fréchet derivative of J with respect to ϕ results in

$$\frac{DJ}{D\phi}\tilde{\phi} = 2\int_0^{y_m}\left(\delta_u(y)\frac{D\delta_u(y)}{D\phi}\tilde{\phi}_u + \delta_w(y)\frac{D\delta_w(y)}{D\phi}\tilde{\phi}_w\right)dy, \tag{5.3}$$

where $\tilde{\phi}$ is an arbitrary test function. To evaluate this expression, the Fréchet differential of $\delta_{u_i}(y)$ must also be computed:

$$\frac{D\delta_{u_i}(y)}{D\phi}\tilde{\phi} = \frac{1}{A}\int_{\mathbf{X}}\int_{\mathbf{Z}}\left(\frac{Du_{i,\mathrm{LES}}}{D\phi} - \frac{Du_{i,\mathrm{RANS}}}{D\phi}\right)\tilde{\phi}\,dx\,dz. \tag{5.4}$$

The second term in the integral can be evaluated using the chain rule (which applies for Fréchet differentiation, see Luenberger (1969)):

$$\frac{Du_{i,\mathrm{RANS}}}{D\phi}\tilde{\phi} = \left(\frac{\mathcal{D}u_{i,\mathrm{RANS}}}{\mathcal{D}\phi} + \frac{\mathcal{D}u_{i,\mathrm{RANS}}}{\mathcal{D}q}\frac{Dq}{D\phi}\right)\tilde{\phi} \tag{5.5}$$

where $\mathcal{D}u_{i,\mathrm{RANS}}/\mathcal{D}\phi$ represents the partial Fréchet derivative with respect to ϕ. For simple models, these derivatives can be computed analytically at virtually no

additional expense. However, for more complicated models, it will be necessary to define an adjoint problem for them. This procedure will now be shown for a general RANS model. The results for specific model formulations will be presented as needed.

Once the RANS sensitivities have been determined, the adjoint source term for the LES adjoint equations needs to be modified to incorporate this information, specifically the last term in (5.5). In order to determine what the source term for the LES adjoint equations should be, it is necessary to examine the structure of the RANS sensitivity operator. In the cases considered here, it takes the form of a linear functional acting on $q'(\vec{x})$:

$$\frac{\mathcal{D}u_{i,\mathrm{RANS}}}{\mathcal{D}q}q' = \int_\Omega \left(\frac{\mathcal{D}u_{i,\mathrm{RANS}}}{\mathcal{D}q_j}(\vec{x}')q_j'(\vec{x}') \right) d\vec{x}'. \tag{5.6}$$

The only way to have this integral evaluated within the inner product formulation is to have the inner product of f^* and q' yield the expression in (5.6). However, the expression found in (5.3) and (5.4) must still be recovered. To this end, the RANS gradient must be weighted by the corresponding term that appears in the cost function, which is accomplished by switching the order of integration:

$$\begin{aligned} \frac{-2}{A}\int_0^{y_m} \delta_{u_i}(y) \int_{\mathbf{X}}\int_{\mathbf{Z}} \left(\int_\Omega \left(\frac{\mathcal{D}u_{i,\mathrm{RANS}}(\vec{x})}{\mathcal{D}q_j}(\vec{x}')q_j'(\vec{x}') \right) d\vec{x}' \right) dy\, dx\, dz = \\ \int_\Omega \left(q_j'(\vec{x}')\frac{-2}{A}\int_0^{y_m}\int_{\mathbf{X}}\int_{\mathbf{Z}} \left(\delta_{u_i}(y)\frac{\mathcal{D}u_{i,\mathrm{RANS}}(\vec{x})}{\mathcal{D}q_j}(\vec{x}') \right) d\vec{x} \right) d\vec{x}'. \end{aligned} \tag{5.7}$$

Therefore, the adjoint source term will be decomposed as follows

$$f_c^* = f^* + f_{q_r^*}^* \tag{5.8}$$

where f^* is the adjoint source term used in Chapter 4 while $f_{q_r^*}^*$ is given by

$$f_{q_r^*,i}^*(\vec{x}) = \frac{-2}{A}\int_0^{y_m}\int_{\mathbf{X}}\int_{\mathbf{Z}} \left(\delta_{u_j}(y)\frac{\mathcal{D}u_{j,\mathrm{RANS}}(\vec{x})}{\mathcal{D}q_i}(\vec{x}') \right) d\vec{x}'. \tag{5.9}$$

The LES adjoint equations are then solved as before to yield the cost function gradient in combination with the solution of the RANS adjoint equations for the direct sensitivity of the RANS state to the control. In this case, however, the LES adjoint source term will be a function of all the spatial variables and not just the wall-normal direction.

5.2.1 RANS Sensitivities

Since the RANS profile potentially changes in response to the LES state and control inputs, the sensitivities of the RANS velocity profiles to these variables must be evaluated. These sensitivities are required in order to compute the necessary gradients that arise in (5.4). Within this framework, it is possible to use many different near-wall RANS models, ranging from the simplest stress balance model to a full set of time-varying TBL equations. In addition, it is possible to prescribe a variety of boundary conditions and source terms from the LES. These include velocities, velocity gradients, pressure gradients, and energy or vorticity fluxes at y_m, and velocities and stresses at the wall. Each wall can then be handled independently.

In order to compute the RANS sensitivities, it is necessary to first define a RANS state, q_r. Given the cost function used in this work, it is necessary that both the RANS streamwise and spanwise velocities, u_{RANS} and w_{RANS}, be elements of q_r. In general, q_r must include all the states that appear in the cost function and auxiliary states which influence these quantities. For example, other elements of q_r could be the wall-normal velocity and eddy viscosity model variables. Given these states, the RANS system can be written generally as

$$\mathcal{R}_q(q_r) = f_r(q, \phi) \tag{5.10}$$

subject to boundary conditions at the wall

$$g_q(q_r|_0) = f_{r,\mathrm{bcw}}(q, \phi), \tag{5.11}$$

and at y_m:

$$h_q(q_r|_m) = f_{r,\mathrm{bcm}}(q, \phi). \tag{5.12}$$

Here the dependence of the operator, source term and boundary conditions on q is meant to couple the RANS solution to the LES solution in a potentially general manner. The RANS dependence on the LES quantities will normally be only at positions above the matching layer, as they are not considered to be physically correct near the wall.

Now, taking the Fréchet partial derivative of (5.10)-(5.12) with respect to q and ϕ yields two equations, one for each sensitivity:

$$\frac{\mathcal{D}\mathcal{R}_q(q_r)}{\mathcal{D}q}\tilde{q} + \frac{\mathcal{D}\mathcal{R}_q(q_r)}{\mathcal{D}q_r}q_r^l = \frac{\mathcal{D}f_r}{\mathcal{D}q}\tilde{q} \tag{5.13}$$

$$\frac{\mathcal{D}\mathcal{R}_q(q_r)}{\mathcal{D}\phi}\tilde{\phi} + \frac{\mathcal{D}\mathcal{R}(q_r)}{\mathcal{D}q_r}q_r^\phi = \frac{\mathcal{D}f_r}{\mathcal{D}\phi}\tilde{\phi}, \tag{5.14}$$

where

$$q_r^l = \frac{\mathcal{D}q_r}{\mathcal{D}q}\tilde{q}$$
$$q_r^\phi = \frac{\mathcal{D}q_r}{\mathcal{D}\phi}\tilde{\phi}.$$

Note that $\tilde{\phi}$ and $\tilde{q}$ refer to perturbations in the LES state and control input, respectively, and are taken to be independent.

With the following definitions

$$\mathcal{R}'_{q,q_r} \equiv \frac{\mathcal{D}\mathcal{R}_q(q_r)}{\mathcal{D}q_r}, \tag{5.15}$$

$$f_r^l \equiv \left(\frac{\mathcal{D}f_r}{\mathcal{D}q} - \frac{\mathcal{D}\mathcal{R}_q(q_r)}{\mathcal{D}q}\right)\tilde{q}, \tag{5.16}$$

(5.13) can be written as the linearized RANS system

$$\mathcal{R}'_{q,q_r}q_r^l = f_r^l(q, q_r). \tag{5.17}$$

The boundary conditions for this equation (using similar notation for the subscripts) are

$$g'_{q,q_r} q_r|_0 = f'_{r,\mathrm{bcw}}(q, q_r, \phi), \tag{5.18}$$

$$h'_{q,q_r} q'_r|_m = f'_{r,\mathrm{bc}}(q, q_r), \tag{5.19}$$

where

$$g'_{q,q_r} \equiv \frac{\mathcal{D} g_q(q_r|_m)}{\mathcal{D} q_r|_m}, \tag{5.20}$$

$$f'_{r,\mathrm{bcw}}(q, q_r) \equiv \left(\frac{\mathcal{D} f_{r,\mathrm{bcw}}}{\mathcal{D} q} - \frac{\mathcal{D} g_q(q_r|_m)}{\mathcal{D} q} \right) \tilde{q}. \tag{5.21}$$

and

$$h'_{q,q_r} \equiv \frac{\mathcal{D} h_q(q_r|_m)}{\mathcal{D} q_r|_m}, \tag{5.22}$$

$$f'_{r,\mathrm{bc}}(q, q_r) \equiv \left(\frac{\mathcal{D} f_{r,\mathrm{bc}}}{\mathcal{D} q} - \frac{\mathcal{D} h_q(q_r|_m)}{\mathcal{D} q} \right) \tilde{q}. \tag{5.23}$$

A similar system can be derived for the sensitivities to ϕ.

Integration by parts now yields the adjoint operator $\mathcal{R}^*_{q,q_r}$ of (5.17) . The adjoint identity then becomes:

$$\langle f'_r(q, q_r), q^*_r \rangle = \langle q'_r, f^*_r \rangle + \mathrm{BT}_r. \tag{5.24}$$

The RANS adjoint source term, f^*_r, is determined such that q'_r can be identified. Similarly, the boundary conditions on q^*_r must be chosen such that all terms not directly proportional to $q'_r|_m$ are zero. It can be seen that this will result in a well posed system by considering that only terms containing a derivative of order two or greater in the wall-normal direction will require an adjoint boundary condition. This arises from the integration by parts. Any terms containing first order derivatives will have boundary terms proportional to elements of q'_r and q^*_r. A derivative of order n on an element of q'_r will result in one term proportional to

q_r' and $n-1$ terms proportional to derivatives of it. Thus, all the boundary terms involving derivatives of q_r' can be removed by setting the appropriate derivatives of q_r^* to zero. This is also the correct number of boundary conditions required for well posedness. Hence, equation (5.24) allows for the identification, in the weak sense, of $\frac{Dq_r}{Dq}$ which can be used to compute the cost function gradients.

5.2.2 RANS Sensitivities for a Simplified System

In order to provide an illustrative example, as well as to derive the equations used in this work, the RANS sensitivities of the previous section will be applied to a simple near-wall model. The model under consideration is the simplest one used by Wang and Moin to provide wall stresses in a trailing edge geometry. It is given by

$$\frac{\partial}{\partial y}\left(\nu+\nu_t^r\right)\frac{\partial u_{i,\mathrm{RANS}}}{\partial y}=0, \qquad i=1,3, \tag{5.25}$$

where ν_t^r is the RANS eddy viscosity given by a damped mixing length model

$$\frac{\nu_r}{\nu}=1+\kappa y^+\left(1-e^{-y^+/A}\right)^2.$$

The boundary conditions are taken to be

$$u_{i,\mathrm{RANS}}|_w = 0, \tag{5.26}$$

$$u_{i,\mathrm{RANS}}|_m = u_{i,\mathrm{LES}}|_m. \tag{5.27}$$

Now, the terms in (5.17) can be identified as

$$\begin{aligned}\frac{\mathcal{D}\mathcal{R}_q(q_r)}{\mathcal{D}q}\tilde{q} &= 0,\\ \mathcal{R}'_{q,q_r}q_r' &= \frac{\partial}{\partial y}(\nu+\nu_t^r)\frac{\partial u'_{i,\mathrm{RANS}}}{\partial y},\\ \frac{\mathcal{D}f_r}{\mathcal{D}q}\tilde{q} &= 0.\end{aligned} \tag{5.28}$$

The boundary conditions in (5.18)-(5.19) then become

$$h'_{q,q_r} q'_r|_m = u'_{i,\mathrm{RANS}}|_m, \tag{5.29}$$

$$f'_{r,\mathrm{bc}}(q, q_r) = \tilde{u}_{i,\mathrm{LES}}|_m. \tag{5.30}$$

The adjoint operator can be determined by integration by parts to be

$$\mathcal{R}^*_{q,q_r} q^*_r = \frac{\partial}{\partial y}(\nu + \nu^r_t)\frac{\partial u^*_{i,\mathrm{RANS}}}{\partial y}. \tag{5.31}$$

Note that in this case, ν_r is not a function of any of the state variables so it can be handled directly in the integration by parts. The boundary terms are

$$\mathrm{BT}_r = \int_{\mathbf{X}}\int_{\mathbf{Z}} (\nu + \nu^r_t)\left(u^*_{i,\mathrm{RANS}}\frac{\partial u'_{i,\mathrm{RANS}}}{\partial y} - u'_{i,\mathrm{RANS}}\frac{\partial u^*_{i,\mathrm{RANS}}}{\partial y}\right) dx\, dy\Big|_0^{y_m}. \tag{5.32}$$

Given these equations, it is now possible to identify the RANS sensitivities at a point $y_0 \in (0, y_m)$. The source term for the adjoint equation is taken to be the Dirac delta function, $\delta(\vec{x} - \vec{x}_0)$, in both the u^* and w^* equations and the boundary conditions are chosen to be:

$$u^*_{i,\mathrm{RANS}}|_0 = u^*_{i,\mathrm{RANS}}|_m = 0. \tag{5.33}$$

With these values, and recalling that $u'_{i,\mathrm{RANS}}|_0 = 0$, (5.24) becomes

$$u'_{\mathrm{RANS}}(\vec{x}_0) + w'_{\mathrm{RANS}}(\vec{x}_0) = \int_{\mathbf{X}}\int_{\mathbf{Y}} u'_{i,\mathrm{RANS}}\frac{\partial u^*_{i,\mathrm{RANS}}}{\partial y}\bigg|_m dx\, dz. \tag{5.34}$$

By noting that the RANS equations are an ODE at each wall-normal location, the delta function used as the RANS adjoint source term will be retained in the x and z directions in the adjoint solution. Hence the sensitivity can be identified as

$$\frac{Du_{i,\mathrm{RANS}}(x, y, z)}{Du_{i,\mathrm{LES}}(x, y_m, z)} = \frac{\partial u^*_{i,\mathrm{RANS}}}{\partial y}(x, y_m, z), \tag{5.35}$$

Since the RANS sensitivities are related to the LES state at only one point, a delta

function must be included in (5.7) in the definition of the operator defining the RANS gradient with respect to the LES. Hence, a delta function must similarly be included in the LES adjoint source term given by (5.9).

5.3 Decoupling the Mean Wall Stress from the Control

Several different control formulations that proved unsuccessful are described in Appendix B, including directly replacing the fixed target in Nicoud *et al.* (2001) with the RANS velocity. From these results, some important requirements on the control were determined. First, the RANS profile must be able to correct itself, i.e. if there is an error, this error must decrease with time. Second, cost functions that measure a ratio of the velocity profiles tend to be unstable and should be avoided. Third, in order for the control to be effective, it must exert most of its effort based on the LES state. These three results imply that the structure of the cost function of Nicoud *et al.* (2001) is a good one to use, and that the RANS equations must somehow be coupled to mean flow information, in this case either the mean pressure gradient, or equivalently, the mean wall stress.

Since coupling the control directly to the RANS equations proved ineffective, it is therefore proposed that the RANS system be used to prescribe the mean wall stress, and the control used to compute the fluctuations about this mean. The RANS system under consideration is readily adapted to that purpose since the average wall stress is easily obtained by using the system as an algebraic wall model as in Wang and Moin (2002). The mean value of the control is then removed, while all the fluctuations are retained. This can be formally justified by considering the control not to be the local wall stress but instead to be a Fourier coefficient in a Fourier series expansion of the wall stress, i.e.

$$\tau^w(x,z) = \sum_{n=-N_x/2}^{N_x/2} \sum_{m=-N_z/2}^{N_z/2} \hat{\phi}_{n,m} e^{i(nN_x x + mN_z z)}, \tag{5.36}$$

with N_x and N_z being the number of Fourier modes in the streamwise and spanwise directions, respectively.

In this formulation, $\hat{\phi}_{n,m}$ will be given by the optimal control as the appropriate Fourier coefficients for all n, m except for $n = m = 0$. The latter coefficient, representing the mean wall stress, will be prescribed by the average of that predicted by the algebraic RANS-based wall model. In order to see how this term can be removed from the control set, consider the cost function gradient identification equation (4.24) written with (5.36) substituted in for $\tilde{\phi}_{n,m}$:

$$\begin{aligned}\frac{DJ}{D\phi}\tilde{\phi} = \int\int \Bigg(u^* \sum_{i=-N_x/2}^{N_x/2} \sum_{j=-N_z/2}^{N_z/2} \tilde{\hat{\phi}}^u_{n,m} e^{i(nN_x x + mN_z z)} \\ + w^* \sum_{i=-N_x/2}^{N_x/2} \sum_{j=-N_z/2}^{N_z/2} \tilde{\hat{\phi}}^w_{n,m} e^{i(nN_x x + mN_z z)} \Bigg) \, dx \, dz,\end{aligned} \tag{5.37}$$

which can be rewritten as

$$\begin{aligned}\frac{DJ}{D\phi}\tilde{\phi} = \sum_{n=-N_x/2}^{N_x/2} \sum_{m=-N_z/2}^{N_z/2} \Bigg(\tilde{\hat{\phi}}^u_{n,m} \int\int u^* e^{i(nN_x x + mN_z z)} \, dx \, dz \\ + \tilde{\hat{\phi}}^w_{n,m} \int\int w^* e^{i(nN_x x + mN_z z)} \, dx \, dz \Bigg).\end{aligned} \tag{5.38}$$

By applying the definition of the Fourier transform, we can see that

$$\frac{DJ}{D\phi}\tilde{\phi} = \sum_{n=-N_x/2}^{N_x/2} \sum_{m=-N_z/2}^{N_z/2} \left(\tilde{\hat{\phi}}^u_{n,m} \hat{u}^*_{-n,-m} + \tilde{\hat{\phi}}^w_{n,m} \hat{w}^*_{-n,-m} \right). \tag{5.39}$$

Thus, the gradients can be identified directly from the Fourier representation of the adjoint solution:

$$\begin{aligned}\frac{DJ}{D\phi^u_{n,m}} &= \hat{u}^*_{-n,-m} \\ \frac{DJ}{D\phi^w_{n,m}} &= \hat{w}^*_{-n,-m}.\end{aligned}$$

Since the gradient of each Fourier coefficient can be identified independently, it is possible to retain only a subset of them in the control formulation. Thus, the mean wall stress can be taken out of the control set and the optimal control problem can still be solved. It should be noted that while the above analysis provides a formal argument for channel flow, a more general Gram-Schmidt procedure could be used to remove the mean wall stress in general. All that is required that it can be decomposed into mean and fluctuating components. In more complex cases, the RANS wall stress distribution can be used as the mean.

Using this control algorithm, it is necessary that the mean wall stress is determined by RANS at the old time to prevent the controller from manipulating the mean stress, while the fluctuating component can be determined by RANS at the new time. For consistency, however, the RANS at the old time is used to define target in the cost function.

The approach can then be summarized as follows: first, the algebraic wall model of Wang and Moin (2002) is used to compute the mean stress at the wall. In this work, the velocity inputs into this model come from the velocity at the first LES grid point away from the wall, although the imposed mean pressure gradient ensures that this technique using the input from any point would correctly predict the mean wall stress in this case. In order to compute the mean wall stress, an RANS solution is performed in the wall-normal direction. These RANS velocities are then used as the target for the optimization procedure. By combining the mean wall stress from the RANS solution and the fluctuating wall stress from the control routine, the LES wall stress is found.

Results for the mean velocity profile using this approach, with the cost function defined over the first three grid cells, are shown in Fig. 5.1 while the rms profiles are presented in Fig. 5.2. Note that the results for the mean velocity profile are almost identical to what was obtained by Nicoud *et al.*. Thus, the model retains the fidelity enabled by the controller but is predictive in that no *a priori* information was needed to prescribe the target profile.

To examine the robustness of this controller, it is tested at different Reynolds

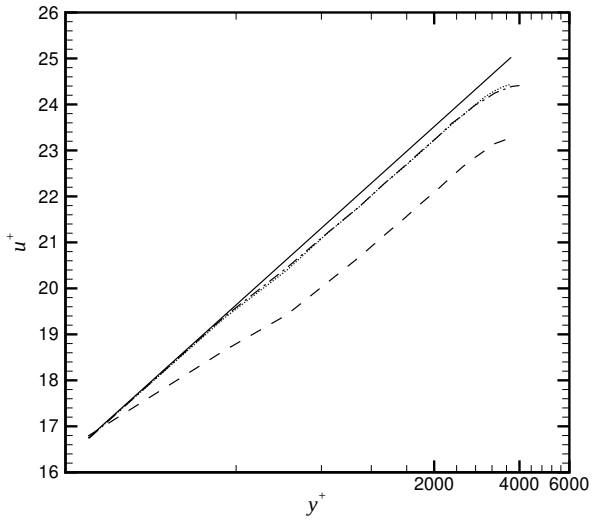

Figure 5.1: Mean velocity profiles at $Re_\tau = 4000$, ——— : $u^+ = 2.41 \log(y^+) + 5.2$, - - - - : Piomelli *et al.* (1989), —·— : present model, ····· : Nicoud *et al.* (2001).

numbers, on a finer grid, and with different SGS models. The Reynolds numbers considered are $Re_\tau = 640, 4000$ and 20000. First, all computations are performed on a grid with $32 \times 33 \times 32$ cells, and all other parameters held constant. It was found, however, that the convergence rate was improved at $Re_\tau = 640$ by increasing μ. This is likely because the first point is below the logarithmic layer and so more control effort is required to increase the slope of the mean velocity. For all Reynolds numbers, though, the mean velocity profiles, shown in Fig. 5.3, accurately capture the logarithmic profile.

In order to validate that the method is independent of the grid spacing, a further computation has been performed at $Re_\tau = 4000$ on a grid with $64 \times 65 \times 64$ cells. This is twice the resolution in each direction as was used in the original case. All other parameters have been kept constant. The mean velocity profile, presented in Fig. 5.4, again compares favorably to the logarithmic profile, demonstrating that this method is robust with respect to grid and Reynolds number changes.

Another important robustness issue to examine is the sensitivity of the control

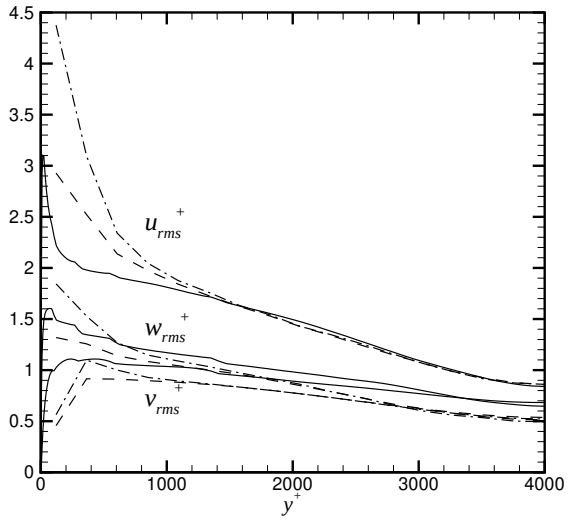

Figure 5.2: RMS of velocity fluctuations at $Re_\tau = 4000$, ——— : Kravchenko *et al.* (1996), - - - - : Piomelli *et al.* (1989), —·— : present model.

to the SGS model. Its relevance was demonstrated by Baggett *et al.* (2000) in considering the LSE wall model applied in different numerical environments. While it was demonstrated that the performance of the LSE approach was sensitive to changes in the numerical method and grid stretching, the technique was significantly more sensitive to different SGS models as evidenced by the large over-prediction of the logarithmic profile when the Cabot and Moin (2000) procedure was used to compute the Smagorinsky coefficient in the near-wall region.

In this study, we consider three models: the dynamic Smagorinsky model, which was used to obtain the previous results, the mixed similarity model Bardina *et al.* (1980), and the procedure of Cabot and Moin (2000). The stress for the mixed similarity model is given by

$$\tau_{ij} = C_{\text{sim}}(\widehat{u_i u_j} - \hat{u}_i \hat{u}_j) + \text{DSM}, \tag{5.40}$$

where the model constant is set to be $C_{\text{sim}} = 0.9$, $\widehat{(\cdot)}$ denotes the same test filter as used in the dynamic procedure, and DSM stands for the stress coming from the

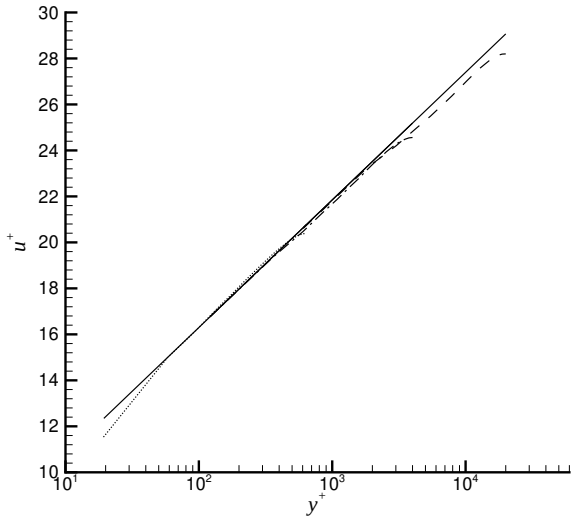

Figure 5.3: Mean velocity profiles computed on a $32 \times 33 \times 32$ grid, —— : $u^+ = 2.41 \log(y^+) + 5.2$, - - - - : $Re_\tau = 20\,000$, —·— : $Re_\tau = 4000$, ····· : $Re_\tau = 640$.

dynamic Smagorinsky model. The results using these three models in conjunction with an algebraic wall model Wang and Moin (2002) are shown in Fig. 5.5. It is clear that these SGS models can produce substantially different behavior in the LES. However, as is also presented in Fig. 5.5, when they are used with the control-based model, the near-wall profiles collapse onto the logarithmic profile (again without changing the optimization parameters). This demonstrates that the control can account for different SGS modeling errors, while the LSE wall model of Nicoud *et al.* Nicoud *et al.* (2001), based on one instance of the control, could not. Further, note that away from the wall, the quality of the mean profile prediction depends weakly on the SGS model used. It can be seen that the more accurate a prediction the model makes without the control, the more accurately the mean velocity will be captured away from the wall. The effect of the control is to ensure that the near-wall mean velocity is computed correctly.

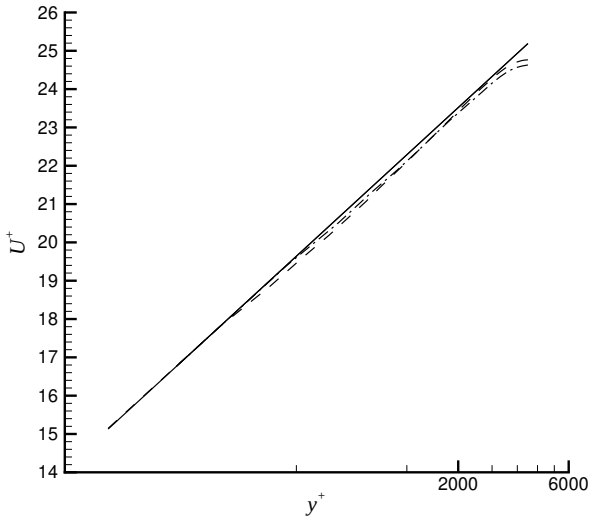

Figure 5.4: Mean velocity profiles for $Re_\tau = 4000$, ——— : $u^+ = 2.41\log(y^+) + 5.2$, - - - - : $64 \times 65 \times 64$ cells, —·— : $32 \times 33 \times 32$ cells.

5.4 Examination of the Control Efforts

5.4.1 Correlations Between the Control and Turbulent Quantities

Previous efforts to understand the control have focused on its effects on the stress balance and turbulent kinetic energy budget (Nicoud *et al.*, 2001). Such an approach aims to evaluate the control based on the changes it makes to the time averaged flow field. Here, we attempt to gain insight into the control through a different statistical measure: its correlations with turbulent quantities. These correlations allow us to examine what the control is reacting to in the turbulent field. The goal is to better understand the instantaneous actions of the control rather than the changes to the time-averaged quantities. In addition, these results may yield insight that could lead to feedback models, since a correlation coefficient with a value of ± 1 would imply that a perfect feedback controller exists.

In this investigation, the control at a point, $\phi(x, y)$, is correlated with various

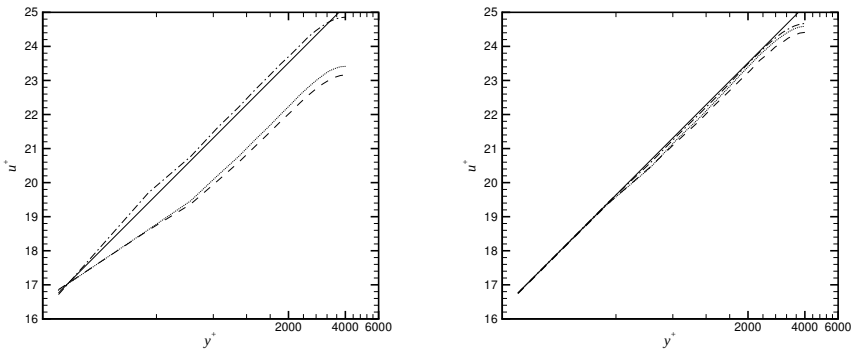

Figure 5.5: Effects of SGS model using an algebraic wall model (Wang and Moin, 2002) (left) and the present control-based wall model (right), ——— : $u^+ = 2.41\log(y^+) + 5.2$, - - - - : dynamic Smagorinsky model, —·— : Cabot and Moin procedure (Cabot and Moin, 2000), ····· : mixed similarity model (Bardina *et al.*, 1980).

turbulent quantities throughout the channel. The results presented this section are computed at $Re_\tau = 4000$ on a grid with $32 \times 33 \times 32$ cells using the dynamic Smagorinsky model. If h is some function of the turbulent field, $h(\vec{x}) = h(\vec{u}, P)$, we can compute the spatial correlation coefficient with the expression

$$C_h^\phi(\vec{x}, \vec{x}') = \frac{\left\langle (h(\vec{x}) - \bar{h})(\phi(\vec{x}') - \bar{\phi}) \right\rangle}{\sigma_h \sigma_\phi}, \tag{5.41}$$

where σ_h and σ_ϕ are the square roots of the variances of h and ϕ with $\vec{x}$ being a location in the channel interior while $\vec{x}'$ is located on the wall. Averaging is performed over wall-parallel planes and in time. Because of the spatial homogeneity in the wall-parallel plane, the correlation is only a function of the spatial separation $C_h^\phi(\vec{x} - \vec{x}')$. The results for the maximum correlation coefficients of a sample of quantities are presented in Table 5.1. In all cases the maximum correlation occurred in the second wall-parallel plane. The streamwise and spanwise locations of the maxima can be seen in the figures that will follow.

These results indicate what the control is and is not reacting to. Perhaps the

h	$\max \lvert C_h^u \rvert$	$\max \lvert C_h^w \rvert$
u	0.46	0.36
v	0.28	0.19
w	0.19	0.34
TKE	0.07	0.03
P^k	0.06	0.03
$u'v'$	0.06	0.03
$\partial u/\partial y$	0.32	0.22
ω_x	0.09	0.29
ω_y	0.17	0.59
ω_z	0.33	0.21
$\lvert\omega\rvert^2$	0.09	0.06
$\partial u/\partial x$	0.59	0.26

Table 5.1: Maximum correlation coefficients for the streamwise (u) and spanwise (w) boundary conditions.

most interesting result is the lack of correlation between the control and quantities related to the shear stress balance and the turbulent kinetic energy (TKE). The previous work of Nicoud *et al.* (2001) focused on the change made by the control in decreasing the Reynolds stress and increasing both TKE production and dissipation near the wall in the average sense. However, these results suggest that the control does not directly respond to these quantities, as their correlation coefficients are quite small. Instead, the flow is manipulated in such a way that indirectly changes these flow characteristics.

To examine the control effects in more detail, it is useful to understand their spatial distribution. Figures 5.6 and 5.7 show both the horizontal and vertical distributions of the coefficient in the plane of its maximum value. The correlation coefficient is maximum in the second plane from the wall and decreases rapidly, consistent with the near-wall cost function construction. Similarly, the effect of the control is also local in the wall-parallel directions. The rapid convergence of the steepest descent algorithm is likely due to this locality since the optimization becomes a solution of many local problems as opposed to one large global problem.

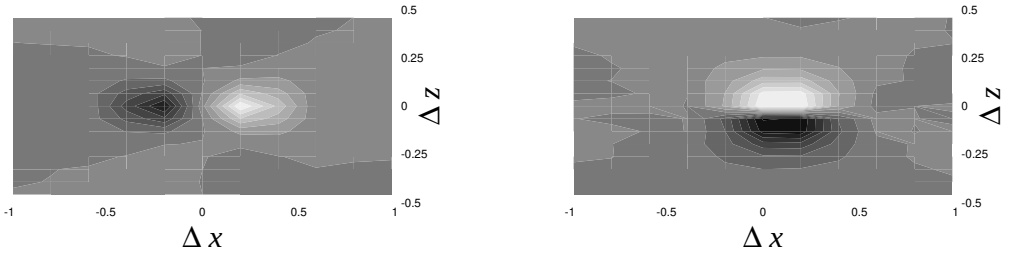

Figure 5.6: Wall-parallel spatial distribution of the correlation coefficients for u': coefficients for ϕ^u (left) and ϕ^w (right) at $y/h = 0.09$ (second wall-normal cell). The scale range is ± 0.46 for ϕ^u and ± 0.36 for ϕ^w, with white being a large positive value and black a large negative value. The domain is ± 5 points in the streamwise direction and ± 6 points in the spanwise direction.

Figures 5.6 and 5.7 also indicate that the wall stresses have significant structure. The large regions of high positive and negative correlations aligned with the streamwise axis, in the case of ϕ^u, and in the spanwise direction, in the case of ϕ^w, also suggest that velocity gradients will be more highly correlated with the control.

The complexity of the controller's actions can be further observed by considering the spatial distributions of additional quantities in Figs. 5.8 and 5.9. Patterns ranging from quadrupoles to "butterflies" are observed, indicating the control does not simply apply a stochastic force to the flow. In all cases, the control is only correlated with the LES over a few grid points, reinforcing that the controller is solving the optimization problem locally. The highest correlations in Table 5.1 are realized with spatial distributions involving only one strong peak, as shown for ϕ^u and $\partial u/\partial x$ in Fig. 5.9 and ϕ^w and ω_y in Fig. 5.10. This suggests that a feedback controller based on these quantities may be effective, although further work remains to develop a feedback law independent of a particular simulation.

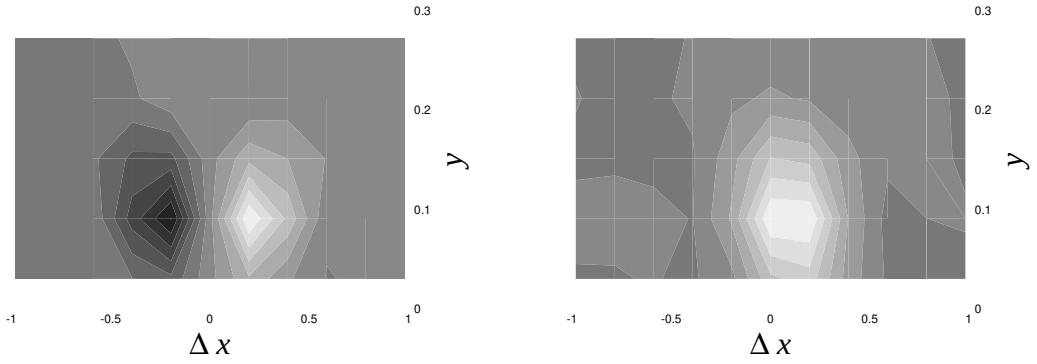

Figure 5.7: Wall-normal spatial distribution of the correlation coefficients for u': coefficients for ϕ^u (left) and ϕ^w (right) at $\Delta z = 0$. The scale range is $\pm.046$ for ϕ^u and ± 0.36 for ϕ^w, with white being a large positive value and black a large negative value. The domain is ± 5 points in the streamwise direction and 5 points in the wall-normal direction.

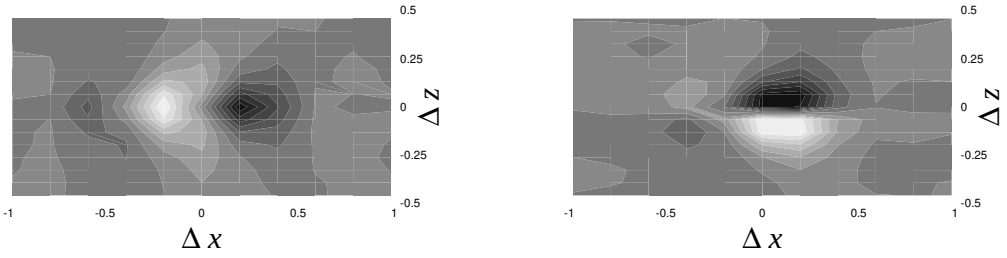

Figure 5.8: Wall-parallel spatial distribution of the correlation coefficients for v: coefficients for ϕ^u (left) and ϕ^w (right) at $y/h = 0.12$ (second wall-normal cell). The scale range is ± 0.28 for ϕ^u and ± 0.19 for ϕ^w, with white being a large positive value and black a large negative value. The domain is ± 5 points in the streamwise direction and ± 6 points in the spanwise direction.

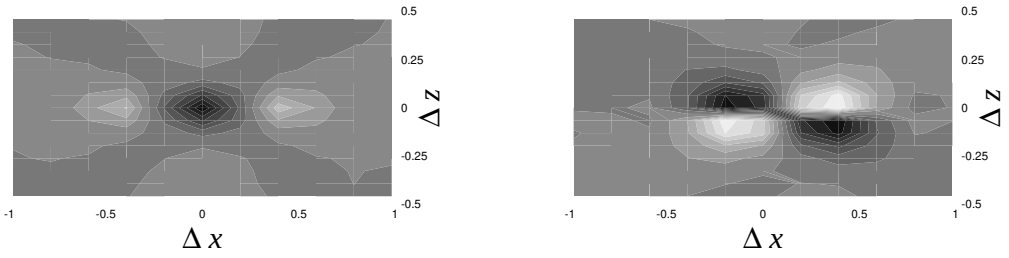

Figure 5.9: Wall-parallel spatial distribution of the correlation coefficients for $\partial u/\partial x$: coefficients for ϕ^u (left) and ϕ^w (right) at $y/h = 0.09$ (second wall-normal point). The scale range is ± 0.59 for ϕ^u and ± 0.26 for ϕ^w, with white being a large positive value and black a large negative value. The domain is ± 5 points in the streamwise direction and ± 6 points in the spanwise direction.

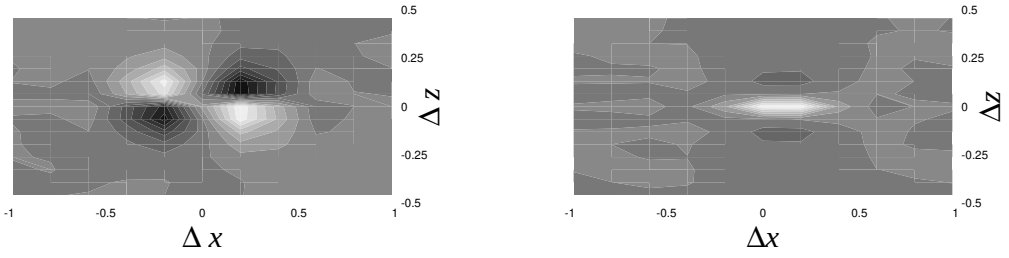

Figure 5.10: Wall-parallel spatial distribution of the correlation coefficients for ω_y: coefficients for ϕ^u (left) and ϕ^w (right) at $y/h = 0.09$ (second grid cell). The scale range is ± 0.17 for ϕ^u and ± 0.59 for ϕ^w, with white being a large positive value and black a large negative value. The domain is ± 5 points in the streamwise direction and ± 6 points in the spanwise direction.

These correlation results have implications in terms of applying the methodology developed here to more complex flows. First, the fact that the correlations all peak near the wall demonstrates that the near-wall construction is indeed appropriate. Tests have been performed using a cost function that includes the entire domain and the structure of the correlation coefficients is almost identical to those shown here. In addition to their wall-normal extent, the streamwise and spanwise correlation lengths suggests that local averaging may be sufficient in flows with no homogeneous directions. These lengths (measuring approximately ± 3 grid points in each direction) can be used to define the averaging operator needed in the cost function formulation while still supplying the controller with the information it requires.

5.4.2 Structure of the Near-Wall Flow

While the correlations presented in the previous section yield some information about how the control responds to the flow, it is also useful to compare instantaneous flow realizations between controlled and uncontrolled cases. The most striking observation is that very little appears to be qualitatively different between simulations using the algebraic model of Wang and Moin (2002) and the control-based framework presented here. This qualitative comparison is demonstrated in the streamwise velocity fluctuations at the first wall-normal plane; contour plots are presented in Fig. 5.11 and show that the near-wall structures have similar spatial scales and organization in both simulations. This indicates that much of the dynamics occurring near the wall in wall modeled simulations is qualitatively independent of the wall boundary conditions. Figures 5.12 and 5.13 show that regions of high streamwise velocity are located near regions of intense streamwise vorticity and wall-normal velocity. This is in contrast to results using stochastic forcing models (Mason and Thomson, 1992; Piomelli *et al.*, 2003) in which the flow appears much more de-correlated. In the present approach, the control does not randomly force the flow but manipulates it specifically because, through the adjoint equations, it is based on the dynamics of the simulation.

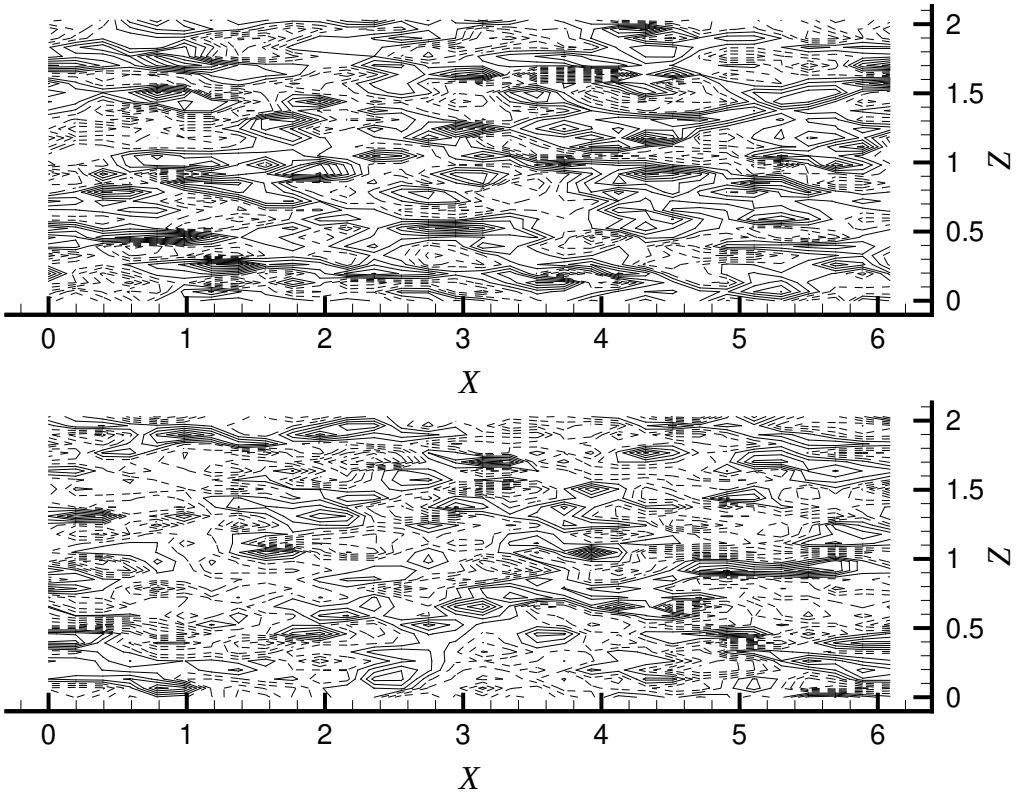

Figure 5.11: Contours of the streamwise velocity fluctuations at the first wall-parallel plane with control (top) and without control (bottom). Contour levels are from $-9u_\tau$ to $13u_\tau$ for the controlled case and from $-8u_\tau$ to $10u_\tau$ for the uncontrolled case with dashed lines representing negative values.

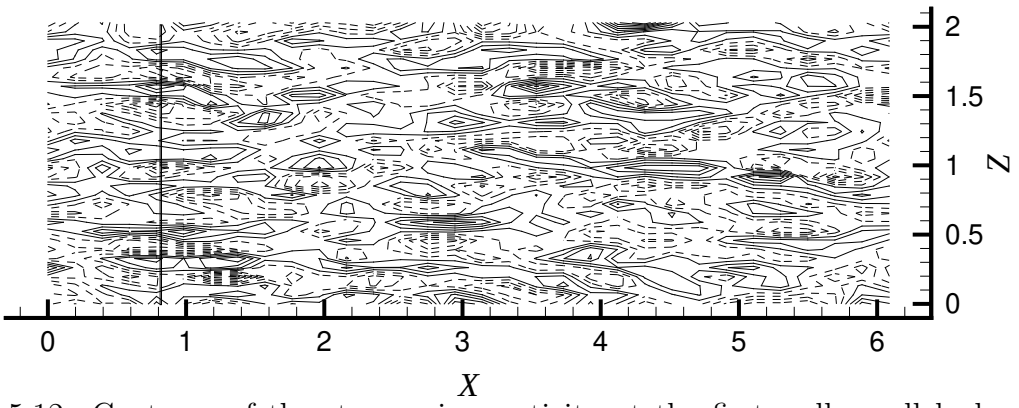

Figure 5.12: Contours of the streamwise vorticity at the first wall-parallel plane with control. Contour levels are from $-134u_\tau/h$ to $203u_\tau/h$ with dashed lines representing negative values.

Many of the features presented in Figs. 5.11 - 5.13 appear qualitatively similar to those observed in resolved lower Reynolds computations (Moin and Kim, 1982). However, the structures in wall-modeled computations are far too large and do not accurately represent the physics of near-wall turbulence. This is primarily due to the grid spacing as the spanwise width of each grid cell is over twice the minimal channel spacing required for self sustaining turbulence (Jimenez and Moin, 1991), and therefore the small near-wall dynamics that contribute to wall turbulence are not resolved. Since the structures cannot realize their correct size, they take on spanwise widths of one or two grid cells. Differentiating the field, to determine quantities such as vorticity, can similarly not recover the underlying physics because the grid is too coarse to support accurate derivatives. Rather, these quantities should be used to understand the dynamics of coarse simulations

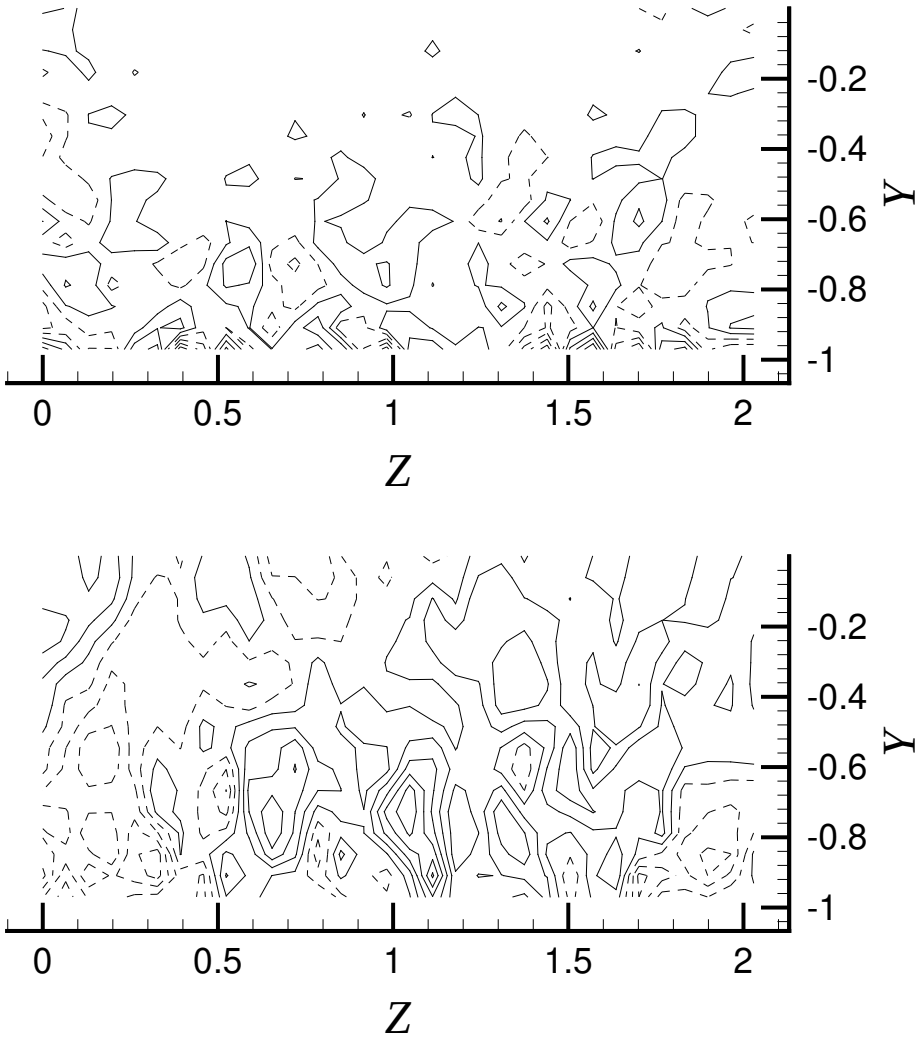

Figure 5.13: Contours of the streamwise vorticity and wall-normal velocity corresponding to the line in Fig. 5.12. Contour levels are from $-134u_\tau/h$ to $203u_\tau/h$ for the streamwise vorticity and from $-3u_\tau$ to $4u_\tau$ for the wall-normal velocity with dashed lines representing negative values.

since these derivatives are used in the governing equations. Therefore the resulting structures are most affected by the grid resolution rather than the wall model.

There is one important way in which the streamwise velocity fluctuations do depend on the control. Without control, the fluctuations are nearly symmetric about zero with a maximum amplitude of approximately $\pm 10 u_\tau$. When the control is activated, the lower bound remains constant while the upper bound increases almost 40%. This affect can be visualized by plotting both contours using the scale of the results without control. As shown in Fig. 5.14, this scaling exaggerates the high-speed regions. While the actual spatial scales of these regions do not vary, the control increases their intensity and results in a velocity distribution that is less symmetric than the uncontrolled case. Because of the underlying dynamics of the simulation, this also results in an increase of intensity of the streamwise vorticity and wall-normal velocity.

To examine this aspect of the control in more detail, comparisons of the wavenumber energy spectra of the streamwise velocity for the control-based wall model and that of Wang and Moin (2002) are presented in Fig. 5.15. In both figures, the spectra are normalized by the square of the streamwise velocity fluctuations to determine how the energy distribution changes with wave number. Very little difference is observed between the two simulations in the streamwise spectra. The spanwise spectra are very flat compared to a resolved computation, which is caused by the poor resolution of this grid. There is apparently a shift of energy from low to high wavenumbers caused by the control. In addition, the two-point correlation functions of the streamwise velocity in both wall-parallel directions are shown in Fig. 5.16. In both the controlled and uncontrolled cases, these correlations are similar, again suggesting that the control does not change the size of the near-wall features.

The data implies that the relevant small scale in these simulations is the grid spacing rather than one determined by the physics. To investigate this issue, a controlled simulation was performed on a grid consisting of $64 \times 65 \times 64$ uniformly distributed cells; double the resolution of the previous simulations in each direction.

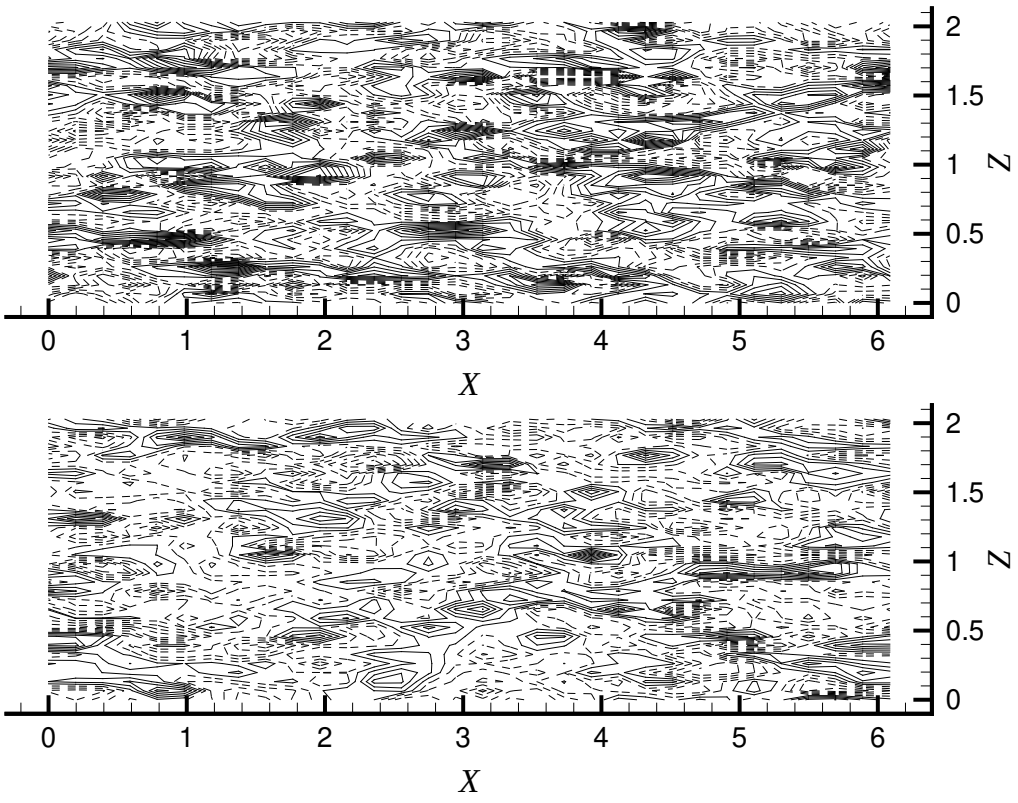

Figure 5.14: Contours of the streamwise velocity fluctuations at the first wall-parallel plane with control (top) and without control (bottom). Contour levels are from $-8u_\tau$ to $10u_\tau$ on both plots with dashed lines representing negative values.

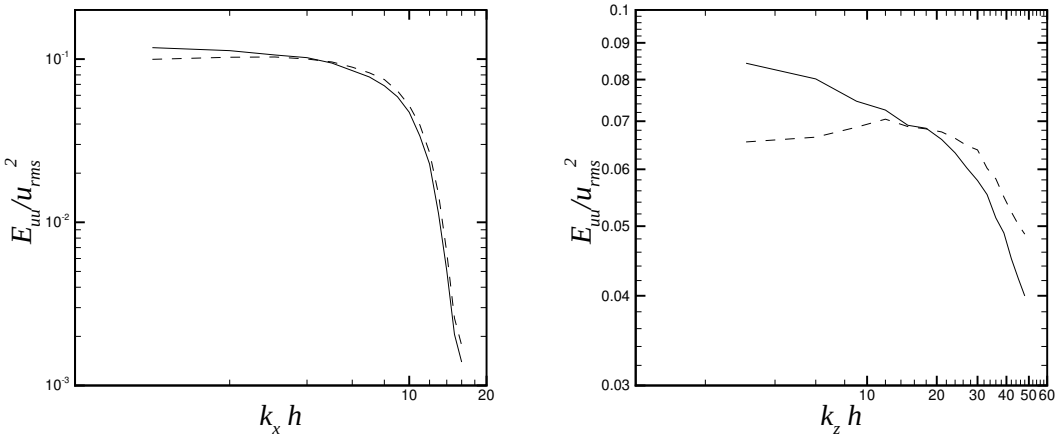

Figure 5.15: Energy spectra of the streamwise velocity in the streamwise (left) and spanwise (right) directions at the first wall-parallel plane: ——— : no control, - - - - : control.

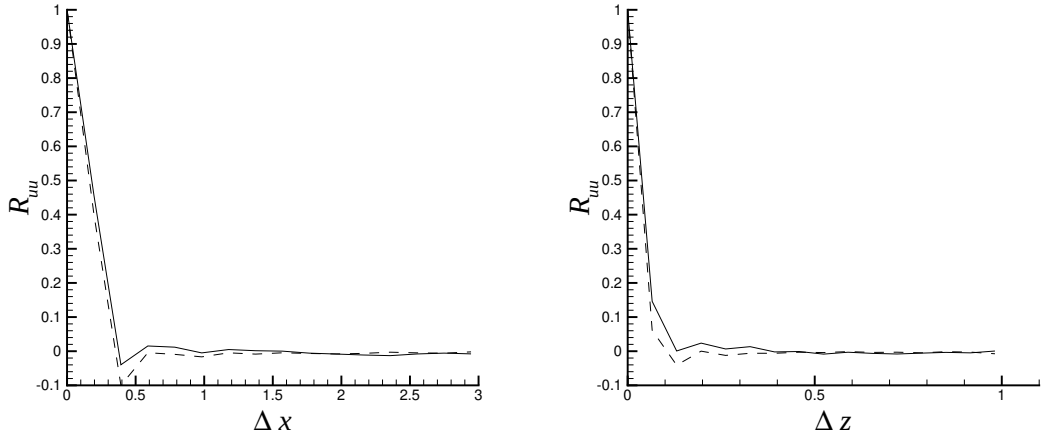

Figure 5.16: Two-point correlation function of the streamwise velocity in the streamwise (left) and spanwise (right) directions at the first wall-parallel plane: ——— : no control, - - - - : control.

Figure 5.17 shows the contours of the streamwise velocity fluctuations in the first wall-parallel plane. The structures are qualitatively similar to those on the coarser grid, except they appear finer. This observation is confirmed by the streamwise and spanwise two-point correlation functions of the streamwise velocity, presented in Fig. 5.18. In both directions, the structure size is reduced by half when the grid spacing is doubled. Wall-normal velocity contours, presented in Fig. 5.19, also demonstrate the same trend. Note that, consistently, the size of the structures increases with the wall-normal distance.

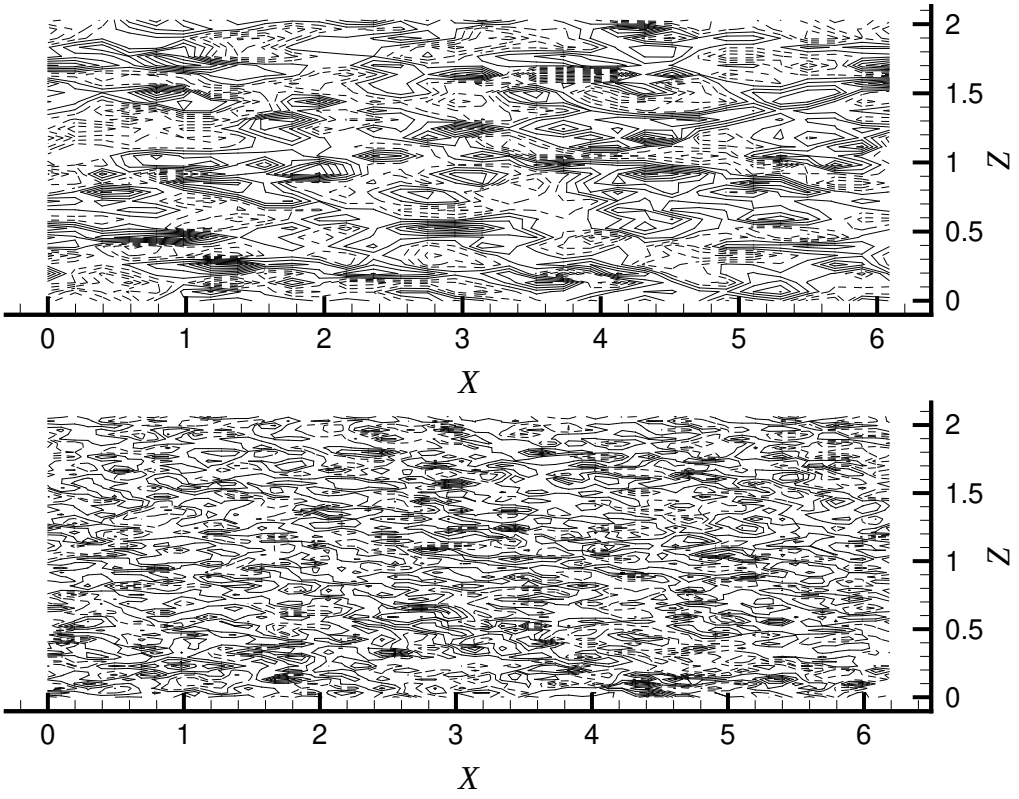

Figure 5.17: Contours of the streamwise velocity fluctuations at the first wall-parallel plane with control on a grid with $32 \times 33 \times 32$ cells (top) and on a grid with $64 \times 65 \times 65$ cells (bottom). Contour levels are from $-9u_\tau$ to $13u_\tau$ in both cases with dashed lines representing negative values.

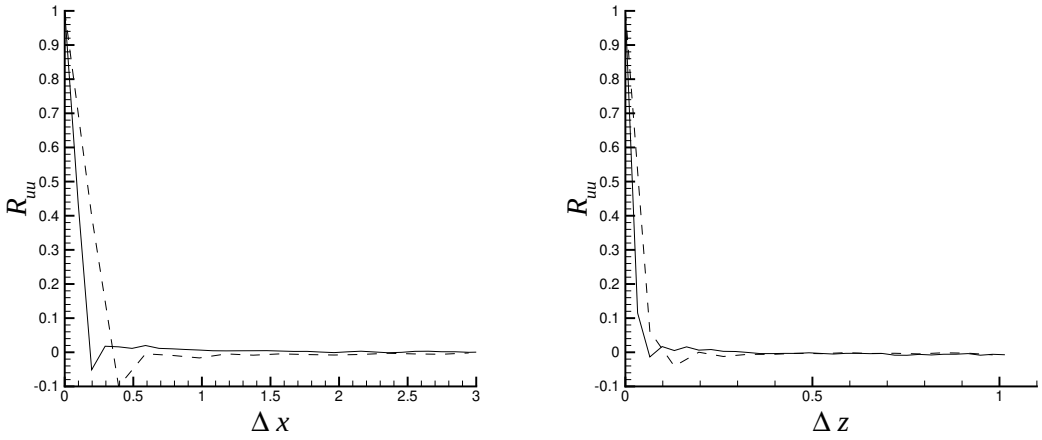

Figure 5.18: Two-point correlation function of the streamwise velocity in the streamwise (left) and spanwise (right) directions at the first wall-parallel plane: —— : $64 \times 65 \times 64$ cells, - - - - : $32 \times 33 \times 32$ cells.

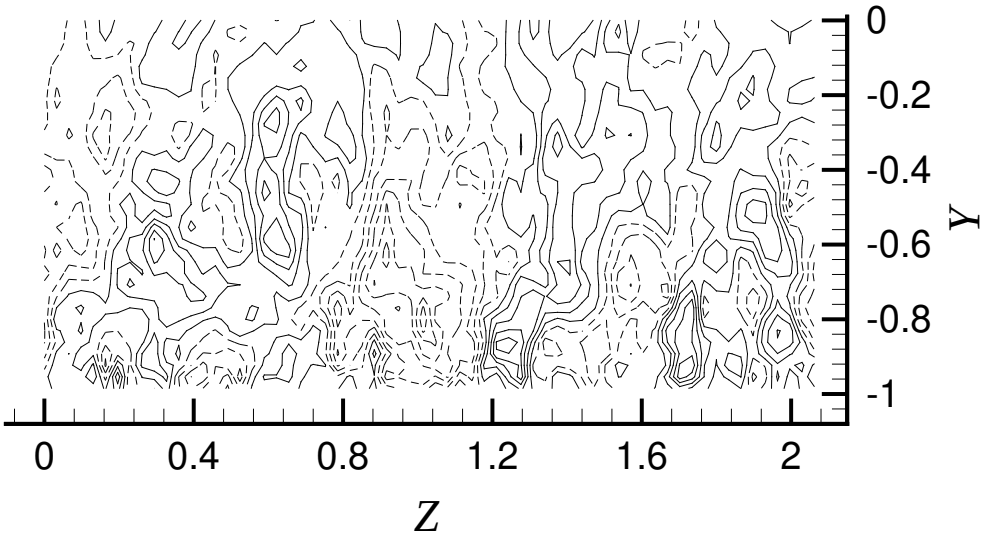

Figure 5.19: Contours of the wall-normal velocity in a streamwise plane on a grid with $64 \times 65 \times 65$ cells. Contour levels are from $-4u_\tau$ to $4u_\tau$ with dashed lines representing negative values.

Chapter 6

Conclusions and Future Work

The two primary goals of this work were to reduce the computational expense of the optimal control wall stress model and to develop a predictive model based on this framework. Both of these goals have been accomplished for high Reynolds number plane channel flow. The method has been shown to produce accurate results over a range of Reynolds numbers and is grid independent. This represents a significant advance in control-based LES wall modeling.

This work has confirmed the results of previous efforts indicating that wall models must compensate for numerical and SGS modeling errors that are present when LES is performed on coarse grids. Many earlier wall models had focused solely on compensating for the unresolved physics, and these have been shown to be inadequate on a coarse grid. A wall model that has proven able to compensate for all three types of errors is the control-based wall modeling studied in this work. The earlier version of this method was unattractive because it was computationally expensive and not predictive due to the fact that the target velocity profiles had to be prescribed.

With the control-based wall model developed in this work, the computational expense has been reduced from $O(10)$ times that of the LES part of the calculation to $O(1)$. Reducing the expense has the additional effect of making the method easier to implement. The most important aspect is to avoid solving the optimization method throughout the entire domain. It has been shown that most of this effort

is wasted, and the prediction of the mean velocity profile remains accurate when solving both the adjoint and LES equations only near the wall in the optimization procedure. Further approximations to the implicit solutions for wall-normal diffusion and the pressure have also contributed to cost reduction without affecting the accuracy of the solution.

The final aspect of reducing the computational expense is to reconsider the derivation of the adjoint equations. Previous work had assumed a form for the adjoint equations based on a Crank-Nicolson numerical technique. There is no *a priori* justification for such a choice. Often, the issue is whether the adjoint equations are derived directly from the discrete system or instead descretized after being derived from the continuous system. While the latter is always more accurate, when an efficient numerical technique is required, the additional expense and complexity of such an approach is often not worth the modest improvement in cost function reduction rate. Since we are already approximating the cost function solution, and since the actual quantity of interest is the time-averaged mean velocity profile, it is reasonable to choose the adjoint system with the computational cost, rather than maximum accuracy, as the primary consideration.

The choice of the discretization is tied directly to the definition of the cost function. It has been demonstrated that defining this function based on the terminal time rather than as a time integral, results in a system that is more robust with respect to temporal discretization. Thus, the adjoint equations are discretized using an explicit Euler scheme. By using such a strategy, the method has been made significantly more computationally tractable.

The other outstanding issue of previous control-based wall models is the reliance on targets chosen *a priori*, making them not predictive. It has been demonstrated in this work that velocity profiles obtained from RANS can be used to determine the targets dynamically during the simulation. However, coupling the RANS solution to the LES presents several difficulties. The primary issue is that the controller can manipulate both the LES and RANS solutions if they are coupled incorrectly.

By coupling the RANS with the controller to set the mean wall stress, the LES

and RANS solutions can be made compatible. This prevents the controller from manipulating the mean wall stress to reduce the cost function by producing an unphysical LES computation. It has been shown that such a coupling results in a simulation as accurate as those which use a fixed target profile.

Given that a wall model has been developed which is computationally simple, efficient, and predictive, many directions for future work are available. One is to apply this method to more complex flows. By using more general near-wall RANS treatments and coupling them to the controller, the techniques presented in this work can be extended to flows in complex geometries. Because of the thin nature of the wall layer, the curvature effects can often be neglected, and the near-wall region can often be approximated as flat plate flow. However, the averaging operation in complex geometries is less clear since there is often no homogeneous direction. The correlation coefficients presented in Chapter 5 demonstrate the the control only responds locally to the flow. Therefore, local averages should be used to define the cost function.

Two important areas for future work are that of heat transfer and compressible flows. To extend this method to such situations, a RANS model for heat transfer must similarly be coupled to the system. Such coupling must ensure that the controller cannot artificially manipulate the RANS heat transfer model, as this type of coupling has proved detrimental in the LES momentum equations. A similar approach must be taken for compressible flows, with RANS models providing the mean distribution of both momentum and thermodynamic variables near the wall. The control-based wall model can then be used to ensure that the LES solution matches the RANS solution near the wall. The mean values for all variables based on the RANS model will have to be used to match the corresponding LES variables at the wall to correctly couple the two simulations.

In addition to these areas, further work will be needed for complex physics simulations where the fluid mechanics represent only part of the problem. One example where wall modeling has already been utilized is in aero-acoustics. While acoustic propagation far from a body can be computed using the Lighthill analogy

with the solution of only the momentum equations, a wall model coupled with a model for near-wall pressure fluctuations could be used to obtain even more accurate information about the acoustic field. Another interesting application would be to use a control-based wall model in flows used for aero-optics investigations. In these flows, the proper affect of the turbulence on the optical propagation must be modeled near the wall since, as was shown in this study, the fluctuations in this region must be enhanced to obtain a correct prediction of the outer flow. Once this model is applied to the optics, the outer flow propagation of the optical beam can be handled using wall modeled LES. Such a method would allow aero-optical computations to be performed at Reynolds numbers of engineering interest.

Appendix A

On the Use of the Method of Incomplete Sensitivities to Generate Wall Models

A.1 Introduction

Large-eddy simulations (LES) of high Reynolds number flows are difficult to perform due to the need to include a large number of grid points in the near wall region. While LES models the small scales of the flow and resolves the large, dynamically important scales, near the wall, eddies scale with the distance from the wall and move increasingly nearer to the wall as the Reynolds number increases. These eddies are dynamically important despite their small size. Unfortunately, the eddy viscosity sub-grid scale (SGS) models only make a small contribution to the total Reynolds stress. This makes these models invalid near the wall Jimenez and Moser (2000), unless the LES grid is sufficiently refined to resolve the near-wall vortical structures. Therefore, the number of grid points for an LES scales as Re_τ^2 in an attached boundary layer Baggett *et al.* (1997). This is only a slight improvement on the scaling for a full direct numerical simulation (DNS) of $Re^{9/4}$.

The technique of wall modeling was developed to reduce the Reynolds number

scaling of LES resolution so that LES could be applied in practical situations. For recent reviews, see Cabot and Moin (2000) and Piomelli and Balaras (2002). The approach has a long history dating back to atmospheric science and oceanographic applications. Limited by the computational power of the time, Deardorff (1970) was the first to implement a model for the wall layer in an LES of a channel flow at infinite Reynolds number. He implemented constraints on wall-parallel velocities in terms of the wall-normal second derivatives to ensure the LES satisfied the log-law in mean. The wall transpiration velocity was set to zero. The first "modern" wall model was developed by Schumann (1975). It is a modern wall model in the sense that the wall stresses are determined directly by an algebraic model. The wall stresses were found by assuming that they were in phase with the velocity at the first off wall grid point and that the deviation from their mean was proportional to the deviation of the velocity from its mean. Since the flow was in a channel, both the mean wall stresses and mean velocities were known. The transpiration velocity was set to zero. Many improvements to this basic model have been proposed and tested, see e.g. Piomelli *et al.* (1989), Mason and Callen (1986), Grötzbach (1987), and Werner and Wengle (1991), although none of these attempts produced a wall model robust enough for use in most engineering flows.

To address this robustness issue in wall modeling, several investigators used more elaborate near-wall flow models to compute the wall stresses (see e.g. Balaras *et al.* (1996) and Cabot and Moin (2000)). This type of approach divides the computational domain into two regions: one near the wall and one away from the wall. A simplified set of equations based on turbulent boundary-layer (TBL) approximations are solved on a near wall grid seperate from the outer LES grid, subject to boundary conditions determined from the outer LES velocity together with the no-slip wall. The computed wall stress is then provided to the LES as a boundary condition. While this method does require the solution of an extra set of equations, the simplifications made in these equations makes its cost much less than the evalutaion of the LES equations. This method was tested in a plane channel, square duct, and rotating channel by Balaras *et al.* (1996) and in a plane channel

and backward-facing step by Cabot and Moin (2000). More recently, Wang and Moin (2002) used a variant of this method to perform an LES of an airfoil trailing edge flow. The results are generally better than those of the algebraic models, since the TBL equations can account for more of the physics of the flow. However, there is insufficient evidence of robustness of this approach, particulaly on coarse meshes and at high Reynolds numbers.

The difficulty of formulating a robust wall model was highlighted by Cabot (1996). In that work, a backward facing step LES was performed using the "exact" time series of the wall stress from a resolved LES as the wall model. The results of this approach were not satisfactory and in fact not an improvement over the other types of wall models previously mentioned. This indicates that SGS and numerical errors play an important role in the coarse grid LES, which has not been accounted for by the previous wall models. To investigate this hypothesis and determine what information a wall model must provide to the LES, Nicoud *et al.* (2001) used optimal control techniques to compute the wall stresses in a channel LES at $Re_\tau = 4000$. A cost function was defined to be the difference between the plane-averaged LES streamwise and spanwise velocity fields and their known mean values (log-law in the streamwise direction and zero in the spanwise direction). Adjoint equations were used to determine the cost function derivatives, and iterations were performed at each time step to determine the best wall stress. Since the iterations were not performed over a large time window, this approach was sub-optimal. Linear stochastic estimation (LSE) was then used to determine a feedback law for the wall stresses based on their correlation with LES velocities obtained from the sub-optimal control algorithm.

Many important lessons were learned from this work involving wall models based on optimal control theory. Unfortunately, this approach proves to be impractical due to the high computational cost required for the suboptimal control since it requires both the solution of adjoint equations and many iterations to achieve convergence in the wall stresses. Furthermore, the cost function is based on known

target data, making the model non-predictive. Baggett *et al.* (2000) also demonstrated that the LSE models generated from such computations are too senstive to the numerical parameters to construct a universal LSE coefficient database. The objective of the present work is to develop a low-cost, robust wall model to achieve the accuracy of the sub-optimal control technique without an *a priori* target solution. A cost function based on a Reynolds-averaged Navier Stokes (RANS) solution will be constructed in Section A.2 to make the model predictive, and in Section A.3, the problem will be formulated in an optimal shape design setting in an attempt to reduce the computational cost. Some test results and discussions are presented in Sections A.4 and A.5. This work originally appeared as Templeton *et al.* (2002).

A.2 Cost function

In order to make the wall model predictive, an easy to evaluate cost function near the wall using quantities not known *a priori* must be defined. To this end, a RANS model is used to provide the target velocity. This is motivated by the recognition that the near-wall region of a high Reynolds number boundary layer is more appropriately modeled by RANS than by a coarse grid LES with filter length larger than the integral scale of the turbulence.

In the present work, the RANS model is obtained from a simplified version of the TBL equation model used by Wang and Moin (2002):

$$\begin{aligned} &\frac{d}{dy}\left[\left(\nu+\nu_t\left(y\right)\right)\frac{du_i}{dy}\right]=\frac{1}{\rho}\frac{\partial p}{\partial x_i}\bigg|_{\text{LES}}, \quad i=1,3 \\ &\nu_t\left(y\right)=\kappa\nu y^+\left(1-e^{-y^+/A}\right)^2, \quad y^+=yu_\tau/\nu. \end{aligned} \tag{A.1}$$

These equations model all Reynolds stresses through a damped mixing length eddy viscosity, and explicitly account for the pressure gradient which is assumed constant across the wall layer and is imposed by the LES. To complete the model, a no slip condition is applied at the wall and the outer boundary is set to be the LES velocity. The resulting velocity profile should be interpreted as the ensemble

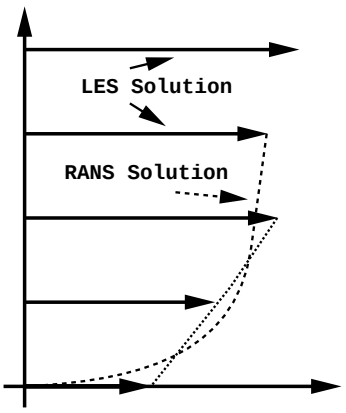

Figure A.1: Diagram of RANS and LES velocities in overlap region.

averaged velocity profile given the local LES state. It can therefore be expected that, on average, the resolved LES should match the RANS solution near the wall. Note that this model is chosen for simplicity in this intial attempt, and there are likely better models for this application that will be explored in future work.

To match the RANS and LES, their grids are produced to overlap at the three LES points closest to the wall, as in Figure A.1. This selection was made to get as many overlap points as possible while remaining in the region where A.1 is a reasonable approximation. Furthermore, the LES velocity too near the wall may well be meaningless Cabot (1996), so using it as a RANS boundary condition could cause the RANS to generate poor results.

In an overlapped region consisting of N LES grid points in the wall-normal direction, cost functions are devised to match the LES and RANS solutions on average. An attractive method in a statistically stationary flow would be to use a running time average to provide the target velocities. However, if the control authority is restricted to the current time, this approach becomes impractical since the flow at the current time would contribute only a small fraction of the total cost function. This makes it difficult to determine the control since the cost function is insensitive to it. If the control is explicitly computed as a function of time, then adjoint equations have to be integrated backward in time to find a correct solution over a sufficiently large time window which contains enough statistical samples.

An alternative is to use the current state as the statistical sample. Thus, the first cost function is defined to be the $\mathcal{L}_2$ difference between the LES and RANS states:

$$J_{\mathcal{L}_2} = \int_S \sum_{n=1}^{N} \left(\left(u_{\mathrm{RANS},1}|_{y_n} - u_{\mathrm{LES},1}|_{y_n} \right)^2 + \left(u_{\mathrm{RANS},3}|_{y_n} - u_{\mathrm{LES},3}|_{y_n} \right)^2 \right) dS, \qquad \text{(A.2)}$$

where S is the surface and y_n are the locations of the n overlap points. In this way, a sufficient number of samples of the flow state are used to make a meaningful average. Also, the cost function is based only on quantities at the current time step, so no history information is required. This type of cost function is also compatible with the gradient evaluation methods used in this work (see Section A.3).

Other cost functions can also be formulated for this problem. A cost function based on the average deviation of the LES and RANS is:

$$J_A = \left(\int_S \sum_{n=1}^{N} \left(\left(u_{\mathrm{RANS},1}|_{y_n} - u_{\mathrm{LES},1}|_{y_n} \right) + \left(u_{\mathrm{RANS},3}|_{y_n} - u_{\mathrm{LES},3}|_{y_n} \right) \right) dS \right)^2. \qquad \text{(A.3)}$$

This cost function is similar to that used by Nicoud *et al.* (2001). However, as shown in Section A.4, this cost function performs quite poorly. Analysis of its gradients indicates that they do not capture the sign information correctly in some regions (gradient computation will be discussed in the next section). In order to retain more information and move in the direction of feedback control, a signed cost function has also been used:

$$J_S = \int_S \sum_{n=1}^{N} \left(\left(u_{\mathrm{RANS},1}|_{y_n} - u_{\mathrm{LES},1}|_{y_n} \right) + \left(u_{\mathrm{RANS},3}|_{y_n} - u_{\mathrm{LES},3}|_{y_n} \right) \right) dS. \qquad \text{(A.4)}$$

When this cost function is used, the control strategy is shifted to force the cost function to zero rather than minimizing it. It was thought that this approach might better take advantage of the method being used for gradient evaluation, but it only resulted in a moderate improvement (see Section A.4)

The choice of N in (A.2) - (A.4) should be made to include as many matching

layers as possible while remaining in the region where the RANS model is a reasonable approximation for the given local flow. Furthermore, the LES velocity too close to the wall may involve large errors Cabot (1996) and thus is not suitable as a RANS boundary condition. In the calculations presented in this article, N has been chosen to be three.

Two important points should now be noted. First, while all the cost functions here are based on matching RANS and LES velocities, other quantities could also be used. These could include matching vorticity or energy fluxes with suitable models. Second, it may not be possible or desirable to reduce the cost function to zero. Doing so could artificially reduce the turbulence fluctuations of the flow. Also, if an inexpensive scheme is required, it may not be possible to fully optimize the solution. Thus, the cost function must act as a suitable quantity for feedback regulation, rather than for minimization.

A.3 Optimization using shape design techniques

Optimal shape design consists of a set of techniques for optimizing a shape to achieve an engineering objective (e.g. Mohammadi and Pironneau (2001)). Several approaches have been developed in this field that have had some success in reducing the computational expense of the optimization procedure. In an attempt to bring these techniques to bear, the wall modeling problem is formulated in this framework.

In general, the formulation is to consider a partial differential equation $A(U,q,a) = 0$ in a region Ω satisfying boundary conditions $b(U,q,a) = 0$ on $\partial\Omega$. The optimization is performed to determine

$$\min_a \{J(U,q,a) : A(U,q,a) = 0 \,\forall x \in \Omega, b(U,q,a) = 0 \,\forall x \in \partial\Omega\} \tag{A.5}$$

for some cost function $J(U,q,a)$. In this formulation, U is the state, q the shape, and a are the control variables. The gradient of the cost function with respect to

the control variables is then:

$$\frac{dJ}{da} = \frac{\partial J}{\partial a} + \frac{\partial J}{\partial q}\frac{\partial q}{\partial a} + \frac{\partial J}{\partial U}\frac{\partial U}{\partial q}\frac{\partial q}{\partial a}. \tag{A.6}$$

The standard technique for solving this equation is to use an adjoint method interfaced with a gradient minimization technique. But, as previously noted, this can be expensive and present data storage difficulties in time-accurate computations. Since it is the last term in (A.6) that requires the adjoint evaluation, Mohammadi and Pironneau (2001) suggest the following assumption when the controls and the cost function share the same support:

$$\frac{dJ}{da} \approx \frac{\partial J}{\partial a} + \frac{\partial J}{\partial q}\frac{\partial q}{\partial a}. \tag{A.7}$$

This assumption is called the method of incomplete sensitivities since the sensitivity to the state gradient is ignored. The use of this method has been explored in this work since it has produced positive results in the optimization of aerodynamic shapes. For examples, see Mohammadi (1999), Mohammadi *et al.* (2000), and Mohammadi and Pironneau (2001), although these are all steady, two-dimensional applications. Since no rigorous proof on the applicability of this technique exists and its usefulness is based on purely empirical studies, it was not known how well it would perform in a full LES. Furthermore, the present cost function is not defined exactly on the support of the control, although it is defined in a small neighborhood of the control. While these factors will produce errors, the gradient evaluation needs only accurately predict the sign of the gradient and capture to some degree the difference in magnitudes of the derivatives with respect to different control parameters. A goal of this work is to determine if the amount of information contained in this gradient is sufficient for application to wall boundary conditions.

In order to apply the incomplete sensitivity assumption, the control must be related to shape design parameters. B-splines spaced evenly along the surface (although not enough to form a complete basis) are used to parameterize deformations normal to the surface. The control parameters, a_i, are then the spline amplitudes.

The gradient of the cost function with respect to these parameters can be computed using finite differences by perturbing each parameter by a small value, ϵ, and then using (A.7) to evaluate the gradient based on the current state information. It is not necessary to recompute the actual geometry or grid because all the state variables of interest can be stored and matched to the new surface. The parameter ϵ is chosen *a priori* by making it small enough such that the gradient values are independent of it.

Once the cost function gradient is known, the new spline amplitudes can be computed by

$$a_i^{k+1} = a_i^k - \rho \frac{\partial \mathcal{J}}{\partial a_i}, \tag{A.8}$$

where ρ is a descent parameter set in advance and k is the iteration count. The new shape is computed by adding the surface perturbations to the previous shape. To relate this to the wall stresses, the RANS model is used to compute the correction to the equivalent slip velocity on the original surface:

$$u_{w,i}^c = f_{\mathrm{RANS},i}\left(y_{new}\right), \quad i = 1, 3, \tag{A.9}$$

where f stands for the RANS model given by (A.1). This approach is inspired by a Taylor series expansion about the wall Mohammadi and Pironneau (2001). In this way, it is not necessary to change the computational geometry of the LES.

The total slip velocity is given by adding the correction $u_{w,i}^c$ to the old wall slip velocity. Corrected wall stresses can then be computed directly by definition

$$\tau_{w,i} = \tau_{w,i}^o + \frac{1}{Re} \frac{-u_{w,i}^c}{\Delta x_2}, \tag{A.10}$$

where Δx_2 is the local wall normal grid spacing.

While this approach avoids the evaluation of a set of adjoint equations, iterations are still required to converge the solution. Additional function evaluations are also often used to determine an optimal choice for ρ at each iteration. In order to make the wall model practical, these costs must be avoided. Therefore, no iterations are performed at each time step. The cost function gradients are computed and used

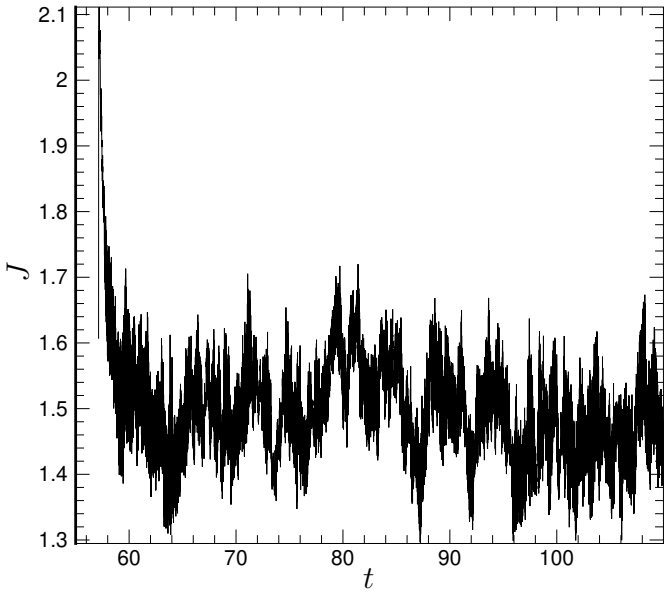

Figure A.2: $\mathcal{L}_2$ cost function history.

in a feedback manner to provide a correction. Every a_i is reset to zero at each time step. Also, ρ is taken to be a fixed parameter similar to the gain in a feedback controller. To make up for some of this lost information, a predictor-corrector approach to the control algorithm is used. This is done by using (A.1) to compute a prediction of the wall stress before the optimization is used. It is expected that the prediction will account for the missing physics in the coarse grid LES while the optimization will correct for the numerical and SGS modeling errors. While this approach must be classified as sub-optimal, it is still reasonable to expect a cost function reduction if at each time step the LES velocity is forced in the direction of the reduced cost function.

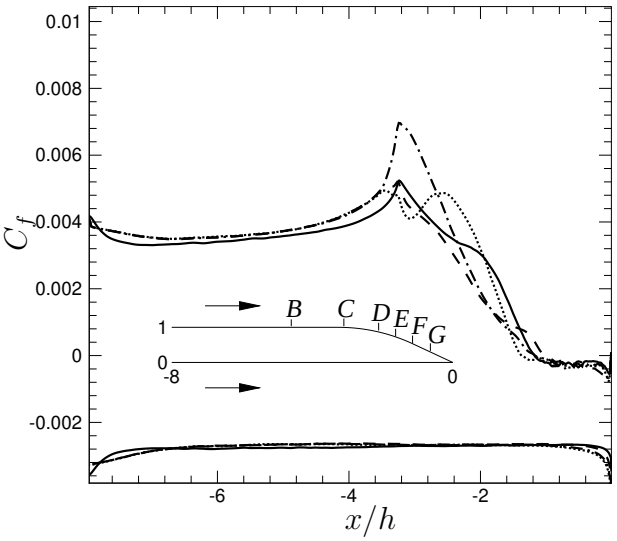

Figure A.3: Time averaged skin friction over the airfoil surface: ---- , $\mathcal{L}_2$ cost function; —·— , average cost function; ····· , signed cost function; —— , full LES of Wang and Moin (2000).

A.4 Results

The application of this method to the trailing edge flow simulated previously by Wang and Moin (2000, 2002) has produced mixed results. The first goal is to justify the incomplete sensitivies assumption. The $\mathcal{L}_2$ cost function history is shown in Figure A.2. While the average value is reduced approximately 15% from the inital value, this is not completely out of the range of the cost function fluctuations. It is therefore inconclusive regarding the validity of the assumption. As shown in Figure A.3, the predicted wall stress matches the full LES wall stress quite well in some regions for the $\mathcal{L}_2$ and signed cost functions, but performs poorly in other regions. The seperation point is predicted reasonably accurately for both these cost functions. As previously indicated, the average cost function performed more poorly. Figure A.4 contains a comparison between the $\mathcal{L}_2$ cost function results and the predictor alone. The new results are much better in the region near the skin friction peak, although they produce a less smooth skin friction profile, and

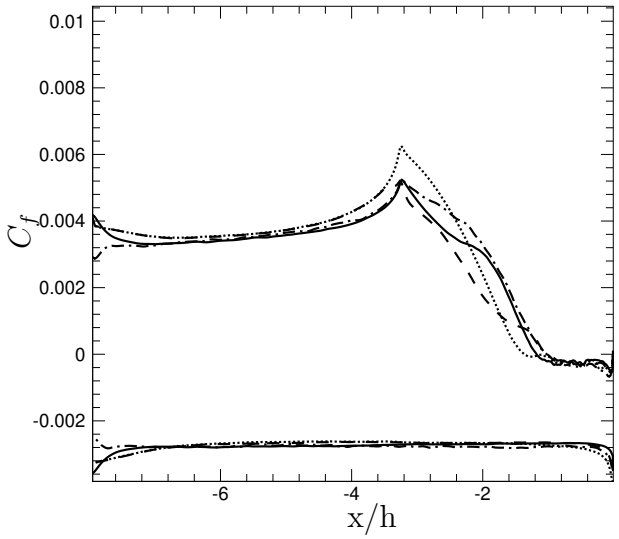

Figure A.4: Time averaged skin friction over the airfoil surface: ---- , $\mathcal{L}_2$ cost function; ····· , predictor only; —— , full LES of Wang and Moin (2000); —·— , TBL model of Wang and Moin (2002).

rather large errors remain in part of the adverse pressure gradient region. Overall, the model demonstrates some improvement over the simple wall model used as a predictor, but is less accurate than the full TBL equation model used in Wang and Moin (2002).

Comparison of the velocities between the full LES and wall modeled LES (based on the $\mathcal{L}_2$ cost function, which produced the best results) are quite good. As shown in Figures A.5 and A.6, the coarse grid LES is able to match the resolved LES very closely. The main (moderate) discrepency occurs in the turbulent intensities near the wall. This is not unreasonable since these quantities were not included in the cost function and it may in fact not be possible to capture these regions accurately because the LES grid does not resolve the intensity peak. When compared to the results of Wang and Moin (2002) using only the predictor, the results are found to be comparable and in fact are worse for the two cost functions not shown. Therefore, it is difficult to draw definitive conclusions about the effect of the gradient based

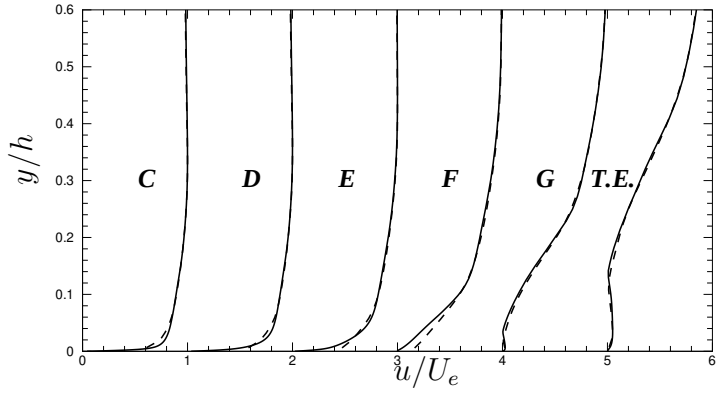

Figure A.5: Mean velocity magnitude profiles at several trailing edge stations: ---- , $\mathcal{L}_2$ cost function; —— , full LES of Wang and Moin (2000). Locations are those indicated in Figure A.3. T.E. is the trailing edge point.

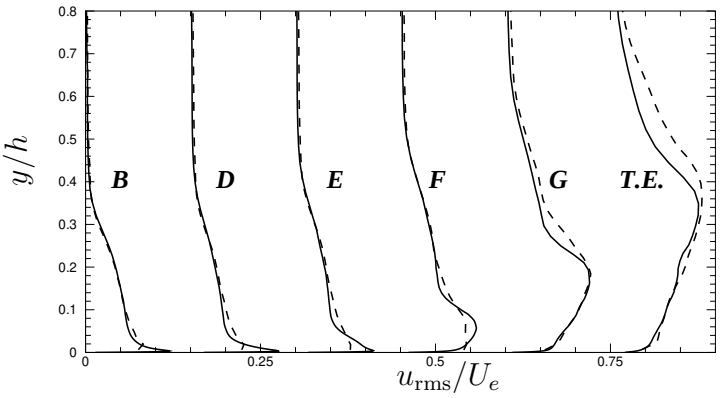

Figure A.6: Streamwise component of turbulence intensities at several trailing edge stations: ---- , $\mathcal{L}_2$ cost function; —— , full LES of Wang and Moin (2000). Locations are those indicated in Figure A.3. T.E. is the trailing edge point.

optimization procedure on the velocity field.

A.5 Channel flow analysis

In order to evaluate the proposed wall model in a more controlled environment, the algorithm has been implemented in the plane channel LES of Nicoud *et al.* (2001). This is a simpler and well known case, so the model can be more readily analyzed. It was immediately noticed that, unlike the trailing edge case, the cost function gradients could not be made independent of the small parameter ϵ used in the finite-difference computation. The gradients monotonically decreased with ϵ until they reached a value of zero. This result indicated that the incomplete sensitivity approach did not accurately capture the gradients in the channel since Nicoud *et al.* (2001) observed non-zero gradients in the sub-optimally controlled channel. The following analysis is used to explain these results, as well as the difficulties encountered with this method in the trailing edge geometry.

Consider a cost function of form

$$J(a) = \int_S f(u(a))dS. \tag{A.11}$$

Since in the current framework, the shape and shape deformations are defined in two dimensions, the surface can be parameterized by taking the y coordinates as a function of x, i.e. $y = g(x)$. Then the cost function becomes

$$J(a) = \int_0^l f(u(x;a))\sqrt{1+g'^2(x)}dx. \tag{A.12}$$

Consider a perturbation to this surface parameterized by $\epsilon h(x)$. In the current context, $h(x)$ would correspond to the spline and ϵ to the small change in the control parameter. The new cost function is computed by considering its sensitivity to geometry only, so

$$J(a+\epsilon) = \int_0^l f(u(x;a))\sqrt{1+(g'(x)+\epsilon h'(x))^2}dx. \tag{A.13}$$

By using a Taylor series expansion, one obtains to $O(\epsilon)$:

$$\sqrt{1+(g'(x)+\epsilon h'(x))^2} \approx \sqrt{1+g'^2(x)} + \epsilon(1+g'^2(x))^{-1/2} g'(x)h'(x). \tag{A.14}$$

When the gradient is computed by taking $(J(a+\epsilon)-J(a))/\epsilon$, the resulting term is

$$\frac{\partial J}{\partial a} \approx \int_0^l f(u(x;a))(1+g'^2(x))^{-1/2} g'(x)h'(x)dx. \tag{A.15}$$

This expression explains the observed cost function gradients. First, it has been demonstrated in both the trailing edge and channel flows that in regions where the surface is flat, the gradients are zero. This is clear since in these regions, $g'(x) = 0$. A similar observation occurs in areas where the surface is a straight line. This is because $g'(x)$ is constant and, in this case, $h(x)$ is symmetric, meaning that whenever $h'(x) > 0$, there is a corresponding x_1 such that $h'(x_1) = -h'(x)$. Thus, unless $f(u(x;a))$ has a very large change between x and x_1, since $g'(x)h'(x) + g'(x_1)h'(x_1) = 0$ the gradient will be very small.

Finally, it has been observed that in regions of curvature away from the direction of perturbation and for a positive definite $f(u(x;a))$ (such as the $\mathcal{L}_2$ cost function), the gradient is always positive. This can be seen by examining the product $g'(x)h'(x)$. In these regions, $g'(x)$ is always negative and increases monotonically in magnitude. By the symmetry of $h(x)$, the regions where $h'(x)$ is positive correspond to $g'(x)$ having a smaller magnitude, and the regions where $h'(x)$ is negative correspond to $g'(x)$ having a greater magnitude. Thus, the positive contribution is greater in magnitude than the negative contribution, and hence the gradient is positive since $f(u(x;a))$ is positive and varies less than the curvature.

The sensitivity computed by this method is then almost exclusively dependent on the curvature of the function whose information is contained in $g'(x)$. It is difficult to determine how this information could be useful in changing the state u such that the given cost function is minimized in a rigorous and well defined manner. For any cost function defined as above, the incomplete sensitivity method will act in a way directly related to the curvature of the surface. If a correlation

exists between reducing this curvature and reducing the cost function, the method may produce reasonable results. However, there is no reason to believe that, in general, reducing surface curvature will be helpful in wall modeling. In fact, as experience in the channel has demonstrated, a region of no curvature still requires control to obtain an accurate solution. Therefore, it is likely that an alternative method must be found for the general application of a wall model.

A.6 Conclusions and future work

Wall modeling using control theory is a promising new approach for developing robust wall models which account for not only the unresolved flow physics but also numerical and SGS modeling errors. In the present work, a methodology has been proposed to overcome the deficiencies of the model of Nicoud *et al.* (2001) and make the control-based wall model predictive and practical in terms of computational expense. Two critical components, namely the use of RANS velocity profiles as the near-wall LES target in the cost function and the incomplete sensitivity method for gradient evaluation have been examined and tested in a turbulent trailing edge flow.

Based on the results, it is clear that the assumption of incomplete sensitivities is not appropriate for LES wall models with the type of cost function considered in this work. This is at least partly due to the cost function measuring the LES state in the flow and not at the wall. A cost function that is more sensitive to the geometry could be better suited, but it is unclear how to formulate such a cost function for a wall model. Furthermore, there is evidence suggesting that in applications similar to this, the gradient calculated with incomplete sensitivities may have not only incorrect magnitude but also incorrect sign Marsden (2004). Clearly, a more accurate means is needed to compute the gradient.

The use of a cost function matching a RANS profile near the wall may however prove useful in LES wall modeling. It has a solid physical basis, although the RANS model used here is rather rudimentary. More robust RANS models, such the k-ω

model are being considered. In addition to choosing an appropriate RANS model, the choice of matching quantities is also an important factor in the performance of the model. Matching LES and RANS velocities may prove not to be the best quantity to minimize for optimal performance of the model. Cost functions based on vorticity or energy could better account for dynamics that are more important to the large scales in the LES. An investigation of these cost functions and implementation of a RANS model is underway in a channel flow.

Appendix B

Unsuccessful Control Formulations

In this work, several approaches were used that did not result in accurate predictions of the mean velocity profile. This appendix describes these methods and presents analysis as to why they were ineffective. The first control formulation considered is the optimal control scheme described in Chapter 4 modified to use the RANS velocity profile as the target. In this case, the mean profile is severely under-predicted, as shown in Fig. B.1. In fact, the computation was terminated before a statistically steady state was reached since the mean velocity profile continued to decline. Examination of the cost function data revealed that the cost function was also steadily decreasing, indicating that the control algorithm was functioning correctly. The result can be understood via a more thorough examination of δ.

In this case, the coupling between the RANS state and the LES occurs through boundary conditions that match the RANS and LES velocities at y_m. Therefore, δ_u can be rewritten as

$$\delta_{u_i}(y,T) = \frac{1}{A}\int\int u_{i,\mathrm{LES}}(x,y_m,z,T) \left(\frac{u_{i,\mathrm{LES}}(\vec{x},T)}{u_{i,\mathrm{LES}}(x,y_m,z,T)} - \frac{u_{i,\mathrm{RANS}}(\vec{x},T)}{u_{i,\mathrm{LES}}(x,y_m,z,T)}\right) dx\,dz. \tag{B.1}$$

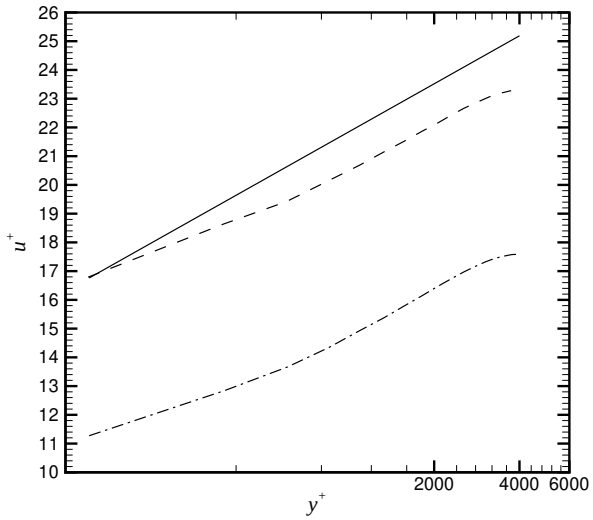

Figure B.1: Mean velocity profiles for $Re_\tau = 4000$, ——— : $u^+ = 2.41 \log(y^+) + 5.2$, - - - - : Piomelli *et al.* (1989), —·— : control-based wall model with RANS target used in cost function of Nicoud *et al.* (2001).

In this formulation, it can be seen that the cost function can be reduced by either reducing the relative difference between the two profiles, or by reducing the velocity at the matching plane. The control is able to reduce this velocity artificially by increasing the mean wall shear stress, which is the only force available to balance the imposed mean pressure gradient. Therefore, this component of cost function reduction is very sensitive to the control. The result is that the cost function is reduced by minimizing the mean velocity, making the mass flow rate un-physically low.

An attempt to remedy this problem was to take the RANS profile as a fixed target based on the velocity field at the old time, i.e. $u_{i,\mathrm{RANS}}|_m = u_{i,\mathrm{LES}}|_m(t = T - \Delta t)$. Similar results were observed, although the decay rate was slower. This can be attributed to the shape of the mean velocity profile obtained with either control-based or standard wall models for this flow. It is observed that over the first three cells, the wall-normal mean velocity gradient is under-predicted by these methods. This leads to a solution with a logarithmic profile which has too small

an intercept. Therefore, when the RANS profile is computed to match this profile, the velocities it predicts are smaller in magnitude than those of the LES. With this RANS profile fixed, the control can reduce the cost function by artificially increasing the wall stress and reducing the LES velocity. Since the RANS profile at the next time step is computed with a lower velocity, it also decreases, forming a feedback loop that again reduces the mass flow rate. Note however that the control sensitivities are smaller in this case, resulting in the slower decay rate.

B.1 Alternative Control Formulations

A problem with any cost function is that, in order to be predictive, the target (whether this be velocity, energy flux, etc) must scale in some sense with the LES. For example, if the LES has a higher velocity, then the predicted RANS velocities will also be high. What is expected is that outer forcing effects (geometry, pressure gradients, inflow/outflow conditions) will be able to equilibrate the system with the help of the controller. We must therefore have a cost function and model that will not have a large impact on this global equilibrium. The previous cost function is an example of a cost function that does not have this property.

In order to alleviate this problem, consider an alternative definition of δ:

$$\delta_u(y) = \frac{1}{A}\int_{\mathbf{Z}}\int_{\mathbf{X}}\left(\frac{u_{\mathrm{LES}}(\vec{x},T)}{u_{\mathrm{RANS}}(\vec{x},T)} - 1\right)dx\,dz. \tag{B.2}$$

Then we have

$$\frac{D\delta_u(y)}{D\phi}\tilde{\phi}_u = \frac{1}{A}\int_{\mathbf{X}}\int_{\mathbf{Z}}\frac{\left(u_{\mathrm{RANS}}\frac{Du_{\mathrm{LES}}}{D\phi} - u_{\mathrm{LES}}\frac{Du_{\mathrm{RANS}}}{D\phi}\right)}{u^2_{\mathrm{RANS}}}\tilde{\phi}_{u_i}dx\,dz. \tag{B.3}$$

Recalling our previous expression for $Du_{\mathrm{RANS}}/D\phi$, this can be rewritten as

$$\frac{D\delta_u(y)}{D\phi}\tilde{\phi}_u = \frac{1}{A}\int_{\mathbf{X}}\int_{\mathbf{Z}}\frac{\left(u_{\mathrm{RANS}}\frac{Du_{\mathrm{LES}}}{D\phi} - u_{\mathrm{LES}}\frac{du_{i,\mathrm{RANS}}}{du_{i,\mathrm{LES}}|_m}\frac{Du_{i,\mathrm{LES}}|_m}{D\phi}\right)}{u^2_{\mathrm{RANS}}}\tilde{\phi}_{u_i}dx\,dz. \tag{B.4}$$

This expression is linear in the sensitivities, so we can use the same approach as before. The only alteration is to change the source terms in the adjoint equations to match the coefficients given in (B.4). However, we must note that in contrast to Nicoud *et al.* (2001), this source term will vary not only in the wall normal direction but also in the wall parallel directions.

Unfortunately, this cost function results in an unstable system. To improve the stability, a new penalty term can be included in the cost function which measures the time derivative of the control

$$J_t = \frac{\alpha_t}{AT} \int_0^T \int \int \left(\frac{\partial \phi}{\partial t} \right)^2 dx\, dz\, dt, \tag{B.5}$$

where α_t is the penalty parameter for this term of the cost function. In order for this to be used in the present control formulation, its Fréchet derivative with respect to the control must be found. When taken directly, it is

$$\frac{DJ_t}{D\phi}\tilde{\phi} = \frac{2\alpha_t}{AT} \int_0^T \int \int \frac{\partial \phi}{\partial t} \frac{\partial \tilde{\phi}}{\partial t}\, dx\, dz\, dt. \tag{B.6}$$

To extract the required information, integration by parts in time is used

$$\frac{DJ_t}{D\phi}\tilde{\phi} = \frac{2\alpha_t}{AT} \frac{\partial \phi}{\partial t} \tilde{\phi} \Big|_0^T - \frac{2\alpha_t}{AT} \int_0^T \int \int \frac{\partial^2 \phi}{\partial t^2} \tilde{\phi}\, dx\, dz\, dt, \tag{B.7}$$

from which the gradient information can be extracted. Note that $\partial^2\phi/\partial t^2$ is zero over one time step in our formulation, so the resulting penalty term acts like a Proportional-Derivative (P-D) controller. However, tests using this cost function have demonstrated that in order for the simulation to be stable, this part of the controller must be the dominant term in the cost function gradient. The resulting mean velocity is then again under-predicted.

In an effort to improve the stability while retaining the same basic formulation, consider the following definition of δ:

$$\delta(y) = \left(\frac{\langle u_{\mathrm{LES}}(\vec{x}, T) \rangle}{\langle u_{\mathrm{RANS}}(\vec{x}, T) \rangle} - 1 \right), \tag{B.8}$$

in this case using the shorthand notation $\langle\cdot\rangle$ for plane averaging. This should somewhat mitigate the large changes in cost function value observed in the code. The Fréchet derivative is then

$$\frac{D\delta}{D\phi}\tilde{\phi} = \delta(y)\left(\frac{1}{A}\int_{\mathbf{X}}\int_{\mathbf{Z}}\left(\frac{\frac{Du_{\text{LES}}}{D\phi}\tilde{\phi}}{\bar{u}_{\text{RANS}}} - \frac{\bar{u}_{\text{LES}}}{\bar{u}^2_{\text{RANS}}}\frac{du_{\text{RANS}}}{du_{\text{LES}}|_m}\frac{Du_{\text{LES}}|_m}{D\phi}\tilde{\phi}\right)dx\,dz\right). \quad \text{(B.9)}$$

In the previous notation, this is

$$\frac{D\delta}{D\phi}\tilde{\phi} = \frac{1}{A}\int_{\mathbf{X}}\int_{\mathbf{Z}}\delta(y)\left(\frac{1}{\bar{u}_{\text{RANS}}}\frac{Du_{\text{LES}}}{D\phi} - \frac{\bar{u}_{\text{LES}}}{\bar{u}^2_{\text{RANS}}}\frac{du_{\text{RANS}}}{du_{\text{LES}}|_m}\frac{Du_{\text{LES}}|_m}{D\phi}\right)\tilde{\phi}\,dx\,dz. \quad \text{(B.10)}$$

However, this cost function is still unstable. Therefore, a different approach will be taken in the coupling of the LES, RANS, and control.

B.2 RANS Sensitivities to Wall Stress Boundary Conditions

In order to reduce the error that is potentially introduced to the RANS system when it is coupled with the LES, the wall stresses will be used directly as an input to the RANS equations. These stresses will be used as boundary conditions in addition to the no-slip condition on the RANS velocity. Because the simplest model of Wang and Moin (2002) is reduces to an analytic solution of an ODE with unknown integration constants, this set of boundary conditions still results in a well-posed system. This may not be the case for more complicated near-wall equations.

Consider the Fréchet derivative of the cost function using this new RANS system:

$$\frac{DJ}{D\phi}\tilde{\phi} = \frac{2}{A}\int_{\Omega}\delta_{u_i}(y)\left(\frac{Du_{i,\text{LES}}(\vec{x},T)}{D\phi} + \frac{Du_{i,\text{RANS}}(\vec{x},T)}{D\phi}\right)\tilde{\phi}\,d\vec{x}. \quad \text{(B.11)}$$

In this case, the last term on the right-hand side of (B.11) is independent of the LES state and is a function of ϕ only. Depending on the RANS model used, this

can either be solved analytically or evaluated through the use of a second adjoint system. With the model used here, the former method is used to determine the RANS sensitivities.

When used in the code, this method produces results similar to those obtained with an algebraic wall model. An explanation is found by examining the magnitudes of the two derivatives in (B.11). The RANS gradient is found to be 2-3 orders of magnitude larger than the gradient from the LES. This is because the RANS system contains no inertia and instead varies linearly with the wall stress only. Therefore, this control attempts to make the RANS profile match that of the LES, instead of the opposite. It is possible that more advanced optimization algorithms could produce better results since they would be more sensitive to the small gradient contributions from the LES state.

This result demonstrates the importance of the structure of the control-based wall stress. Because of the imposed mean pressure gradient and the formulation of the RANS equations, the RANS profile must be correct in the mean. However, the wall stresses that move the RANS profile closer to the LES profile do not significantly increase the quality of the LES solution. This indicates that the specific stresses given to the LES are important and react to the realization of the turbulence.

Bibliography

Arunajatesan, S. and Sinha, N. 2001 Unified unsteady RANS-LES simulations of cavity flowfields. *AIAA Paper 2001-0516*.

Baggett, J. 1997 Some modeling requirements for wall models in Large-Eddy simulation. *Annual Research Briefs*, pp. 123–134. Stanford, CA: Center for Turbulence Research.

Baggett, J. 1998 On the feasibility of merging LES with RANS for the near-wall region of attached turbulent flows. *Annual Research Briefs*, pp. 267–277. Stanford, CA: Center for Turbulence Research.

Baggett, J., Jimenez, J. and Kravchenko, A. 1997 Resolution requirements in large-eddy simulation of shear flows. *Annual Research Briefs*, pp. 51–66. Stanford, CA: Center for Turbulence Research.

Baggett, J., Nicoud, F., Mohammadi, B., Bewley, T., Gullbrand, J. and Botella, O. 2000 Sub-optimal control based wall models for LES - including transpiration velocity. *Proceedings of the 2000 Summer Program*, pp. 331–342. Stanford, CA: Center for Turbulence Research.

Bagwell, T., Adrian, R., Moser, R. and Kim, J. 1993 Improved approximation of wall shear stress boundary conditions for large eddy simulation. *Near-Wall Turbulent Flows* (ed. R. So, C. Speziale and B. Launder). New York, NY: Elsevier Science.

Balaras, E., and Benocci, C. 1994 Subgrid scale models in finite difference simulations of complex wall flows. *Tech. Rep.* CP-551. AGARD.

Balaras, E., Benocci, C. and Piomelli, U. 1996 Two-layer approximate boundary conditions for large-eddy simulations. *AIAA Journal* **34**, 1111–1119.

Bardina, J., Ferziger, J. and Reynolds, W. 1980 Improved subgrid scale models for large-eddy simulation. *AIAA Paper 80-1357*.

Bewley, T. and Moin, P. 1997 Optimal and robust approaches for linear and non-linear regulation problems in fluid mechanics. *AIAA Paper 97-1872*.

Bewley, T., Moin, P. and Temam, R. 2001 DNS-based predictive control of turbulence: a benchmark for feedback algorithms. *J. Fluid Mech.* **447**, 179–225.

Blake, W. 1975 A statistical description of pressure and velocity fields at the trailing edge of a flat strut. *Tech. Rep.* 4241. David Taylor Naval Ship R & D Center, Bethesda, MD.

Brown, A., Hobson, J. and Wood, N. 2001 Large-eddy simulation of neutral turbulent flow over rough sinusoidal ridges. *Boundary-Layer Meteorology* **98** (3), 411.

Cabot, W. 1996 Near-wall models in large-eddy simulations of flow behind a backwards facing step. *Annual Research Briefs*, pp. 199 –210. Stanford, CA: Center for Turbulence Research.

Cabot, W. 1997 Wall models in large eddy simuation of separated flow. *Annual Research Briefs*, pp. 97–106. Stanford, CA: Center for Turbulence Research.

Cabot, W. and Moin, P. 2000 Approximate wall boundary conditions in the large-eddy simulation of high Reynolds number flow. *Flow, Turbulence and Combustion* **63** (1-4), 269–291.

Carati, D. 2001 Large-eddy simulation for turbulent flows: from mathematical foundations to practical applications. Université Libre de Bruxelles.

Caruelle, B. and Ducros, F. 2003 Detached-eddy simulations of attached and detached boundary layers. *Int'l. J. Comp. Fluid Dyn.* **17** (6), 433–451.

Catalano, P., Wang, M., Iaccarino, G. and Moin, P. 2003 Numerical simulation of the flow around a circular cylinder at high Reynolds numbers. *Int'l. J. Heat & Fluid Flow* **24** (4), 463–469.

Cederwell, R. 2001 Large-eddy simulation of the evolving stable boundary layer over flat terrain. PhD thesis, Stanford University.

Chang, Y. and Collis, S. 1999 Active control of turbulent channel flows based on large eddy simulation. Paper No. FEDSM-99-6929. ASME.

Chow, F. K., Street, R., Xue, M. and Ferziger, J. 2005 Explicit filtering and reconstruction turbulence modeling for large-eddy simulation of neutral boundary layer flow. *Journal of the Atmospheric Sciences* **62** (7), 2058–2077.

Deardorff, J. 1970 Numerical study of three dimensional turbulent channel flow at large Reynolds numbers. *J. Fluid Mech.* **4**, 453–480.

Dennis, J. 1983 *Numerical Methods for Unconstrained Optimzation and Nonlinear Equations*. New York: Prentice-Hall.

Germano, M. 1999 From RANS to DNS: towards a bridging model. *Direct and Large Eddy Simulation III*, pp. 225–236. Kluwer, Germany.

Germano, M., Piomelli, U., Moin, P. and Cabot, W. 1991 A dynamic subgrid-scale eddy-viscosity model. *Phys. Fluids A* **3** (7), 1760–1765.

Ghosal, S., Lund, T., Moin, P. and Akselvoll, K. 1995 A dynamic localization model for large-eddy simulation of turbulent flows. *J. Fluid Mech.* **286**, 229–255.

Grötzbach, G. 1987 Direct numerical and large eddy simulation of turbulent channel flows. *Encyclopedia of Fluid Mechanics* (ed. N. Cheremisinoff). West Orange, NJ.

Hoffman, G. and Benocci, C. 1995 Approximate wall boundary conditions for large eddy simulations. *Advances in Turbulence V* (ed. R. Benzi). Kluwer, Berlin.

Iovieno, M., Passoni, G. and Tordella, D. 2004 A new large-eddy simulation near-wall treatment. *Phys. Fluids* **16** (11), 3935–3944.

Jimenez, J. and Moin, P. 1991 Minimal flow unit in near-wall turbulence. *J. Fluid Mech.* **225**, 213–240.

Jimenez, J. and Moser, R. 2000 LES: where we are and what we can expect. *AIAA J.* **38** (4), 605–612.

Jimenez, J. and Vasco, C. 1998 Approximate boundary conditions for turbulent simulations. *Proceedings of the 1998 Summer Program*, pp. 399 – 412. Stanford, CA: Center for Turbulence Research.

Kerstein, A., Ashurst, W., Wunsch, S. and Nilsen, V. 2001 One-dimensional turbulence: vector formulation and application to free shear flows. *J. Fluid Mech.* **447**, 85–109.

Kim, J. and Moin, P. 1985 Application of a fractional-step method to incompressible Navier-Stokes equations. *J. Comp. Phys.* **59** (2), 308–323.

Kravchenko, A., Moin, P. and Moser, R. 1996 Zonal embedded grids for numerical simulations of wall-bounded turbulent flows. *J. Comp. Phys.* **127** (2), 412–423.

Le, H., Moin, P. and Kim, J. 1997 Direct numerical simulation of turbulent flow over a backward-facing step. *J. Fluid Mech.* **330**, 349–374.

Lilly, D. 1992 A proposed modification of the Germano subgrid-scale closure method. *Phys. Fluids A* **4** (3), 633–635.

Luenberger, D. 1969 *Optimization by Vector Space Methods*. New York, NY: John Wiley & Sons, Inc.

Marsden, A. 2004 Aerodynamic noise reduction using shape optimization. PhD thesis, Stanford University.

Mason, P. and Callen, N. 1986 On the magnitude of the subgrid-scale eddy coefficient in large eddy simulations of turbulent channel flow. *J. Fluid Mech.* **162**, 439–462.

Mason, P. and Thomson, D. 1992 Stochastic backscatter in large-eddy simulation of boundary layers. *J. Fluid Mech.* **242**, 439–462.

Meneveau, C. and Katz, J. 2000 Scale-invariance and turbulence models for large-eddy simulation. *Annu. Rev. Fluid Mech.* **32**, 1–32.

Mohammadi, B. 1999 Dynamical approaches and incomplete gradients for shape optimization. *AIAA Paper 99-3374*.

Mohammadi, B., Moldho, J. and Santiago, J. 2000 Design of minimal dispersion fluidic channels in a CAD-free framework. *Proceedings of the 2000 Summer Program*, pp. 49–62. Stanford, CA: Center for Turbulence Research.

Mohammadi, B. and Pironneau, O. 2001 *Applied Shape Optimization for Fluids*. Oxford: Oxford University Press.

Moin, P. 2001 *Fundamentals of Engineering Numerical Analysis*. Cambridge University Press.

Moin, P. and Kim, J. 1982 Numerical investigation of turbulent channel flow. *J. Fluid Mech.* **118**, 341–377.

Moin, P. and Mahesh, K. 1998 Direct numerical simulation: A tool in turbulence research. *Ann. Rev. Fluid Mech.* **30**, 539–578.

Moser, R., Kim, J. and Mansour, N. 1999 Direct numerical simulation of turbulent channel flow up to $Re_\tau = 590$. *Phys. Fluids* **11** (4), 943–945.

Nadarajah, S. and Jameson, A. 2000 A comparison of the continuous and discrete adjoint approach to automatic aerodynamic optimization. *AIAA Paper 2000-0667*.

Nicoud, F., Baggett, J., Moin, P. and Cabot, W. 2001 Large eddy simulation wall-modeling based on suboptimal control theory and linear stochastic estimation. *Phys. Fluids* **13** (10), 2968–2984.

Nicoud, F., Winckelmans, G., Carati, D., Baggett, J. and Cabot, W. 1998 Boundary conditions for LES away from the wall. *Proceedings of the 1998 Summer Program*, pp. 413–422. Stanford, CA: Center for Turbulence Research.

Nikitin, N., Nicoud, F., Wasistho, B., Squires, K. and Spalart, P. 2000 An approach to wall modelling in large-eddy simulations. *Phys. Fluids. Letters* **12** (7), 1629.

Piomelli, U. and Balaras, E. 2002 Wall-layer models for large-eddy simulations. *Ann. Rev. Fluid Mech.* **34**, 349–374.

Piomelli, U., Balaras, E., Pasinato, H., Squires, K. and Spalart, P. 2003 The inner-outer layer interface in large-eddy simulations with wall-layer models. *Intl. J. Heat & Fluid Flow* **24**, 538–550.

Piomelli, U., Ferziger, J., Moin, P. and Kim, J. 1989 New approximate boundary conditions for large eddy simulations of wall bounded flows. *Phys. Fluids* **1** (6), 1061–1068.

Quemere, P., Saguat, P. and Couaillier, V. 2000 A multidomain/multiresolution method with application to large-eddy simulation. *Comptes Rendus de l'Academie des Sciences, Serie II* **328** (1), 87–90.

Sagaut, P. 2002 *Large Eddy Simulation for Incompressible Flows*. Berlin: Springer.

Schmidt, R., Kerstein, A., Wunsch, S. and Nilsen, V. 2003 Near-wall LES closure based on one-dimensional turbulence modeling. *J. Comp. Phys.* **186** (1), 317–355.

Schumann, U. 1975 Subgrid scale model for finite difference simulations of turbulent flows in plane channels and annuli. *J. Comp. Phys.* **18** (4), 376–404.

Smagorinsky, J. 1963 General circulation experiments with the primitive equations. *Monthly Weather Review* **91**, 99–164.

Spalart, P., Jou, W.-H., Strelets, M. and Allmaras, S. 1997 Comments on the feasibility of LES for wings, and on a hybrid RANS/LES approach. *Advances in DNS/LES*, pp. 4–8. Ruston, LA: First AFOSR International Conference on DNS/LES.

Spalart, P., Moser, R. and Rogers, M. 1991 Spectral methods for the Navier-Stokes equations with one infinite and two periodic directions. *J. Comp. Phys.* **96** (2), 297–324.

Speziale, C. 1998 Turbulence modeling for time-dependent RANS and VLES: a review. *AIAA J.* **36** (2), 173–184.

Strelets, M. 2001 Detached eddy simulation of massively separated flows. *AIAA Paper 2001-0879*.

Templeton, J., Wang, M. and Moin, P. 2002 Towards LES wall models using optimization techniques. *Annual Research Briefs*, pp. 189–200. Stanford, CA: Center for Turbulence Research.

Wang, M. and Moin, P. 2000 Computation of trailing-edge flow and noise using large-eddy simulation. *AIAA J.* **38** (12), 2201–2209.

Wang, M. and Moin, P. 2002 Dynamic wall modeling for large-eddy simulation of complex turbulent flows. *Phys. Fluids* **14** (7), 2043–2051.

Werner, H. and Wengle, H. 1991 Large eddy simulation of turbulent flow over and around a cube in a plate channel. *Proceedings of the Eighth Symposium on Turbulent Shear Flows*, pp. 1941–1946.